

352.15: 500-169-SDL 14

ESSA TR ERL 169-SDL 14

A UNITED STATES  
DEPARTMENT OF  
**COMMERCE**  
PUBLICATION



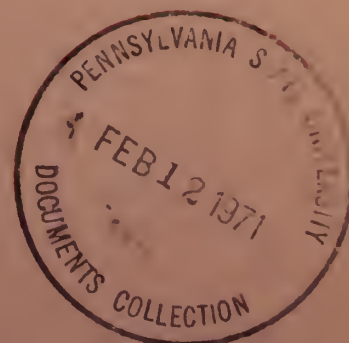
# ESSA Technical Report ERL 169-SDL 14

U.S. DEPARTMENT OF COMMERCE  
Environmental Science Services Administration  
Research Laboratories

## Extreme Ultraviolet Flashes of Solar Flares Observed Via Sudden Frequency Deviations

RICHARD F. DONNELLY

BOULDER, COLO.  
SEPTEMBER 1970



# ESSA RESEARCH LABORATORIES

The mission of the Research Laboratories is to study the oceans, inland waters, the lower and upper atmosphere, the space environment, and the earth, in search of the understanding needed to provide more useful services in improving man's prospects for survival as influenced by the physical environment. Laboratories contributing to these studies are:

**Earth Sciences Laboratories:** Geomagnetism, seismology, geodesy, and related earth sciences; earthquake processes, internal structure and accurate figure of the Earth, and distribution of the Earth's mass.

**Atlantic Oceanographic and Meteorological Laboratories:** Oceanography, with emphasis on the geology and geophysics of ocean basins, oceanic processes, sea-air interactions, hurricane research, and weather modification (Miami, Florida).

**Pacific Oceanographic Laboratories:** Oceanography; geology and geophysics of the Pacific Basin and margins; oceanic processes and dynamics; tsunami generation, propagation, modification, detection, and monitoring (Seattle, Washington).

**Atmospheric Physics and Chemistry Laboratory:** Cloud physics and precipitation; chemical composition and nucleating substances in the lower atmosphere; and laboratory and field experiments toward developing feasible methods of weather modification.

**Air Resources Laboratories:** Diffusion, transport, and dissipation of atmospheric contaminants; development of methods for prediction and control of atmospheric pollution (Silver Spring, Maryland).

**Geophysical Fluid Dynamics Laboratory:** Dynamics and physics of geophysical fluid systems; development of a theoretical basis, through mathematical modeling and computer simulation, for the behavior and properties of the atmosphere and the oceans (Princeton, New Jersey).

**National Severe Storms Laboratory:** Tornadoes, squall lines, thunderstorms, and other severe local convective phenomena toward achieving improved methods of forecasting, detecting, and providing advance warnings (Norman, Oklahoma).

**Space Disturbances Laboratory:** Nature, behavior, and mechanisms of space disturbances; development and use of techniques for continuous monitoring and early detection and reporting of important disturbances.

**Aeronomy Laboratory:** Theoretical, laboratory, rocket, and satellite studies of the physical and chemical processes controlling the ionosphere and exosphere of the earth and other planets.

**Wave Propagation Laboratory:** Development of new methods for remote sensing of the geophysical environment; special emphasis on propagation of sound waves, and electromagnetic waves at millimeter, infrared, and optical frequencies.

**Institute for Telecommunication Sciences:** Central federal agency for research and services in propagation of radio waves, radio properties of the earth and its atmosphere, nature of radio noise and interference, information transmission and antennas, and methods for the more effective use of the radio spectrum for telecommunications.

**Research Flight Facility:** Outfits and operates aircraft specially instrumented for research; and meets needs of ESSA and other groups for environmental measurements for aircraft (Miami, Florida).

ENVIRONMENTAL SCIENCE SERVICES ADMINISTRATION

BOULDER, COLORADO 80302



U. S. DEPARTMENT OF COMMERCE

Maurice H. Stans, Secretary

ENVIRONMENTAL SCIENCE SERVICES ADMINISTRATION

Robert M. White, Administrator

RESEARCH LABORATORIES

Wilmot N. Hess, Director

ESSA TECHNICAL REPORT ERL 169-SDL 14

# Extreme Ultraviolet Flashes of Solar Flares Observed Via Sudden Frequency Deviations

RICHARD F. DONNELLY

SPACE DISTURBANCES LABORATORY  
BOULDER, COLORADO  
September 1970

---

For sale by the Superintendent of Documents, U. S. Government Printing Office, Washington, D. C. 20402  
Price \$1.00



TABLE OF CONTENTS

	Page
LIST OF FIGURES	v
LIST OF TABLES	vii
ABSTRACT	viii
1. INTRODUCTION	1
2. RADIATION DETECTOR CHARACTERISTICS	1
3. WAVELENGTH DEPENDENCE OF SOLAR FLARE RADIATION in the 1-1030 <sup>o</sup> Å range.	5
4. STATISTICAL CHARACTERISTICS OF SUDDEN FREQUENCY DEVIATIONS AND EUV FLASHES	8
4.1 Time of Occurrence	8
4.2 Intensity	11
4.3 Rise Time	15
4.4 Duration	18
4.5 Fine Time-Structure, Complexity and Quasi-Periodicity	18
5. RELATIONSHIP OF EUV FLASHES DEDUCED FROM SFD'S WITH OTHER FLARE RADIATION	25
5.1 Hard X-Ray Bursts (> 10 keV)	25
5.2 Soft X-Ray Bursts ( $\lambda > 1\text{Å}$ )	26
5.3 Ultraviolet Flashes (1030-3000Å)	29
5.4 White Light Flares	29
5.5 Low-Chromosphere Optical Line Emission	30
5.6 H $\alpha$ Flares	32
5.6.1 Area Dependence	32
5.6.2 Intensity Dependence	32
5.6.3 Sunspot Dependence	33
5.6.4 Association of EUV Bursts with the H $\alpha$ Explosive Phase	33
5.6.5 Dependence on Location of the H $\alpha$ Flare	35
5.6.5.a Dependence of Occurrence on Central Meridian Distance	35
5.6.5.b Peculiar Long-Duration Events	38
5.6.5.c Limb Flares	48
5.6.6 Bright Impulsive H $\alpha$ Kernels	48
5.7 Relation to Surges, Sprays and Eruptive Prominences	50
5.8 Microwave Bursts	51
6. SFD'S FOR FAMOUS FLARES	56
7. CONCLUSIONS, RECOMMENDATIONS, AND SPECULATIONS	56
8. ACKNOWLEDGEMENTS	67
9. REFERENCES	68
APPENDIX A	72
1. Procedures for Analyzing SFD Data to Deduce the 10-1030 <sup>o</sup> Å Flux Enhancement: Brief Descriptions	72
2. Sensitivity of Frequency Deviations to Solar Bursts	76
3. Comments on SFD Observations	81
4. Miscellaneous Unpublished Studies of SFD'S	81
APPENDIX B	85



## LIST OF FIGURES

	Page
1. SFD sensitivity to ionizing radiations as a function of radiation wavelength.	2
2. The dependence of SFD's on the impulsiveness of the flare enhancements of ionizing radiation, $t_c$ = the effective electron-loss rate in the ionosphere.	4
3. Monthly rate of occurrence of SFD's at Boulder from October, 1960 through June, 1970.	10
4. Diurnal dependence of Boulder SFD's.	10
5. Seasonal dependence of Boulder SFD's.	12
6. Intensity distribution of all Boulder SFD's.	13
7. Intensity distribution of selected Boulder SFD's.	14
8. Rise-time distribution of Boulder SFD's.	17
9. Duration distribution of Boulder SFD's.	19
10. An EUV flare with quasi-periodic fine structure.	22
11. Spectrum of fine structure.	23
12. Distribution of fine structure periods.	23
13. Comparison of timing of hard X-ray burst and SFD of 2141 UT March 1, 1969, OSO 5 X-ray observations made by Frost (1969).	27
14. Illustration of components of flare radiation. The impulsive component A occurs concurrently at centimeter wavelengths, hard X-rays, certain EUV wavelengths, certain spatial portions of H $\alpha$ flares, and occasionally in white light. The gradual or slow component, B occurs with slightly different time dependence in soft X-rays, certain other RUV wavelengths, most of the H $\alpha$ flare, and centimeter wavelengths where it is sometimes called a postburst increase. The Type IV Component, C, occurs mainly at radio wavelengths.	28
15. EUV burst, 5324 $\overset{\circ}{\text{A}}$ Fe emission and H $\alpha$ flare of 2010 UT April 21, 1969.	31
16. The dependence of the association of SFD's with explosive-phase H $\alpha$ flash on the intensity of the SFD. The number at the bottom of each histogram bar denotes the number of events involved.	34
17. The association of SFD's and H $\alpha$ explosive-phase flares as a function of H $\alpha$ flare importance and brightness. The number at the bottom of the histogram bars denotes the number of events involved.	36
18. Association of an EUV burst with a small bright H $\alpha$ kernel.	37
19. Dependence of EUV flashes on the central meridian distance of the associated H $\alpha$ flare for 1964-1968 for all H $\alpha$ flare classifications.	39
20. Dependence of EUV flashes on the central meridian distance of the associated H $\alpha$ flare for 1966 for all H $\alpha$ flare classifications.	40
21. Dependence of EUV flashes on the central meridian distance of the associated H $\alpha$ flare for 1967 for all H $\alpha$ flare classifications.	41
22. Dependence of EUV flashes on the central meridian distance of the associated H $\alpha$ flare for 1968 for all H $\alpha$ flare classifications.	42
23. Dependence of EUV flashes on the central meridian distance of the associated H $\alpha$ flare for 1964-1968 for all H $\alpha$ flare classifications of importance $\geq 1$ .	43
24. An example of an SFD with an unusually long duration of positive frequency deviation. The station-identification break is shown by SB.	46
25. Peak 606 MHz emission versus peak 10-1030 $\overset{\circ}{\text{A}}$ flux enhancement. EL denotes East Limb flare location, $\bullet$ Central Meridian Distance (CMD) $\geq 70^\circ$ , $\odot 20^\circ < \text{CMD} < 70^\circ$ , and $\oplus \text{CMD} \leq 20^\circ$ .	53
26. Peak 1415 MHz emission versus peak 10-1030 $\overset{\circ}{\text{A}}$ flux enhancement.	53

	Page
27. The average of peak radio emissions observed at 2695, 2700, and 2800 MHz versus peak 10-1030Å flux enhancement.	54
28. Peak 4995 MHz emission versus peak 10-1030Å flux enhancement.	54
29. Peak 8800 MHz emission versus peak 10-1030Å flux enhancement.	55
30. Peak 10700 MHz emission versus peak 10-1030Å flux enhancement.	55
31. Boulder SFD observations for the flare of 1924 UT May 21, 1967.	58
32. Normalized 10-1030Å flux enhancement as a function of time for the flare of 1924 UT May 21, 1967.	59
33. SFD and 10-1030Å flux enhancement as a function of time for the flare of 1710 UT July 8, 1968.	60
34. Boulder SFD observations for the flare of 1740 UT March 12, 1969 (a) Oblique-Path Observations $\Delta\phi(10-1030\text{\AA}, t)$ for this event is presented in McIntosh and Donnelly (1970). (b) Near Vertical-Incidence Observations.	61
35. Boulder SFD observations for the flare of 2009 UT April 21, 1969 $\Delta\phi(10-1030\text{\AA}, t)$ for this event is discussed in section 5.6.6.	63
36. Models for the impulsive EUV flash.	66
37. Examples of electron density and loss time constant as a function of height.	74
38. An example of the wavelength dependence of SFD sensitivity to ionizing radiations for $f_{\nu} = 2 \text{ MHz} \rightarrow f_{\nu} = 2 \text{ MHz}$ , $f_{\nu} = 5 \text{ MHz} \rightarrow f_{\nu} = 5 \text{ MHz}$ .	80
39. Examples of consistency in midlatitude SFD observations.	82

LIST OF TABLES

	Page
1. Radiation detector characteristics of sudden frequency deviations.	6
2. $R_f$ , $\phi_f$ and $R\phi$ as a function of wavelength.	7
3. Transmissions used in Boulder SFD observations.	9
4. Estimates of peak $10\text{-}1030\overset{\circ}{\text{A}}$ flux enhancements.	16
5. SFD's with complex time structure.	21
6. Some statistical properties of SFD events.	24
7. Contingency table for SFD's and $H\alpha$ flares with an explosive-phase.	34
8. Long duration events.	44
9. Association of SFD's with surges and sprays.	50
10. Famous events.	57
11. Boulder SFD events 1968 through June 1970.	85

## ABSTRACT

The properties of EUV flashes from solar flares measured via a type of ionospheric event, called a sudden frequency deviation (SFD), are presented. These results are based on ten years of observations at Boulder wherein about 2000 SFD events were detected and scaled.

The characteristics of SFD's as a detector of solar radiation are discussed. SFD's are sensitive to bursts of solar radiation at wavelengths in the 1-1030Å range. Unlike most detectors of solar radiations, SFD's are sensitive to the impulsiveness of the solar radiation and are insensitive to the non-flare radiation. The sensitivity of SFD's to 1-1030Å bursts depends upon the spectrum of the 1-1030Å radiation, the solar zenith angle, time of day and season, the pre-flare electron density as a function of height, the upper atmospheric constituent densities, and other ionospheric disturbances. The main assets of SFD observation are 1 sec. time resolution, low cost, ground-based equipment, and essentially continuous daylight coverage.

The wavelength spectrum of the radiation responsible for SFD's is revised. The characteristics of He II 303.8Å, OV 629.7Å, HLyγ 972.5Å, CIII 977.0Å and HLyα 1215.7Å have essentially the same time dependence as the 1-1030Å flash responsible for SFD's. Soft X-rays (2-20Å) and certain EUV lines that are normally coronal lines have a much slower time dependence than the 1-1030Å flash and contribute little to SFD's.

The rise time, duration, intensity, and fine time-structure of SFD's are statistically studied. Although most SFD's have some fine structure, quasi-periodicity in EUV flashes is quite rare. When it does occur, it usually is weak relative to the peak 10-1030Å flux enhancement. Previously unpublished SFD data for famous flares are given in detail. A revised list of Boulder SFD observations is given for 1968 through June, 1970, when routine Boulder SFD observations were terminated.

Present knowledge of the close association of EUV flashes with hard X-ray bursts, white-light emission and microwave radio bursts are reviewed. The relationship of EUV flashes to small bright impulsive kernels in Hα and other optical observations of solar flares are presented and the location of these kernels discussed. The intensity of EUV flashes is shown to depend upon the central meridian distance of the flare location; the intensity decreases at the limb. Several models for the impulsive EUV source region are proposed.

Key Words: sudden frequency deviations, extreme ultraviolet, X-ray, solar flare, white-light flare, ionosphere.

EXTREME ULTRAVIOLET FLASHES OF SOLAR FLARES OBSERVED  
VIA SUDDEN FREQUENCY DEVIATIONS

Richard F. Donnelly

1. INTRODUCTION

A sudden frequency deviation (SFD) is a type of sudden ionospheric disturbance (SID) caused by bursts of X-rays and extreme ultraviolet (EUV) radiation from solar flares. In effect, SFD observations are detectors of impulsive solar ionizing-radiation in the 1-1030Å wavelength range. This report presents our knowledge of EUV flashes of solar flares based on about ten years of SFD observations at Boulder, Colorado.

An SFD is an event in which the received frequency of a high-frequency radio-wave reflected, usually from the F-region of the ionosphere, increases suddenly, peaks, and then decays to the transmitted frequency. The frequency deviation sometimes has several peaks and usually takes on negative values during the decaying portion. The start-to-maximum time is typically about one minute, and the peak frequency deviation is usually less than 1/2 Hz. Those SFD's observed on paths reflected from the bottom of the E layer or from sporadic E are sensitive only to 1-10Å flare radiation and are generally smoother, slower, and much smaller than those observed on paths reflected from the F-region. In this report, the term "SFD" will refer to events observed on paths reflected from the F-region or upper-E-region, unless noted otherwise. These SFD's differ from most types of SID effects in that the frequency deviation is proportional to the time rate of change of electron density primarily in the E and F1 regions produced by flare radiation in the 10-1030Å range, rather than being proportional to the D-region electron-density enhancement produced by 1-10Å flare radiation.

In the next section, we first treat SFD observations as detectors of solar-flare ionizing radiation and present the characteristics of this detector, in a way analogous to reports on satellite X-ray measurements. Wavelength dependence of the radiation responsible for SFD's and the statistical characteristics of SFD's are then reviewed, and the characteristics of EUV flashes of solar flares based on SFD observations and their relationships to other solar flare radiations are discussed.

2. RADIATION DETECTOR CHARACTERISTICS

Figure 1 shows a typical curve of the sensitivity  $S(\lambda)$  of SFD's to radiation incident from above the earth's atmosphere as a function of the wavelength ( $\lambda$ ) of the ionizing radiation.  $S(\lambda)$  is defined by

$$S(\lambda) = \frac{\Delta f(f_v)}{R_t R_\chi \Delta \phi(\lambda) d\lambda} \quad (1)$$

where  $\Delta f$  is the frequency deviation in Hz,  $\Delta \phi$  is the radiation enhancement in ergs  $\text{cm}^{-2} \text{sec}^{-1} \text{Å}^{-1}$ ,  $R_t$  is a dimensionless factor that accounts for the time dependence of  $\Delta \phi$ ,  $R_\chi$  accounts for the solar zenith angle dependence and  $f_v$  is the equivalent vertical-incidence frequency of the SFD probing radio wave. For fast EUV bursts and an overhead sun,  $R_t = R_\chi = 1$ ;  $S(\lambda)$  is derived in Appendix A.

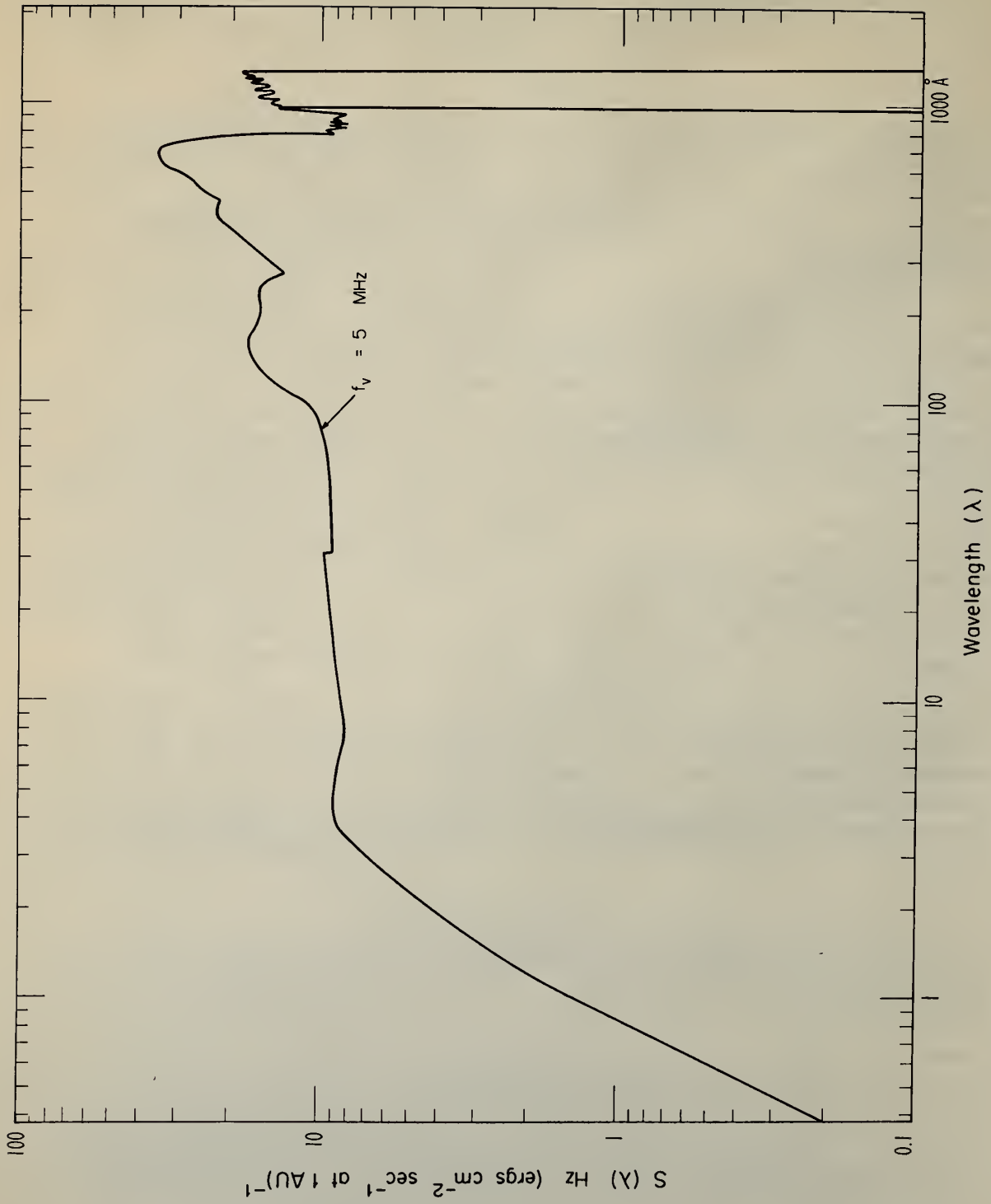


Figure 1. SF D sensitivity to ionizing radiations as a function of radiation wavelength.

The value of  $S(\lambda)$  drops off rapidly with decreasing wavelength below about  $1\text{Å}$  because radiation at those wavelengths produces ionization mainly low in the dense D-region and negligible ionization in the E and F regions. In the D-region, most of the freed electrons are rapidly lost via attachment to form negative ions. The electrons that remain free have such a high collision frequency with the neutral gas that they do not interact effectively with the probing radio wave. The sensitivity drops off abruptly with increasing wavelength at about  $1030\text{Å}$  because radiation at wavelengths higher than  $1027\text{Å}$  is very ineffective at ionizing any of the major constituents of the upper atmosphere. There is a similar dropoff near  $800\text{Å}$  because molecular nitrogen ceases to be ionized, and another dropoff above  $900\text{Å}$  because atomic oxygen ceases to be ionized. The remaining variation in sensitivity throughout the  $1\text{-}1030\text{ Å}$  range is a consequence of the variation with wavelength of the absorption cross sections of the major constituents of the upper atmosphere.

The sensitivity of frequency deviations to solar flare radiation varies with solar zenith angle, frequency of the probing radiowave, season, and numerous other factors. These effects are discussed in detail in Appendix A. Despite these complexities, SFD observations are much like a very broad-band satellite detector. The solar zenith angle dependence of SFD's is analogous to the aspect angle dependence of satellite measurements. Just as satellite X-ray observations are complicated by particle radiation, SFD's are complicated by other types of ionospheric disturbances. Because of the "noise" from small ionospheric fluctuations that are always present, the smallest  $1\text{-}1030\text{ Å}$  flux enhancement detectable by midlatitude SFD observations under the best conditions is about  $4 \times 10^{-3} \text{ ergs cm}^{-2}\text{sec}^{-1}$ , and, more typically,  $10^{-2} \text{ ergs cm}^{-2}\text{sec}^{-1}$ . The frequency deviation is linearly related to the  $1\text{-}1030\text{ Å}$  flux enhancement for enhancements less than  $1 \text{ ergs cm}^{-2}\text{sec}^{-1}$ , above which a small nonlinearity may occur after the EUV flash has been in progress for about 100 sec.

The main difference between SFD detection of  $1\text{-}1030\text{ Å}$  radiation and satellite broadband radiation detectors is that SFD's are sensitive to the impulsiveness of the  $1\text{-}1030\text{ Å}$  radiation. Figure 2 illustrates this feature. The solid curve represents the time dependence of a burst of ionizing radiation. The dashed curve illustrates the time dependence of the time-rate-of-change of electron density and, hence, the SFD, for the case where the rise time ( $t_m$ ) and decay time ( $t_d$ ) of the burst are much less than the effective electron-loss time constant in the E and F1 regions of the ionosphere. In this case, the SFD time dependence is essentially the same as that of the incident radiation enhancement, except late in the decay stage. The dash-dot curve illustrates the case when the rise and decay times of the burst of radiation are comparable to the effective electron-loss time constant. The SFD in this case has a time dependence similar to the radiation burst but the distortion is quite apparent. The SFD data can be used to estimate the radiation burst by computing the effects of the electron loss processes. The dotted curve illustrates the case when the burst time constants are much larger than the ionospheric electron-loss time constants. The SFD is relatively small and highly distorted with respect to the time dependence of the radiation burst. Considering the "noise" in SFD data caused by non flare-related ionospheric fluctuations and our lack of precise knowledge of the electron loss rates as a functions of height at the time of a particular SFD, it is usually impractical to reconstruct the radiation enhancement from SFD measurements in this

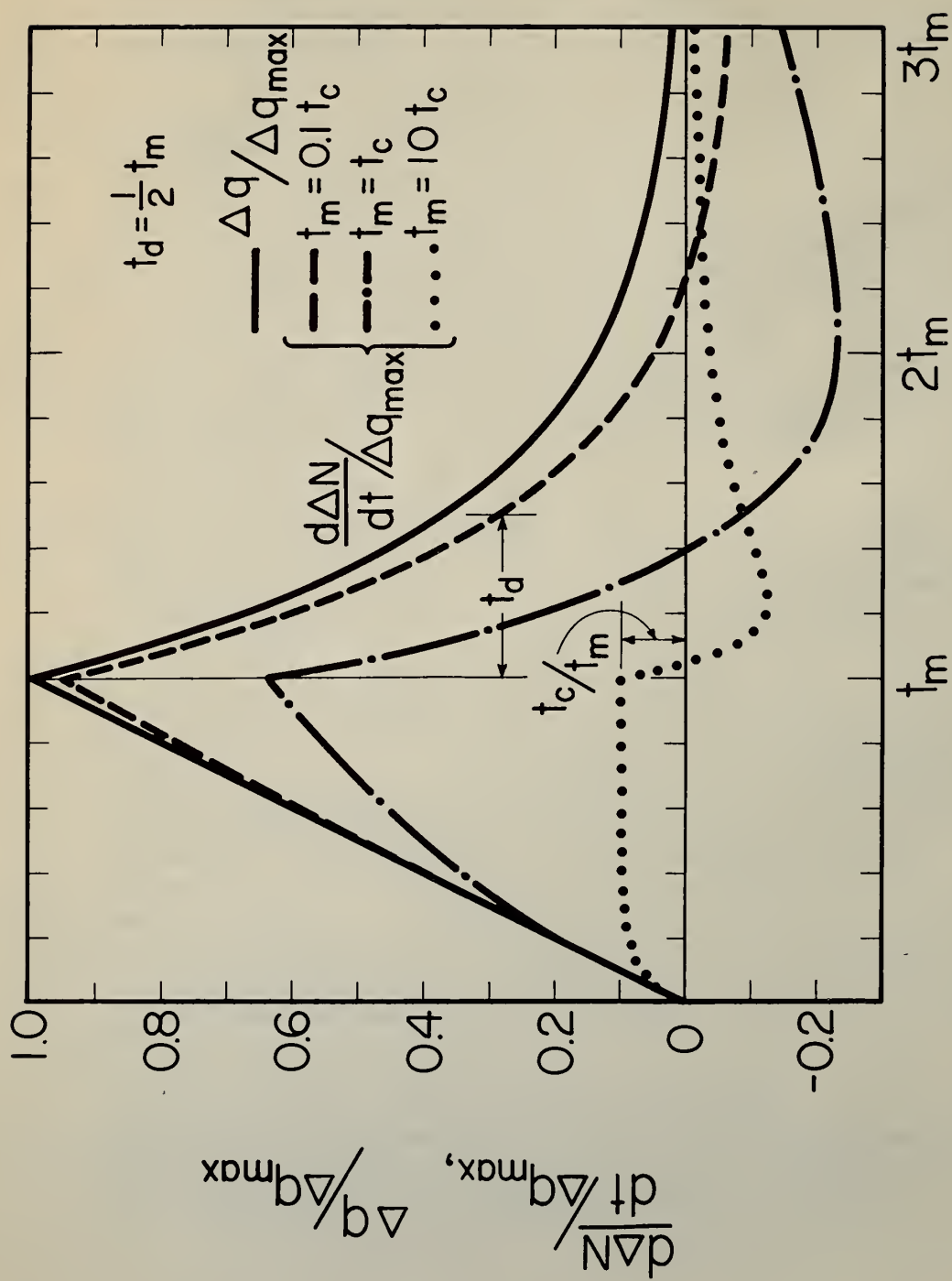


Figure 2. The dependence of SFED's on the impulsiveness of the flare enhancements of ionizing radiation,  $t_c$  = the effective electron-loss rate in the ionosphere.

case. The electron-loss time constant in the E and F1 region is typically between 15 and 60 sec; hence, SFD observations are relatively insensitive to radiation bursts with smooth rises of five minutes or more. Obviously, one major limitation of SFD observations is that they give no information on the non-flare 1-1030 Å radiation. The above discussion qualitatively explains the "impulsiveness" dependence of SFD's; Appendix A gives more quantitative information of some of the complexities involved. Table 1 summarizes some of the basic characteristics of SFD's as a detector of 1-1030 Å flux enhancements.

### 3. WAVELENGTH DEPENDENCE OF SOLAR FLARE RADIATION WITHIN THE 1-1030 Å RANGE

Information on the wavelength dependence of the 1-1030 Å flare radiation comes mainly from many satellite experiments, particularly the EUV observations of Hall and Hinteregger (1969). Donnelly (1968a,b) has examined the relationship between these various satellite observations and SFD's. The results are summarized in table 2 and include some corrections and additions. Most of the corrections involve an improved estimate of the preflare EUV flux based on OSO 3 measurements (Hall, 1969) of absolute EUV flux near the time of the EUV flares upon which the results in table 2 are based, and on improved information of the variation of some EUV lines with respect to the 10.7 cm flux based on Hall et al. (1969) and Hinteregger and Hall (1969). Considering the scatter in the ratio of their EUV flux measurements to the radio flux, the preflare EUV flux estimates may easily be in error by a factor of two. In table 2, the symbol  $R_f$  indicates how much of an observed SFD is produced by the flare radiation at a particular emission line or wavelength range. The quantity  $\phi_f$  is useful for estimating the flare radiation enhancement at particular wavelengths from SFD observations. The quantity  $\phi_f$  for the entire 1-1030 Å range is approximately 0.08 ergs  $\text{cm}^{-2}$ . The intensity of the flare radiation enhancement at a particular wavelength relative to the total enhancement in the 1-1030 Å range is indicated by  $R\phi$ . Most of the entries in table 2 are based on only a few events and should therefore be considered as preliminary rough estimates. More narrowband satellite measurements in the 20-1030 Å range are needed for more flares and wavelengths to complete our knowledge of the spectrum of the ionizing radiation that produces SFD's.

One interpretation of the results in table 2 is that the EUV recombination continuum and line emission from the more abundant solar constituents H, He, O, C, and N, are the main cause of SFD's observed on paths reflected from the F region. However, another interpretation includes a bremsstrahlung continuum throughout the 1-1030 Å in addition to the above radiations. McClinton (1968) and Grebenkemper's (1969) 1085-1350 Å and 1225-1350 Å measurements for the proton flare of August 28, 1966, are consistent with a continuum enhancement and not explainable by an enhancement of Lyman  $\alpha$ . They suggest that the EUV and white light flash are bremsstrahlung emission from an optically thick source region. Some of the 1-1030 Å burst is undoubtedly bremsstrahlung emission; but how much is not known. The sum of  $R_f$  in table 2 accounts for only half the SFD; part of the remaining half could be some type of continuum emission. Part of the continuum emission Hall and Hinteregger (1969) observed in the hydrogen recombination continuum wavelength range could have been a broader-band continuum emission. No such continuum is known to have been observed.

Table 1 Radiation Detector Characteristics of Sudden Frequency Deviations

Wavelength Range  $\approx 1-1030 \text{ \AA}$ .

Dynamic Range:

Minimum detectable flux enhancement  $\approx 10^{-2} \text{ ergs cm}^{-2} \text{ sec}^{-1}$ .

Maximum measureable flux enhancement  $\approx 10 \text{ ergs cm}^{-2} \text{ sec}^{-1}$ .

The minimum level is a consequence of "noise" in the frequency deviations produced by ionospheric variations that are usually present and unrelated to flares. The maximum level is a consequence of ionospheric absorption of the SFD probing radio waves (induced by the  $1-10 \text{ \AA}$  flare radiation) and the lowering of their height of reflection to the bottom of the E layer because of the flare-induced electron density enhancement in the E and F1 regions.

Solar Zenith Angle ( $\chi$ ) Dependence of Sensitivity:  $R_{\chi} \approx \cos \chi$

Rise Time ( $t_r$ ) Dependence of Sensitivity:  $R_t \approx 1$  for  $t_r \leq 10 \text{ sec}$ ; for  $t_r > 10 \text{ sec}$ ,  $R_t \approx \frac{t_c}{t} (1 - e^{-(t/t_c)})$  for a linear rise, where  $t_c$  is the effective electron-loss time constant in the ionosphere; for more general relations, see Donnelly (1969a).

Time Resolution:  $\approx 1 \text{ sec}$  for Boulder observations with  $\Delta f$  structure  $\geq 1 \text{ kHz}$  processed with 1 minute  $\geq 1.4$  inches of chart record. Higher resolution could be achieved if needed. A resolution of 1 sec means that two impulses of  $1-1030 \text{ \AA}$  radiation separated by  $\geq 1 \text{ sec}$  could be distinguished as more than one pulse. Fine structure with rise times  $t_r \geq 1 \text{ sec}$  are measureable. Structure with  $t_r < 1 \text{ sec}$  would still be evident in SFD data, although their rise times would be immeasurable. No SFD has been observed at Boulder that contained significant unresolved structure.

Relative Intensity Resolution  $\approx 10^{-2} \text{ ergs cm}^{-2} \text{ sec}^{-1}$  or 1% of maximum  $\Delta f$  ( $1-1030 \text{ \AA}$ ), whichever is larger, for resolution of intensity of fine structure having  $t_r \leq 10 \text{ sec}$ .

Wavelength Resolution: At best, one can estimate the radiation in the following wavelength groups:  $1-10 \text{ \AA}$ ,  $10-100 \text{ \AA}$  +  $910-1030 \text{ \AA}$ ,  $100-400 \text{ \AA}$  +  $800-910 \text{ \AA}$ , and  $400-800 \text{ \AA}$ .

Spatial Resolution: None.

Absolute Intensity Accuracy: typically  $\sim$  a factor of 4; i.e. the real flux should be within the range  $1/4$  x's to  $4$  x's the given value. This poor accuracy is a consequence of our inadequate knowledge of the spectrum of the  $1-1030 \text{ \AA}$  flare radiation, of the ionospheric electron loss rates along the paths of the SFD probing radiowaves, etc.

Absolute Timing Accuracy  $\approx \pm 2 \text{ sec}$ , for Boulder observations with  $\Delta f$  structure  $\geq 1 \text{ kHz}$  processed with 1 minute  $\geq 1.4$  inches of chart record.

Time Coverage  $\approx 45\%$ . SFD's are observed only during the daytime. Ionospheric storms and other ionospheric disturbances undoubtedly prohibit the observation of some small SFD's. (see below).

Data Storage: Two weeks of three channels of SFD data and one time code channel recorded on one 1800' reel of  $1/4$ " magnetic tape.

Data Processing: Standard audio spectrum analyzers used to obtain records of frequency deviation versus time.

Interfering Ionospheric Phenomena for Midlatitude SFD Observations:

Sporadic E - Causes anomalous propagation of the probing radio waves making the SFD observations temporarily insensitive to EUV flashes.

Traveling Ionospheric Disturbances - rarely occur at the time of an SFD.

Common Acoustic-Gravity Waves - always present, the main source of interference with small SFD's, minimized by using one-hop oblique propagation paths of 500-1500 km ground length.

Magnetic and Ionospheric Storms - For a day or more after some large solar flares, the ionosphere is disturbed with small fluctuations because of the ionospheric effects of particle radiation from the flare, or the SFD probing radiowaves may be reflected at an anomalously low height.

Short Wave Fadeouts - During some flares the  $0.5-8 \text{ \AA}$  x-ray enhancement is so large and consequently the D-region ionization and radiowave absorption are enhanced so much, that the SFD probing radiowave is lost in the radio noise and local interference.

Advantages of SFD's as Detectors of  $1-1030 \text{ \AA}$  Impulsive Flare Radiation: Inexpensive, high time resolution and accuracy, good relative intensity resolution, good time coverage, ground-based, easy maintenance, broadband, and convenient high-density data storage.

Disadvantages of SFD's as Radiation Detectors: No spatial resolution, poor wavelength resolution, poor absolute intensity accuracy, high value of minimum detectable flux enhancement, insensitive to non-impulsive radiation, tedious process for converting  $\Delta f$  to  $\Delta \lambda$ , and influenced by unknown time variations of the upper atmosphere and ionosphere.

Table 2. Rf,  $\phi f$  and R $\phi$  as a Function of Wavelength

Definitions:  $Rf = 100\% \frac{\Delta f_c}{\Delta f_o} \left| f_v = 5\text{MHz}; t = t_p \right.$   $\phi f = R_t R_\chi \frac{\Delta \phi_o(\lambda_1 - \lambda_2, t_\phi)}{\Delta f_o(f_v = 5\text{MHz}, t_p)}$  ergs cm<sup>-2</sup>

and  $R\phi = 100\% \frac{\Delta \phi_o(\lambda_i, t_\phi)}{\Delta \phi(1-1030\text{\AA}, t_\phi)} = 100\% \frac{\phi f(\lambda_i)}{\phi f(1-1030\text{\AA})}$

where:  $\Delta f_c$  is the frequency deviation (Hz) computed from the observed radiation enhancement  $\Delta \phi_o$ ,  $\Delta f_o$  is the observed frequency deviation,  $f_v$  is the equivalent vertical incidence frequency of the SFD probing frequency,  $t$  is time and  $t_p$  is the time of the peak of  $\Delta f_o$ ,  $R_t$  and  $R_\chi$  are correction factors to account for the rise time of the SFD relative to the electron loss time constant and for the solar zenith angle dependence, respectively,  $\lambda_1 - \lambda_2$  is the wavelength range of  $\Delta \phi_o$  or  $\lambda_i$  is the wavelength of a line, and  $t_\phi$  is the time of the peak of  $\Delta \phi(1-1030\text{\AA})$ .

Radiation Wavelength $\text{\AA}$	Ion	Rf, %	$\phi f$ , ergs cm <sup>-2</sup>	R $\phi$ , %	Number of Events Studied	Reference Number	Comments
<1 (>10 keV)		0	$8.0 \times 10^{-6}$	-0.001	13t, 56s*	3	
0.5-3		0.08	$7.0 \times 10^{-5}$	0.09	4t*	1	$\Delta \phi(1-8\text{\AA})$ decays slower than $\Delta \phi(1-1030\text{\AA}, t)$ .
1-8		2.4	$6.3 \times 10^{-3}$	7.8	9t	1	$\Delta \phi(8-20\text{\AA})$ rises, peaks, and decays slower than $\Delta \phi(1-1030\text{\AA}, t)$ .
8-20		<2.1	$<4.6 \times 10^{-3}$	<5.8	12t	1	Good time dependence agreement with $\Delta \phi(1-1030\text{\AA}, t)$ .
303.8	He II	5.9	$5.2 \times 10^{-3}$	6.6	8t, 1s	1, 2	
335.3	Fe XVI	<0.6	$<4.0 \times 10^{-4}$	0.5	1t	1, 2	
368.1	Mg IX	0.4	$2.9 \times 10^{-4}$	0.4	1t, 1s	1, 2	Appears to be slower than $\Delta \phi(1-1030\text{\AA})$ .
465.2	Ne VII	0.3	$2.0 \times 10^{-3}$	0.2	1s	1, 2	
554	Group O IV	4.0	$2.8 \times 10^{-3}$	3.4	1s	1, 2	
584.3	He I	0.6	$3.7 \times 10^{-4}$	0.5	1s	1, 2	
629.7	O V	1.2	$7.8 \times 10^{-4}$	1.0	4t, 1s	1, 2	Good time dependence agreement with $\Delta \phi(1-1030\text{\AA}, t)$ .
760	Group O V	0.6	$3.6 \times 10^{-4}$	0.5	1s	1, 2	
765.1	N IV	0.8	$4.7 \times 10^{-4}$	0.6	1s	1, 2	
790	Group O IV	2.3	$1.6 \times 10^{-3}$	2.0	1s	1, 2	
834	Group O II&III	2.2	$2.1 \times 10^{-3}$	2.7	1s	1, 2	
680-911	H Cont	8.1	$9.3 \times 10^{-3}$	12.	1s	1, 2	
949.7	H I Ly $\delta$	0.2	$1.7 \times 10^{-4}$	0.2	1s	1, 2	Good time dependence agreement with $\Delta \phi(1-1030\text{\AA}, t)$ .
972.5	H I Ly $\gamma$	0	$3.3 \times 10^{-4}$	0.4	1t, 1s	1, 2	
977.0	C III	6.2	$6.4 \times 10^{-3}$	8.0	2t, 1s	1, 2	Good time dependence agreement with $\Delta \phi(1-1030\text{\AA}, t)$ .
990	Group N III	1.4	$2.0 \times 10^{-3}$	2.5	1s	1, 2	
1025.7	H I Ly $\beta$	2.3	$1.3 \times 10^{-3}$	1.6	1s	1, 2	
1031.9	O VI	0.1	$3.2 \times 10^{-3}$	4.1	1s	1, 2	
1085	Group N II	0	$1.1 \times 10^{-3}$	1.4	1s	1, 2	**
1175	Group C III	0	$1.7 \times 10^{-2}$	21.	1s	1, 2	Good time dependence agreement with $\Delta \phi(1-1030\text{\AA}, t)$ .
1206.5	Si III	0	$1.4 \times 10^{-2}$	17.	1s	1, 2	Good time dependence agreement with $\Delta \phi(1-1030\text{\AA}, t)$ .
1215.7	HI Ly $\alpha$	<0.1	$\sim 8. \times 10^{-2}$	$\sim 100.$	2, 2t, 1s	1, 2	Good time dependence agreement with $\Delta \phi(1-1030\text{\AA}, t)$ .
1080-1225		0	$1.4 \times 10^{-4}$	17.	1t	4	Good time dependence agreement with $\Delta \phi(1-1030\text{\AA}, t)$ .
1238.8	NV	0	$6.1 \times 10^{-4}$	0.8	1s	1, 2	Good time dependence agreement with $\Delta \phi(1-1030\text{\AA}, t)$ .
1225-1350		0	$7.3 \times 10^{-3}$	9.1	1t	4	
6563	H $\alpha$	0	$3.5 \times 10^{-3}$	<4.3	3t	5	Good time dependence agreement with $\Delta \phi(1-1030\text{\AA})$ to within the time resolution of white light photographs.
3500-6500	White Light	0		$\sim 100.$	4t	6	
3-10 cm	radio	0	$2.4 \times 10^{-8}$	$3 \times 10^{-5}$	43t		

All results based on only one or two events should be considered as unverified rough estimates only. Rf and  $\phi f$  are based on SFD observations at  $f_v = 5\text{MHz}$  and should not be applied when  $f_v \neq 5\text{MHz}$ . If Rf were based on  $f_v = 2\text{MHz}$ , then  $Rf \approx 100\%$  for 1-10 $\text{\AA}$  and  $\approx 0$  for  $\lambda > 10\text{\AA}$ . The reference  $f_v = 5\text{MHz}$  was chosen because it is about the lowest value of  $f_v$  for Boulder SFD observations for which  $\Delta f_o$  is not highly sensitive to the preflare electron concentration height-profile.

\*t, with high time resolution; s, low time resolution.

\*\*In view of results in ref. (4), there "Ly $\alpha$ " observations may have been influenced by a continuum enhancement.

References: 1. Donnelly (1969a, b) 2.  $\Delta \phi_o(\lambda_i)$ , Hall and Hinteregger (1969); 3. Kane and Donnelly (1970); 4.  $\Delta \phi_o(\lambda_1 - \lambda_2)$ , McClinton (1968) and Grebenkemper (1969); 5.  $\Delta \phi_o(\text{H}\alpha)$ , Thomas (1970); 6. McIntosh and Donnelly (1970).

The nonflare EUV "continuum" (other than recombination continua) observed by satellites is not a continuum in the true sense in that it may consist of small unresolved lines plus light scattered in the spectrometer from strong lines at other wavelengths, as well as any true continuum emission. Therefore, even if a small "continuum" enhancement were observed, it would be difficult to determine whether it were a true continuum. The results in table 2 for wavelengths outside of the 1-1030 Å range will be discussed in Section 5. Since almost all of an SFD is produced by the 10-1030 Å flux enhancement and very little by 1-10 Å radiation, and since 1-10 Å radiation is generally much slower than the radiations mainly responsible for SFD's, we will frequently refer to SFD's in the rest of this report as being caused by, or providing information about, the impulsive 10-1030 Å flux enhancement of flares.

#### 4. STATISTICAL CHARACTERISTICS OF SUDDEN FREQUENCY DEVIATIONS AND EUV FLASHES

SFD observations were made in Boulder under the direction of Dr. K. Davies for about 10 years, which amounts to nearly  $4 \times 10^4$  hours of daylight observation. About  $2 \times 10^3$  SFD's were detected, scaled and tabulated. Preliminary lists of Boulder SFD's have been published in NOAA's Solar Geophysical Data since 1963. Revised lists have been published by Agy et al. (1965) for October 1960 through December 1962, by Baker et al. (1968) for 1963 through 1967, and in Appendix B of this report for 1968 through June, 1970, when Boulder SFD observations were terminated. Tabulated information for all SFD's observed in Boulder is available either in computer listings or punched card form from World Data Center A, Upper Atmosphere Geophysics, NOAA, Boulder, Colorado, 80302. Table 3 documents the main transmission frequencies and propagation paths used in the Boulder SFD observations.

Previous studies of the characteristics of SFD's were made by Chan and Villard (1963), based on about one year of SFD observations, and by Agy et al. (1965), based on about two years of observations. The results of these studies, include the following:

- (1) Diurnal Dependence: The number of SFD's observed and the percentage of H $\alpha$  flares accompanied by SFD's varied with the hour of day because of the solar zenith angle dependence of SFD's.
- (2) Seasonal Dependence: The percentage of flares during SFD observing periods that were accompanied by SFD's varied from month to month but exhibited no distinct seasonal dependence. (a seasonal dependence is presented in the next section).
- (3) Rise Time: The start-to-maximum times of SFD's were most commonly one to two min. and the average value increases slightly with increasing importance of the associated H $\alpha$  flare.
- (4) Duration: The start-to-end times for SFD's ranged from 1 to 15 min. with the most common duration being from 2 to 5 min. The SFD duration tends to increase with the importance classification of the H $\alpha$  flare.

##### 4.1 Time of Occurrence

Figure 3 shows the monthly rate of occurrence of SFD's observed at Boulder for the past ten years. The solar minimum in 1964 is quite evident, but probably the most striking features of this figure are the large spikes caused by certain active

Table 3. Transmissions Used in Boulder SFD Observations

Call Letters	Transmitter		Frequency		Dates of SFD Observations	
	Location	D(km)	MHz	From	To	
WWV	Greenbelt, Md	2420	20	09/01/60 09/08/61	06/02/61 01/17/62	
WWV	" "	"	15	12/21/60 01/17/62	01/10/61 09/19/66	
WWV	" "	"	10	12/15/60 01/11/61	12/20/60 09/19/66	
WWV	" "	"	5	02/09/63	07/15/63	
KKE42	Sunset, Colo.	25	4	07/30/61	05/23/69	
KKE42	" "	"	5.054	08/04/61	02/17/67	
KKE42	" "	"	5.1	02/17/67	05/23/69	
KKE42	" "	"	3.3	06/04/65	04/15/69	
KKE42	" "	"	2	09/27/67	05/23/69	
KC2xBI	Akron, Colo.	170	5.1	11/24/65	01/05/66	
WWI	Havana, Ill.	1290	9.9825	04/13/66	01/04/67	
WWI	" "	"	9.9	01/04/67	01/08/69	
WWI	" "	"	8.9	08/03/66	06/08/70	
WWI	" "	"	11.1	08/08/66	05/12/70	
WWI	" "	"	12.1	09/19/66	01/08/69	
WWI	" "	"	13	09/19/66	07/01/70	

D = Approximate ground range from the transmitter to receivers located near Boulder, Colo.

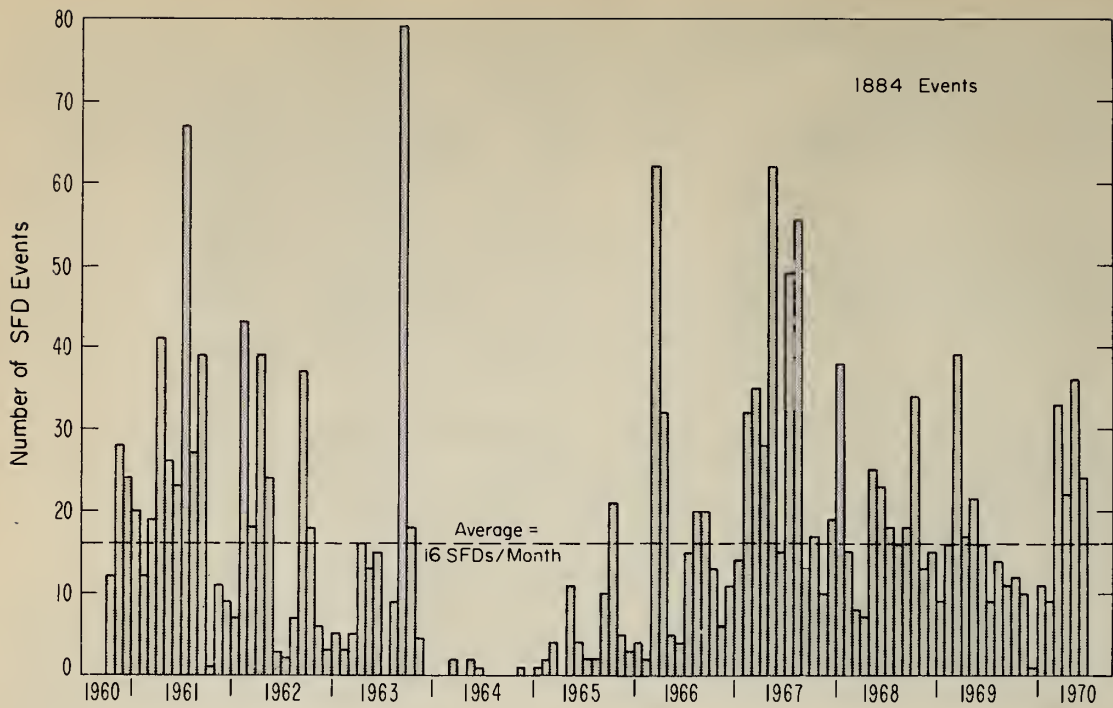


Figure 3. Monthly rate of occurrence of SFD's at Boulder from October, 1960 through June, 1970.

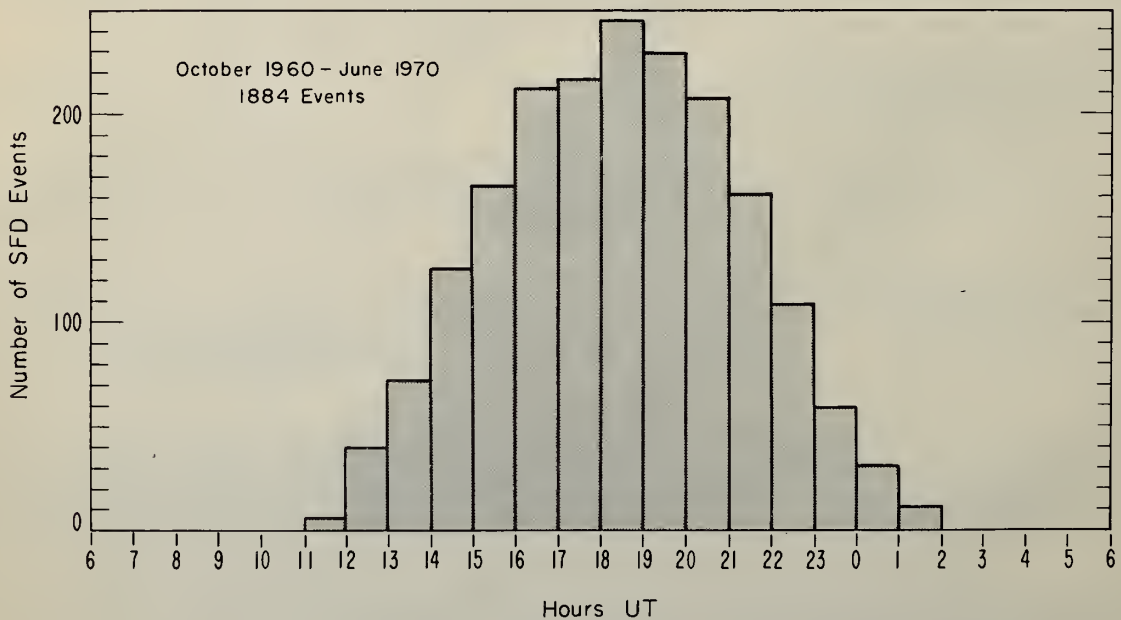


Figure 4. Diurnal dependence of Boulder SFD's.

regions which were prolific producers of H $\alpha$  flares and EUV bursts, e.g. in March 1966. Figure 4 shows the number of SFD's as a function of hour, which agrees in shape with the results of Chan and Villard (1963). This diurnal dependence is caused mainly by the diurnal variation of solar zenith angle; however, a precise analytic formula for the solar zenith angle dependence of SFD's has not yet been developed. (see appendix A).

The occurrence of SFD's as a function of month of the year is shown at the top of figure 5. Note the low values in November, December, and January. The dip at winter solstice is probably caused by the large values of solar zenith angle and low number of hours of daylight. The second graph in figure 5 gives the monthly average number of events per hour of observation for solar zenith angles  $\leq 80^\circ$ . The winter solstice dip is only partially removed, which shows that the solar zenith angle effect is more complicated than just a dependence on hours of daylight. Note the peaks in occurrence near vernal and autumnal equinoxes. These peaks are probably the side effects of the main unexpected feature of this figure, namely the dip at summer solstice. It appears also in the percentage of H $\alpha$  flares (during Boulder SFD observations when the solar zenith angle  $\leq 80^\circ$ ) that were accompanied by SFD's.

The original SFD records were searched and it was found that Sporadic E (Es), a thin but dense layer of ionization that rather sporadically forms at heights near 110 km, severely influenced the SFD observations, particularly in June, and in some years also in May or July. Sporadic E is known to occur at midlatitudes primarily in the daytime in June (see fig. 3.30 of Davies, 1965). The effect on SFD's of the type of Es involved, i.e., blanketing Es, is that probing radio waves are reflected from heights at about 110 km and are cut off from probing the upper-E and F regions. At such times, SFD observations are sensitive mainly to 1-10 Å soft X-rays, which usually do not produce much frequency deviation; they are insensitive to the 10-1030 Å impulsive radiations that normally produce SFD's. Hence, Es acts like a shutter to SFD observations. When the shutter is open, normal SFD's are observed; hence, their average frequency deviation exhibits no peculiarity. When Es occurs or the shutter is closed, SFD events go undetected; therefore, the effective observing period is reduced near the summer solstice. The presence of Es effects is readily evident in frequency deviation measurements processed with spectrum analyzers. Future SFD observations should routinely list periods with Es. Note that the above diurnal and seasonal dependences of SFD's are related to variations in the sensitivity of SFD's to EUV flashes and not to diurnal or seasonal dependences in the solar EUV flashes.

#### 4.2 Intensity

Figures 6 and 7 show the distribution of Boulder SFD's with respect to peak frequency deviation. Note that the intensity intervals are uniform on a log scale, i.e., each interval is a constant multiple of the adjacent interval. In figure 6, each interval includes the number at the upper end of its range and excludes that at the lower end while the converse is true for figure 7, but the results appear to be independent of this difference in definition of intervals. Figure 7 shows similar results by Strauss et al. (1969) using just SFD's reported on 11.1 MHz and confined to observing periods when the solar zenith angle was not too large.

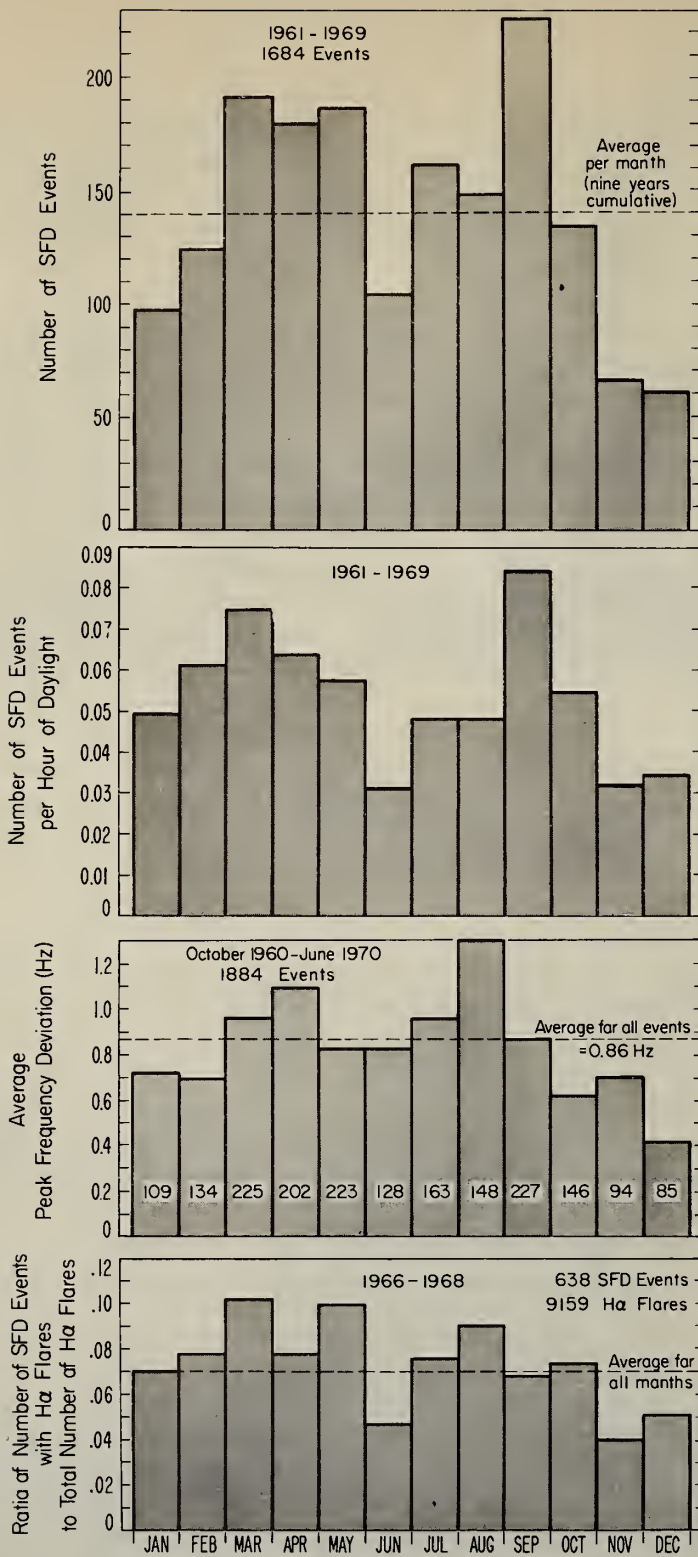


Figure 5. Seasonal dependence of Boulder SFD's.

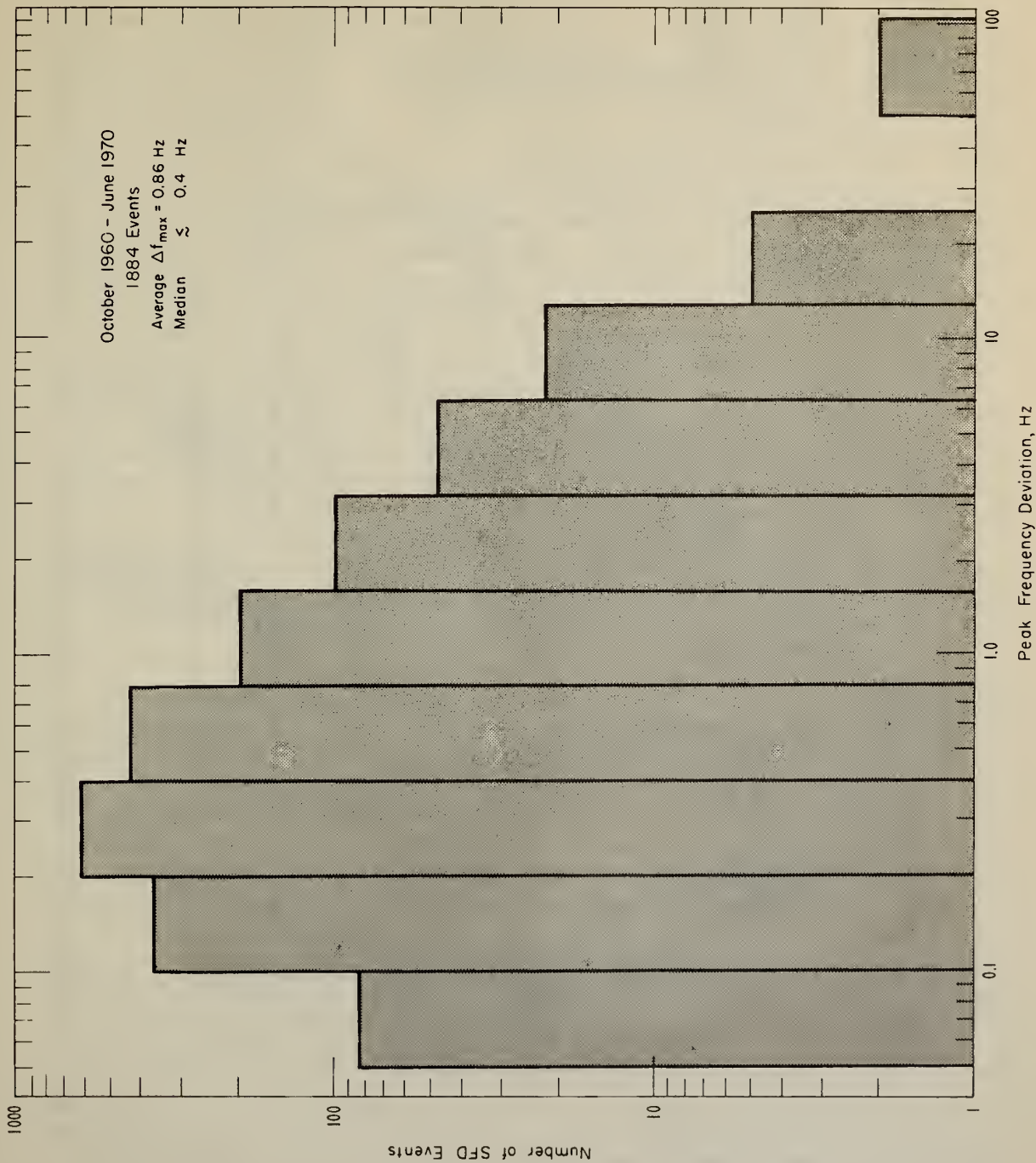


Figure 6. Intensity distribution of all Boulder SFD's.

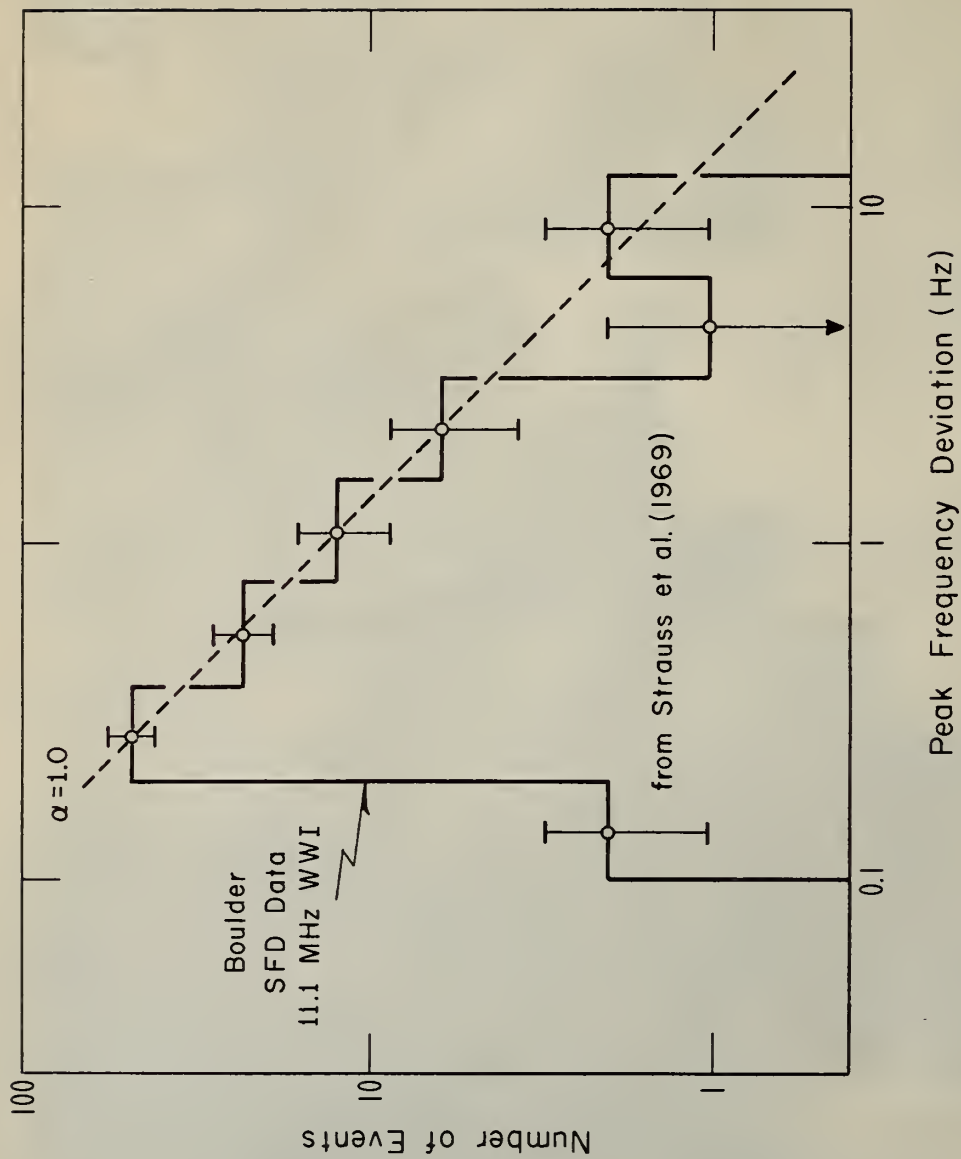


Figure 7. Intensity distribution of selected Boulder SFD's.

They found that above 0.2 Hz the distribution was well fit by a straight line of near unity negative slope; hence, considering the logarithmic choice of intervals, they found that the distribution of SFD's by peak frequency deviation exhibited approximately an inverse squared dependence on the peak frequency deviation. The results in figure 6 for all events shows a similar dependence, except for those below about 0.2 Hz, where some SFD's are probably not detected because of background noise from nonflare ionospheric variations. The relationship also appears to break down above 10 Hz, but this may be the consequence of too few events at such large intensities for a 10 year set of data to sufficiently describe the distribution there. The data used in figure 6 are much less homogeneous than those used in figure 7 (e.g., see table 3), so it is somewhat surprising that they are so similar. Although the peak 10-1030 Å flux enhancement depends on the start-to-maximum time of the SFD as well as on the peak frequency deviation (see fig. 2) the results in figures 6 and 7 suggest nevertheless, that the number of EUV flashes have a distribution roughly inversely proportional to the square of the intensity of the 10-1030 Å flux enhancement ( $\text{ergs cm}^{-2}\text{sec}^{-1}$  at 1AU).

Note that in figure 5, the average peak frequency deviation decreases near the winter solstice, believed to be the consequence of the relatively large solar zenith angles. The average peak frequency deviation in June is not unusually low, despite the summer solstice dip in the other data in figure 5, because the Es effect simply reduces the SFD observing period per day without affecting those SFD's that are observed between periods of Es.

The intensity of EUV emission from flares depends upon the location of the flare on the sun; evidence supporting this result and the details of the dependence are presented in sections 5.1 and 5.6.5. Only a small percent of Boulder SFD's, mostly large SFD's, have been analyzed in detail to estimate the 10-1030 Å flux enhancement,  $\Delta\phi(10-1030 \text{ \AA})$ . The peak flux estimates for the analyzed events are given in table 4.

#### 4.3 Rise Time

Figure 8 shows the distribution of start-to-maximum times of SFD's. No SFD's have been observed at Boulder with start-to-maximum times less than 10 sec. The individual spikes recorded in some SFD's during the rise to maximum frequency deviation may have rise times less than 10 sec, but in ten years of observations, no spike has been observed with a rise time of less than 2 sec. (In order to preserve a time resolution of 1 sec in processing the SFD data, the spikes referred to above are those with peak frequency deviations of greater than 0.8 Hz). These lower limits for rise times are also real lower limits for flashes of 10-1030 Å solar radiation.

The maximum in the distribution of start-to-maximum times of SFD's in figure 8 is believed to be a consequence of a maximum in the distribution of start-to-maximum times of the 10-1030 Å flux enhancement; however, this result needs further confirmation by satellite EUV observations. The sensitivity of SFD's to the time-dependence of the 10-1030 Å flux enhancement discussed in section 2 partially causes the peak observed near one minute; but, considering the sharpness of almost all SFD peaks and that the filtering effect should produce blunt peaks, we believe that this peak near start-to-maximum times of one-minute also occurs in the start-to-maximum time distribution of 10-1030 Å bursts. Nevertheless, because of the uncertainty of the SFD filtering effect, independent measurements will be necessary for confirmation.

Table 4. Estimates of Peak 10-1030Å Flux Enhancements

(a) Complete List of Large Events Observed at Boulder,  
 $\Delta\phi_{\max}(10-1030\text{\AA}) \geq 2.0 \text{ ergs cm}^{-2}\text{sec}^{-1}$  at 1 AU.

Date	Time UT		*1	Accuracy	Date	Time UT		*1	Accuracy
	Start	Peak				Start	Peak		
11/12/60	1324	1327.5	11	A	08/28/66	1523.4	1527.2	9	B
01/30/61	2002	2004	2	A	02/27/67	1640.0	1643.8	3	B
09/28/61	2212	2217	3	A	05/21/67	1920.8	1925.4	3	B
03/01/62	1636	1639.4	7	A	05/23/67	1835.5	1841	> 8	B
04/19/62	1935.3	1935.9	5	B	05/23/67	1936.4	1942	3	B
04/20/62	1958	2000.7	2	B	07/08/68	1707.3	1710	2	B
04/27/62	1410	1412.5	3	A	08/08/68	1814.9	1816.4	5	B
04/15/63	1614	1617	3	A	03/12/69	1738.6	1741.3	4	B
08/18/63	1757	1758	3	A	04/21/69	2006.1	2008.7	3	B
09/16/63	1303	1304	6	A	01/28/70	1916.9	1918.7	2	A
09/20/63	2356	2359	4	A	03/01/70	1530.1	1531.0	2	A
03/30/66	1248	1252	4	A	03/01/70	2001.8	2005.4	3	A
07/07/66	0025.7	0037- 0045	5	B					

(b) Partial List of Medium Sized Events Observed at Boulder,  
 $0.5 \leq \Delta\phi_{\max}(10-1030\text{\AA}) < 2.0 \text{ ergs cm}^{-2}\text{sec}^{-1}$  at 1 AU.

Date	Time UT		*1	Accuracy	Date	Time UT		*1	Accuracy
	Start	Peak				Start	Peak		
01/31/61	1511	1514	1.5	A	08/01/67	1727.5	1732	1.7	A
06/15/61	1635	1641	1.1	A	08/18/67	2120.0	2135.5	0.5	B
09/04/61	1430	1432	1.5	A	08/29/67	1329.7	1332	1.5	A
09/04/61	1513	1513.5	0.6	A	08/29/67	1941.8	1944.9	0.5	B
09/04/61	1911	1915	0.7	A	01/11/68	1659.2	1702	0.9	A
09/27/61	1952	1954	0.8	A	01/29/68	1538.2	1539	0.7	B
03/13/62	1448.5	1450	1.4	A	02/01/68	1801.7	1802.7	0.7	B
10/13/62	1805.2	1805.5	0.5	A	02/01/68	1917.1	1919.2	0.8	A
04/19/63	1754	1758	1.0	A	02/14/68	1534.2	1535.4	0.7	A
09/15/63	2017	2018.5	0.7	A	03/21/68	1913.3	1915	0.8	A
09/17/63	1927	1928	0.7	A	03/25/68	1459.2	1505.0	1.1	A
09/19/63	2257	2300	1.3	A	09/29/68	1617.1	1620	1.8	B
05/20/65	2320	2321	0.9	A	11/01/68	2002.7	2004.5	1.2	B
06/05/65	1808	1810	0.7	A	01/17/69	1704.1	1704.8	1.8	A
10/02/65	1413	1414	0.5	A	02/09/69	1723	1725	1.0	A
03/20/66	1759	1802.6	0.6	B	02/27/69	1403	1408	0.8	B
03/31/66	1856	1905.0	0.5	B	03/01/69	2139.8	2148	1.2	A
04/12/66	1718	1719	0.6	B	03/27/69	1323	1341	1.7	A
06/25/66	1527	1534.4	1.1	B	05/17/69	1922.4	1934	0.5	A
09/18/66	1453	1456	0.6	B	06/06/69	1604.1	1606.4	1.5	A
10/13/66	1334	1344	1.1	B	08/11/69	1215.4	1221	1.2	A
10/24/66	1502	1503	0.7	A	10/08/69	1630.2	1630.8	0.9	A
12/09/66	1756	1800	0.9	B	10/24/69	2111.8	2114	0.7	A
03/04/67	1715.6	1716.2	1.1	B	11/20/69	1619.6	1620.9	1.0	A
03/26/67	1604.6	1606.7	0.7	B	11/22/69	2123.6	2124.5	1.4	A
05/21/67	1534.3	1539.8	1.0	B	03/26/70	1726.6	1728.3	0.6	A
07/24/67	0033.3	0035	0.6	B	03/26/70	2004.3	2007.8	0.5	A
07/26/67	2329.3	2331	0.6	A	05/09/70	1559.8	1600.6	0.9	A

Accuracy: A - Absolute flux-enhancement accurate to within a factor of 10, usually analyzed by methods 4 or 5 discussed in the Appendix; B - Absolute flux enhancement accurate to within a factor of 4, usually analyzed by methods 3, 2 or 1 in the Appendix.

\*1  $\Delta\phi_{\max}(10-1030\text{\AA}) \text{ ergs cm}^{-2}\text{sec}^{-1}$  at 1 AU.

January 1967 - June 1970

884 Events

Average Start-to-Maximum Time  $\approx$  2.1 min.  
Median  $\approx$  1.4 min.  
Minimum  $\approx$  10 sec.

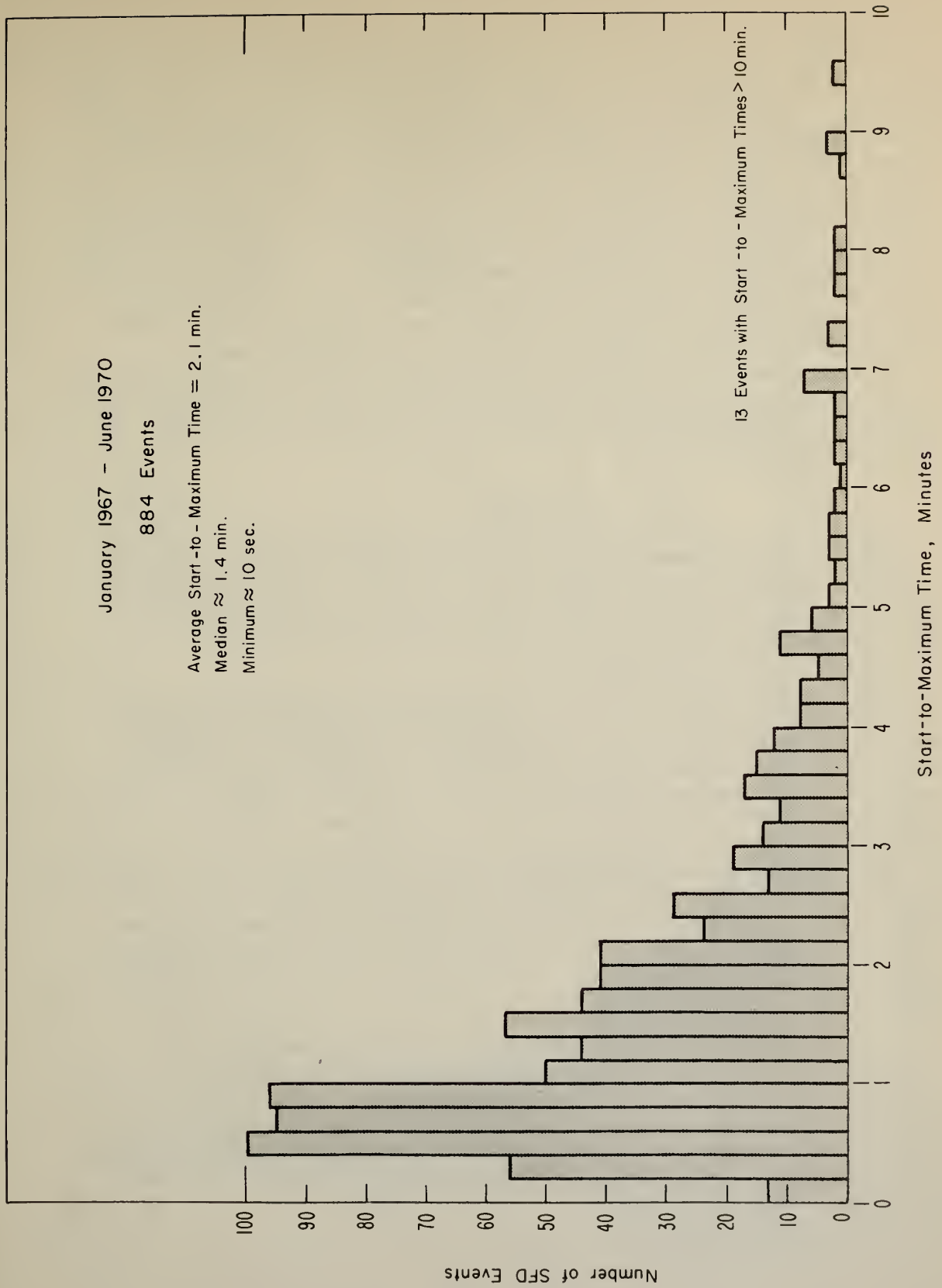


Figure 8. Rise-time distribution of Boulder SFD's.

In general, the peak time of the radiation flash is greater than or equal to the SFD peak time and less than or equal to the time when the frequency deviation equals zero at the onset of the negative decay stage of the SFD (Chan and Villard, 1963). The peak times are equal only if the main SFD peak is sharp and the frequency deviation quickly drops to negative values. This is usually the case, but extensive tabular information on the time from the SFD peak to the start of the SFD negative decay stage is presently not available. The main zero-crossing time would be quite helpful in studying the start-to-maximum time distribution of 10-1030 Å flux enhancements; unfortunately at the end of ten years of observations, we now realize that this time should have been scaled in the routine data processing. Future scaling of SFD measurements should include scaling the main zero crossing time.

No clear dependence of the start-to-maximum time of SFD's on season or time of day was found. The start-to-maximum time statistically tends to increase with increasing peak frequency deviation, but then this is generally true of any type of solar flare radiation.

#### 4.4 Duration

Figure 9 shows the distribution of start-to-end times of SFD's. No clear diurnal or seasonal dependence of SFD duration was found. The end time of an SFD is when the frequency deviation appears to return to the preflare level; usually an indistinct time because the frequency deviation returns asymptotically to the preflare level. Start-to-end times of an SFD undoubtedly underestimate the end times of the 10-1030 Å flux enhancement.

A much more meaningful characteristic time is the decay time constant of the 10-1030 Å radiation. However, the decay time constant is difficult to determine from the SFD data, since the time constant depends critically on the accuracy of frequency deviation recorded during the decay phase of an SFD event. In addition the 10-1030 Å flux estimate during the SFD decay stage is very sensitive to errors in our estimate of the electron loss rates in the ionosphere. Furthermore, the slow radiations, like soft X-rays, are increasing during this time, while the impulsive EUV radiations that are mainly responsible for SFD's are decreasing. Hence, SFD's provide little useful information about the duration or decay times of solar flare radiations. At best, the fact that the minimum SFD duration is about one minute sets a one-min. minimum for the duration of 10-1030 Å bursts. Also, since the duration for half the SFD events exceeds 5 min., the duration of 10-1030 Å flares usually exceeds 5 min.

#### 4.5 Fine Time-Structure, Complexity and Quasi-Periodicity

Most SFD's exhibit some fine time-structure; but according to Chan and Villard (1963) only about 18% of SFD's have two or more major peaks. However, most large SFD's ( $\Delta f_{\max} \geq 5\text{Hz}$ ) have a significant fine structure. Recent studies have suggested a quasi-periodicity in the impulsive emission of flares (Parks and Winckler, 1969a,b; Janssens and White, 1970). Because of the physical significance of such a quasi-periodicity, a detailed study of the periodicity of structure in SFD's was made and the results are reported below.

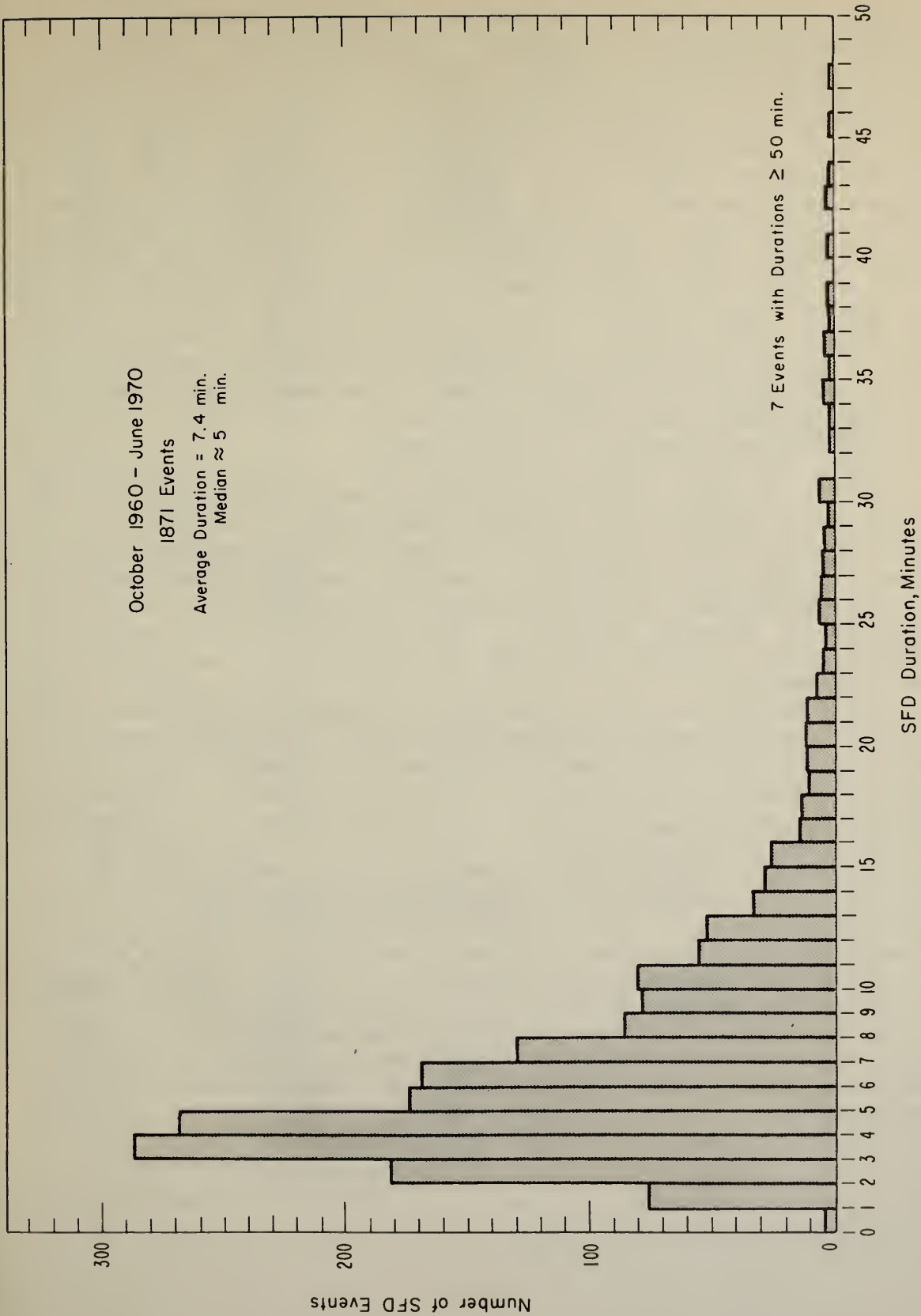


Figure 9. Duration distribution of Boulder SFD's.

Structured SFD's were selected for study using the following criteria: (a) the peak frequency deviation  $\Delta f_{\max} \geq 0.5\text{Hz}$ , (b) the number of major peaks  $\geq 4$  and (c) the  $\Delta f(t)$  trace was well defined, i.e. free of smearing, fuzziness or spread. Criteria (a) and (c) were necessary to be able to accurately scale  $\Delta f(t)$  and compute  $\Delta\phi(10-1030 \text{ \AA}, t)$ . The "major peaks" in criterion (b) means either the main peak ( $\Delta f_{\max}$ ) or a peak with  $\Delta f_{\text{peak}} \geq 1/3 \Delta f_{\max}$  and the adjacent minimums in  $\Delta f$  being  $\leq 2/3 \Delta f_{\text{peak}}$ . Boulder SFD's from March 1966 through June 1969 were systematically searched and then several older events were added to the study. The first criterion (a) eliminated about three-fifths of all SFD's from the study. Criterion (b) eliminated about four-fifths of the remaining events. Less than 7% of all SFD's satisfied all the criteria which means that relatively few SFD's exhibit pronounced complexity, much less quasi-periodicity.

The list of complex events studied with information on the "periodicity" of their structure is given in table 5. For these events, the 10-1030  $\text{\AA}$  flux as a function of time was computed, plotted, and processed by a Fast Fourier Transform subroutine. The spectrum was plotted and examined for quasi-periodic peaks. Ten events devoid of fine structure were similarly spectrum analyzed to examine the noise in Fast Fourier Transform spectra for this type of data.

Figure 10 shows the best example of a quasi-periodic SFD. In this case, the fine structure of the SFD is still quite apparent in the computed  $\Delta\phi(10-1030 \text{ \AA}, t)$  flux. The ruled lines below the  $\Delta\phi(10-1030 \text{ \AA}, t)$  curve in figure 10 point out sequences of peaks that are quasi-periodic, but not uniformly spaced. Figure 11 shows the spectrum of the structure for the same event. Several of the spectrum peaks correspond to the same frequencies for which the rulings are shown in figure 10, namely frequencies  $f_b$ ,  $f_c$ ,  $f_d$  and  $f_e$ . Note that  $f_c \approx 2f_b$ ,  $f_d \approx 3f_b$  and  $f_e \approx 2f_a$ . Also the spectrum exhibits a tendency towards peaks at odd harmonics of  $f_a$  and minimums at even harmonics of  $f_a$ .

Figure 12 shows the distribution of major periods of the EUV fine-structure. There is a cut-off in structure for periods less than 5 sec. Most events have their main periodicity in the 10-30 sec range. Some of the events in table 5 were not periodic. For most of the events, the fine-structure in  $\Delta\phi(10-1030 \text{ \AA}, t)$  was relatively small compared to  $\Delta\phi_{\max}(10-1030 \text{ \AA})$ , which is denoted by comment "A" in table 5; hence, events with strong quasi-periodicity, like that shown in figure 10, are very rare. Consequently, if there is a physical process in the flare region causing the periodic structure; it probably does not play a major role in most flares.

Two classes of processes may be involved in producing the quasi-periodic fine structure: (1) fixed location emission regions that oscillate in intensity as a consequence of either magnetohydrodynamic waves in the flare region or bunches of energetic particles mirroring back and forth along magnetic tubes or (2) several emission cores, spatially separated, that occur at different times during the flare in a time sequence, where each core produces one peak but the set of peaks occur nearly uniformly spaced in time, either accidentally or as a consequence of a spatial structure in the flare region.

The statistical properties of SFD's are summarized in table 6.

Table 5. SFD's with Complex Time Structure

Date	Approximate SFD Peak Time UT	Periods of Fine Structure sec	Comments
11/12/60	1328	37, 118, 67, 46, 22	A, C, D
09/28/61	2217	37, 21	A, C
03/01/62	1639	67, 25	A
04/20/62	2001	20	A
05/01/62	1917	50, 21	A
03/20/66	1858	30	A, B
03/20/66	2002	11	A
03/21/66	2027	14	A
03/30/66	1250	32	A
03/31/66	1902	35	A, B
04/12/66	1718	--	B
07/07/66	0027	15, 11	A
08/28/66	1527	36, 25	A, D
09/18/66	1456	28	A
09/20/66	1712	23, 35, 70, 122	C, D
02/24/67	1905	85, 30	A, D
02/27/67	1644	17, 20	A, D
03/22/67	0031	22	A, B
03/27/67	2112	14, 7	C
03/28/67	1738	9, 12	D
04/11/67	2110	14, 17	
05/20/67	2004	--	B
05/21/67	1539	31	A
05/21/67	1924	6, 11, 39, 20, 73	A
05/23/67	1838	43, 15, 21, 9	A, D
05/23/67	1938	--	A, B
05/03/68	2128	17, 27	
07/08/68	1710	21, 11, 43	A, C, D
07/09/68	1812	28, 130, 64	C, D
08/08/68	1816	17, 11	
08/21/68	1841	64, 29, 120	A, C, D
09/29/68	1619	17, 8, 32	A, C, D
12/29/68	1922	17	A, B
02/09/69	1725	8, 5	
02/27/69	1407	14	
03/01/69	2141	34, 100	A
03/12/69	1740	--	B
03/12/69	2008	104	
03/20/69	1632	60, 21	A
03/20/69	2149	--	B
03/27/69	1330	28	A
03/29/69	2001	9, 18	C
04/21/69	200.	--	A
05/02/69	1749	10, 18, 76	D
05/22/69	1901	27	A
05/22/69	1935	15, 33	A
05/29/69	1942	20	
06/11/69	1621	38, 24, 73, 19	C, D, > 10 major peaks.

Lettered Comments: A - Fine structure strong in SFD but relatively weak in  $\Delta\phi(10-1030\text{\AA}, t)$  because of a large slow enhancement in  $\Delta\phi(10-1030\text{\AA})$ . B - Strong fine structure in SFD but most of it not quasi-periodically spaced. C - Nearly harmonic relationship among some of the major periods of fine structure. D - Much quasi-periodic fine time-structure in SFD.

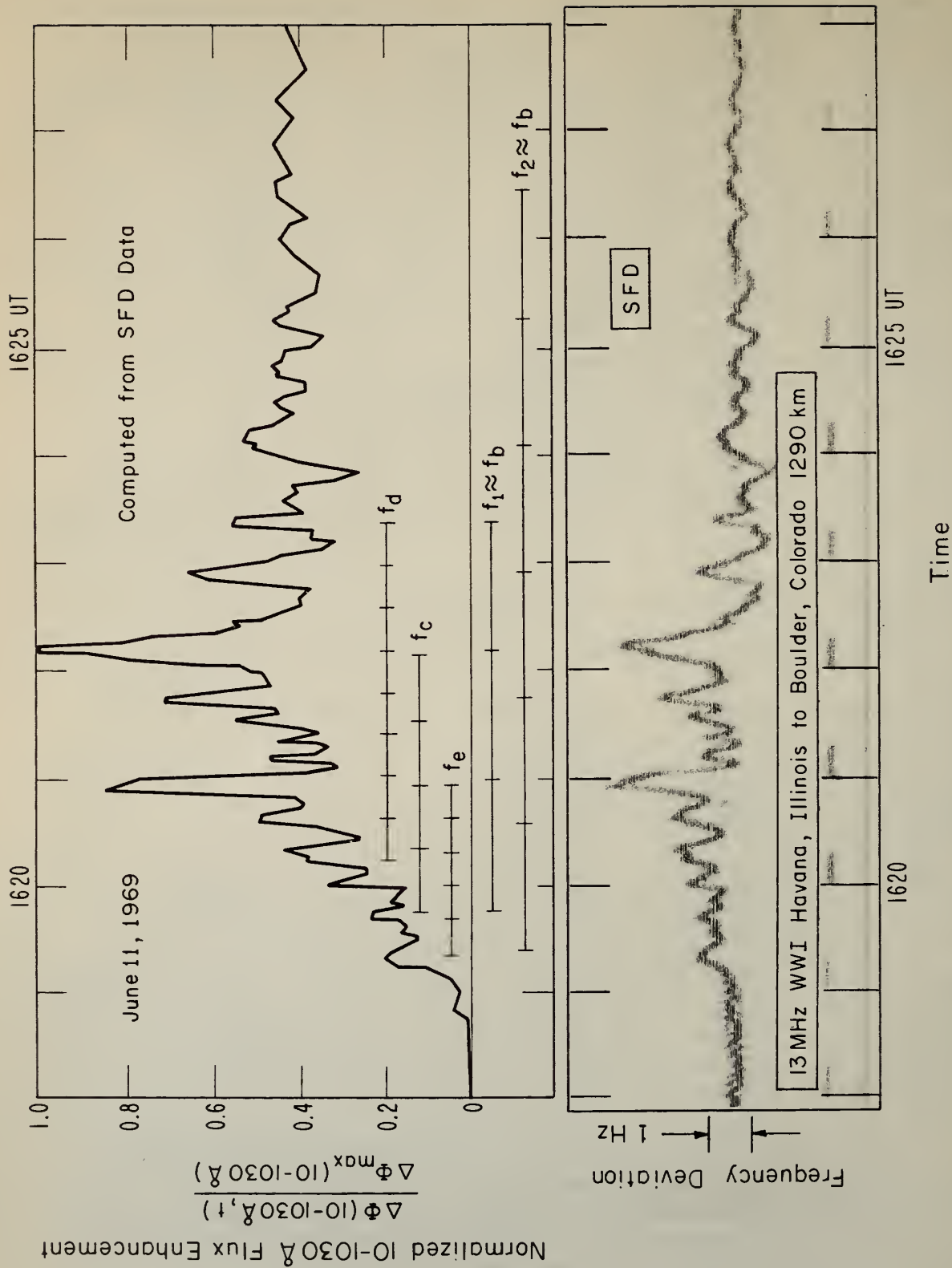


Figure 10. An EUV flare with quasi-periodic fine structure.

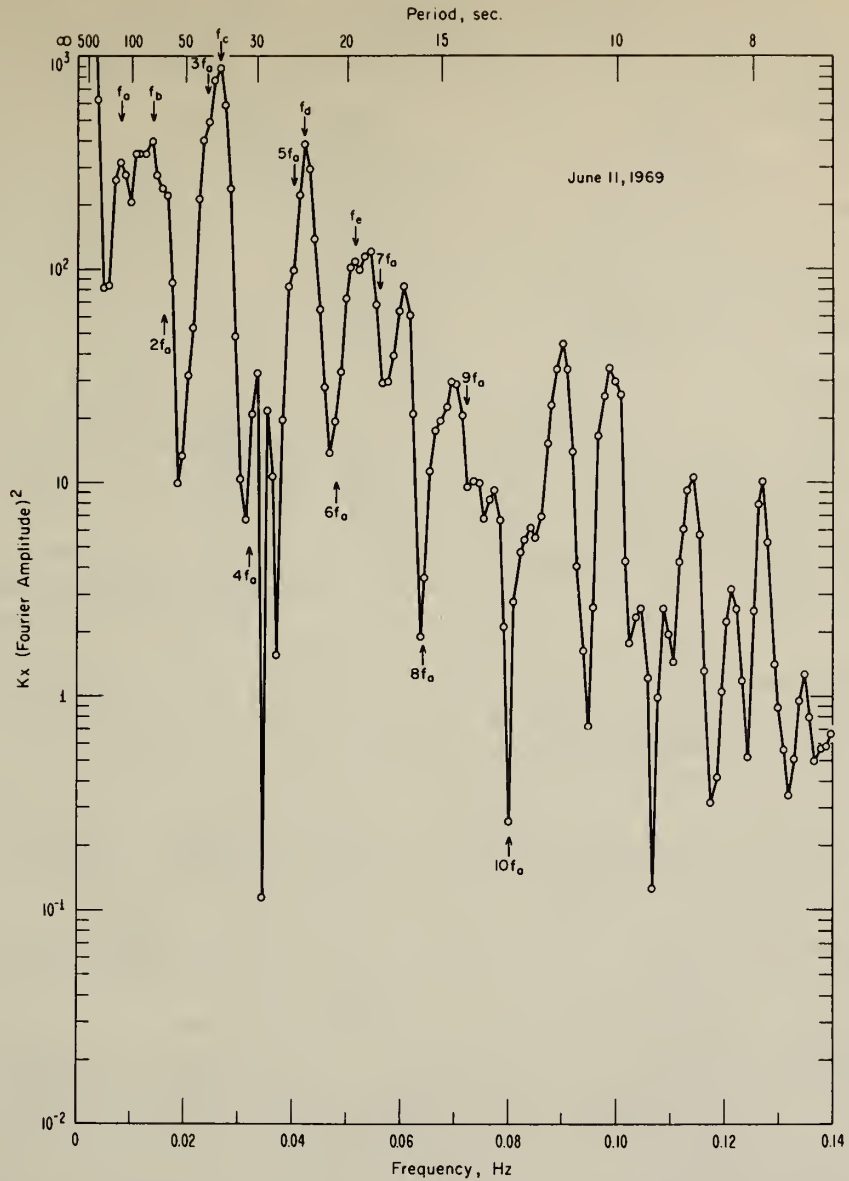


Figure 11. Spectrum of fine structure.

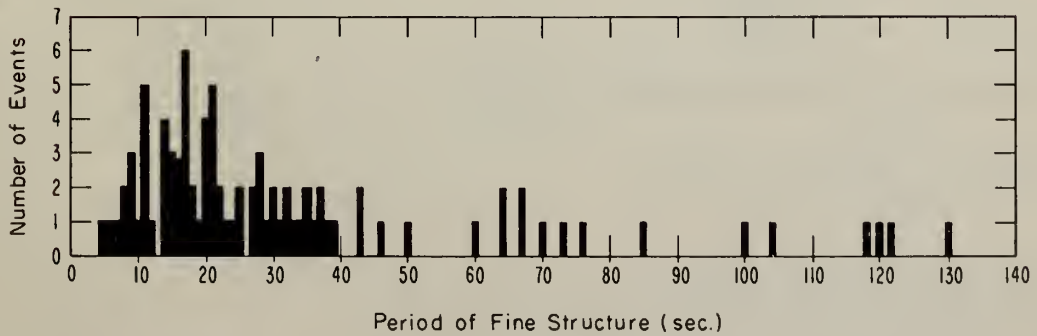


Figure 12. Distribution of fine structure periods.

Table 6. Some Statistical Properties of SFD Events

Characteristics	Amounts	References
<u>Start-to-Maximum Time</u>		
For Boulder SFD events, average:	2.1 min	sect. 4.3
median:	1.4 min	sect. 4.3
minimum:	10 sec	sect. 4.3
Most common value		
for importance 1- and 1 H $\alpha$ flares:	1 min	Agy, Baker and Jones (1965)
for importance 2 and 3 H $\alpha$ flares:	2 min	
<u>Duration</u>		
For all Boulder SFD events, average:	7.4 min	sect. 4.4
median:	5 min	sect. 4.4
<u>Peak Frequency Deviation</u>		
Maximum for a		
two-hop propagation path, 1936 UT 4/19/62	61 Hz	Donnelly (1967)
one-hop propagation path, 1816 UT 8/08/68	53 Hz	sect. 6
For all Boulder SFD events average:	0.86Hz	sect. 4.2
median:	< 0.4 Hz	sect. 4.2
<u>Peak <math>\Delta\phi(10-1030\text{\AA})</math>, ergs cm<sup>-2</sup> sec<sup>-1</sup> at 1 AU</u>		
Maximum, 1527 UT 8/28/66	9	Donnelly (1968a, c)
1841 UT 5/23/67	8-2	Donnelly (1969d) see also Garriott et al. (1967, 1969)
Minimum detectable:	10 <sup>-2</sup>	
<u>Fine Time-Structure</u>		
Percentage of SFD events with		
1 major peak:	82%	Chan and Villard (1963)
2 major peaks:	14%	
more than 2 major peaks:	4%	
(peak=major peak if 1/2 maximum peak of SFD)		
Quasi-periodicity of fine structure (rare and weak)		
Minimum major periodicity:	5 sec	sect. 4.5
Median major periodicity:	22 sec	sect. 4.5
<u>Median Time by which SFD Maximum Precedes</u>		
<u>Area of H<math>\alpha</math> Flare</u>		
for importance 1- H $\alpha$ flares:	< 2 min	Agy, Baker and Jones
for importance 1 H $\alpha$ flares:	2 min	
for importance 2 and 3 H $\alpha$ flares:	< 2.5 min	
<u>H<math>\alpha</math> Flares Accompanied by SFD's</u>		
for importance 3 H $\alpha$ flares:	80-83%	Chan and Villard (1963) and Agy, Baker, and Jones (1965)
for importance 2 H $\alpha$ flares:	49%	
for importance 1 H $\alpha$ flares:	21%	
for importance 1- H $\alpha$ flares:	4-10%	
<u>SFD's Accompanied by H<math>\alpha</math> Flares</u>		
for all importance classes:		
for importance 3 H $\alpha$ flares:	88%	Donnelly (1967)
for importance 2 H $\alpha$ flares:	1%	
for importance 1 H $\alpha$ flares:	3%	
for importance 1- H $\alpha$ flares:	21%	
	63%	
<u>Impulsive 2800 Mc/s Bursts Accompanied</u>		
by SFD's		
	46%	Chan and Villard (1963)
<u>SFD's Accompanied by Impulsive 2800 Mc/s Bursts</u>		
	38%	Chan and Villard (1963)

## 5. RELATIONSHIP OF EUV FLASHES DEDUCED FROM SFD'S WITH OTHER FLARE RADIATION

### 5.1 Hard X-Ray Bursts ( $\geq 10$ keV)

Kane and Donnelly (1970) studied the relationships between SFD's and satellite measurements of hard X-ray emission ( $\lambda < 1 \text{ \AA}$  or photon energies  $> 10$  keV) and established the following:

- (1) The occurrence of an EUV flash large enough to produce a distinct SFD ( $\Delta\phi(1-1030\text{\AA}) > 10^{-2} \text{ ergs cm}^{-2}\text{sec}^{-1}$  at 1AU) is accompanied by the occurrence of a hard X-ray burst.
- (2) The intensity of 10-1030  $\text{\AA}$  flashes observed via SFD's is approximately linearly proportional to the hard X-ray flux, the ratio of 10-1030  $\text{\AA}$  flux ( $\text{ergs cm}^{-2}\text{sec}^{-1}$  at 1AU) to the hard X-ray flux being about  $10^5$  (see table 2 of this report).
- (3) The ratio of 10-1030  $\text{\AA}$  flux to the hard X-ray flux varies on the average with the central meridian distance (CMD) of the associated H $\alpha$  flare, generally decreasing with increasing CMD.
- (4) The detailed time structure of the EUV flash deduced from SFD's is very similar to that of the impulsive hard X-ray burst (see also Donnelly, 1969c).

Kane and Donnelly (1970) have proposed a model to explain the above results wherein non-thermal electrons with a power law energy distribution (energy decreasing with increasing electron energy  $\geq 10$  keV) produce the hard X-ray burst via bremsstrahlung emission in a region of ambient hydrogen or proton density  $< 10^{12} \text{ cm}^{-3}$ , and they produce the EUV emission via collisional ionization and excitation with subsequent recombination and line emission at the bottom of this region where the ambient hydrogen density  $> 10^{12} \text{ cm}^{-3}$ . The CMD dependence in (3) above was suggested to be caused by absorption of the EUV emission in the solar atmosphere.

Numerous hard X-ray bursts have been observed that were not accompanied by an SFD (Kane and Donnelly, 1970), but this is probably because these events were too small for the EUV flash to be detected by SFD's. I would expect any impulsive hard X-ray flare (rise time  $\leq 1$  minute) with a peak flux greater than  $10^{-5} \text{ ergs cm}^{-2}\text{sec}^{-1}$  at 1AU at photon energies  $\geq 10$  keV that was not a near-limb event to surely be accompanied by an SFD providing good quality SFD observations were being made; so far, no such event has been found that was not accompanied by an SFD.

The detailed CMD dependence of the ratio of hard X-ray flux to EUV flux during impulsive bursts is not yet precisely known. Also, for a given small range in CMD, this flux ratio varies appreciably from one flare to another, perhaps because of experimental errors in the EUV estimates (see sec. 2) or perhaps because of varying amounts of EUV absorption depending upon whether or not filaments or other active region structures lie along our line of sight to the impulsive EUV source regions. These items will probably require simultaneous EUV and hard X-ray measurements via satellite that are more sophisticated than those planned for the present solar cycle. The long-duration events, the CMD dependence of occurrence and average size of SFD's, and the limb events, discussed in section 5.6.5, further determine the nature of this CMD dependence.

Kane and Donnelly (1970) suggest that the size of the EUV flash is more dependent upon the total energy flux above 10 keV for the impulsive X-ray burst than upon the spectrum of the hard X-ray radiation. A more precise determination of this result for more events seems desirable. Also, although the detailed time dependences of EUV flashes and hard X-ray bursts for impulsive events are very similar, there occasionally appear to be slight impulsive differences (Donnelly, 1969c) that need further confirmation to prove whether they are real or are caused by experimental faults. Furthermore, Kane and Anderson (1970) have found that the decay time of a hard X-ray burst decreases with increasing photon energy, or the spectrum varies with time. Although the time dependence of the EUV flash agrees closely with the hard X-ray burst, e.g. the EUV decay time of the fast spikes in the August 8, 1968 event (Donnelly, 1969c) appear to be as fast as that of the hard X-ray burst to within a few seconds, there must be a systematic difference in timing with increasing hard X-ray energy, considering Kane and Anderson's result. This systematic difference should be quantitatively determined with better EUV measurements for more events.

Slow differences between hard X-ray bursts and the 10-1030 Å emission deduced from SFD's are to be expected, both because of errors in estimating the electron-loss rates in the ionosphere (see sec. 2) and because SFD's respond to the whole 1-1030 Å wavelength range, which includes slow soft X-rays and slow EUV emissions in addition to the impulsive EUV emissions that are related to the hard X-ray burst (see sec. 3). Figure 13 shows a hard X-ray burst observed by Frost (1969) and the associated SFD which is an example of good timing agreement in the impulsive bursts but also of a slow difference in time dependence. Note that the SFD remains above its preflare level until 2148.3 UT; the major peak in the 1-1030 Å flux enhancement (not shown) occurs at about 2148 UT, well after the major hard X-ray peaks and the corresponding secondary peaks in the 1-1030 Å flux. This is one of the long duration events discussed in section 5.6.5 and is associated with a near-limb flare (89°W). I interpret this as a case where the impulsive EUV emission is relatively small compared to the slow soft X-ray and slow EUV emissions because the impulsive EUV emission encounters relatively high absorption in the solar atmosphere. The slow emissions are probably associated with rising arches and suffer negligible absorption because of the high solar altitude of their source region.

## 5.2 Soft X-Ray Bursts ( $\lambda > 1\text{\AA}$ )

Soft X-ray flares generally start earlier, rise more smoothly, peak later, and last longer than the EUV flashes that cause SFD's (Donnelly, 1968d, 1969b). Soft X-ray bursts contribute less than about 5% to the peak frequency deviation (see table 2) and less than 14% to the energy flux enhancement in the 1-1030 Å range at the time of the main impulsive peak in the 1-1030 Å flux. Note that this latter result is not the same as the percent ratio of peak soft X-ray flux to peak 1-1030 Å flux, which would be > 14%. Figure 14 illustrates that the soft X-ray flare is a different component of the flare than the impulsive component that radiates the EUV flash that produces SFD's. There are a few cases of broad-band soft X-ray observations that suggest a small impulsive component but for all practical purposes it is buried

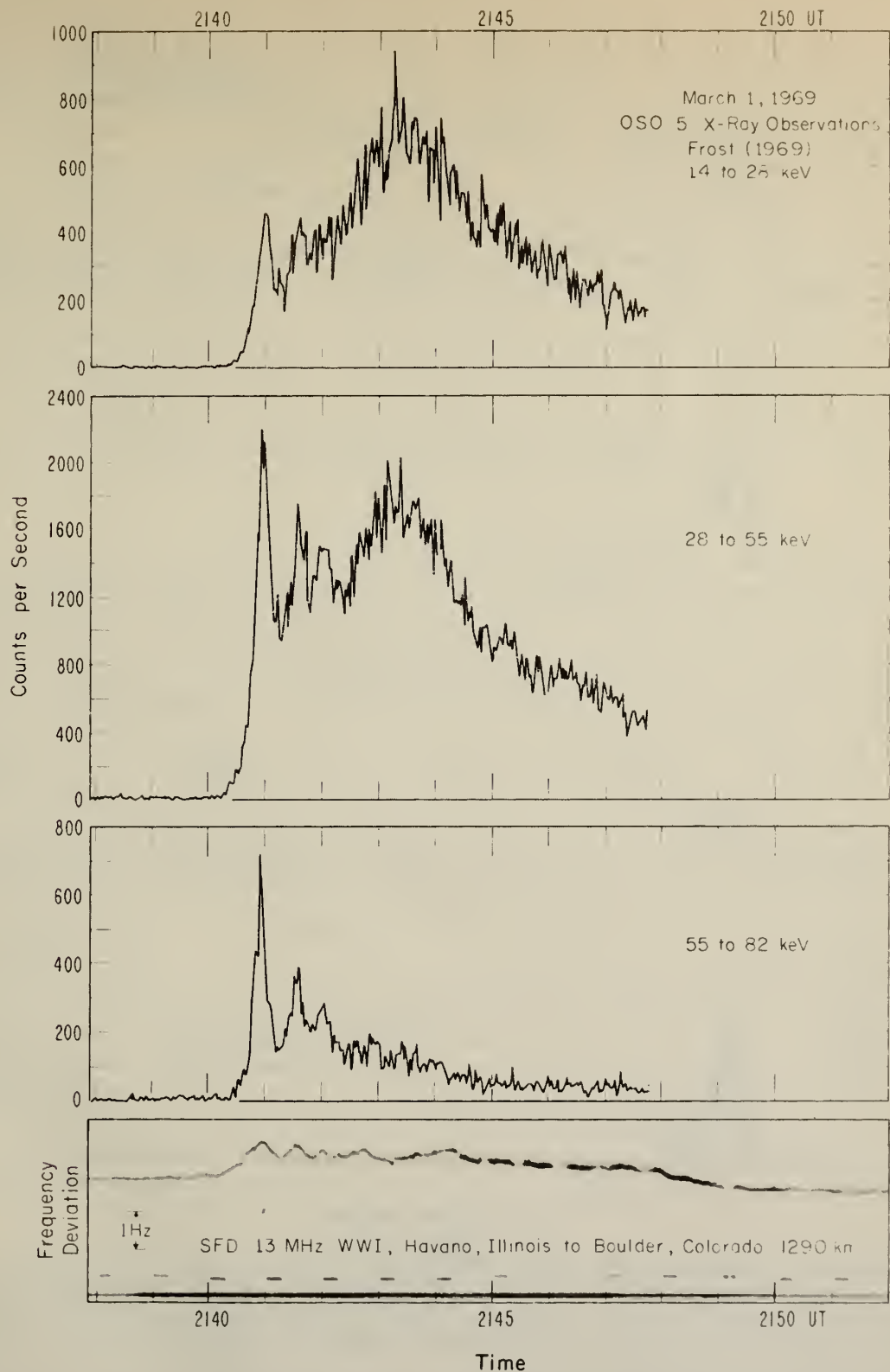


Figure 13. Comparison of timing of hard X-ray burst and SFD of 2141 UT March 1, 1969, OSO 5 X-ray observations made by Frost (1969).

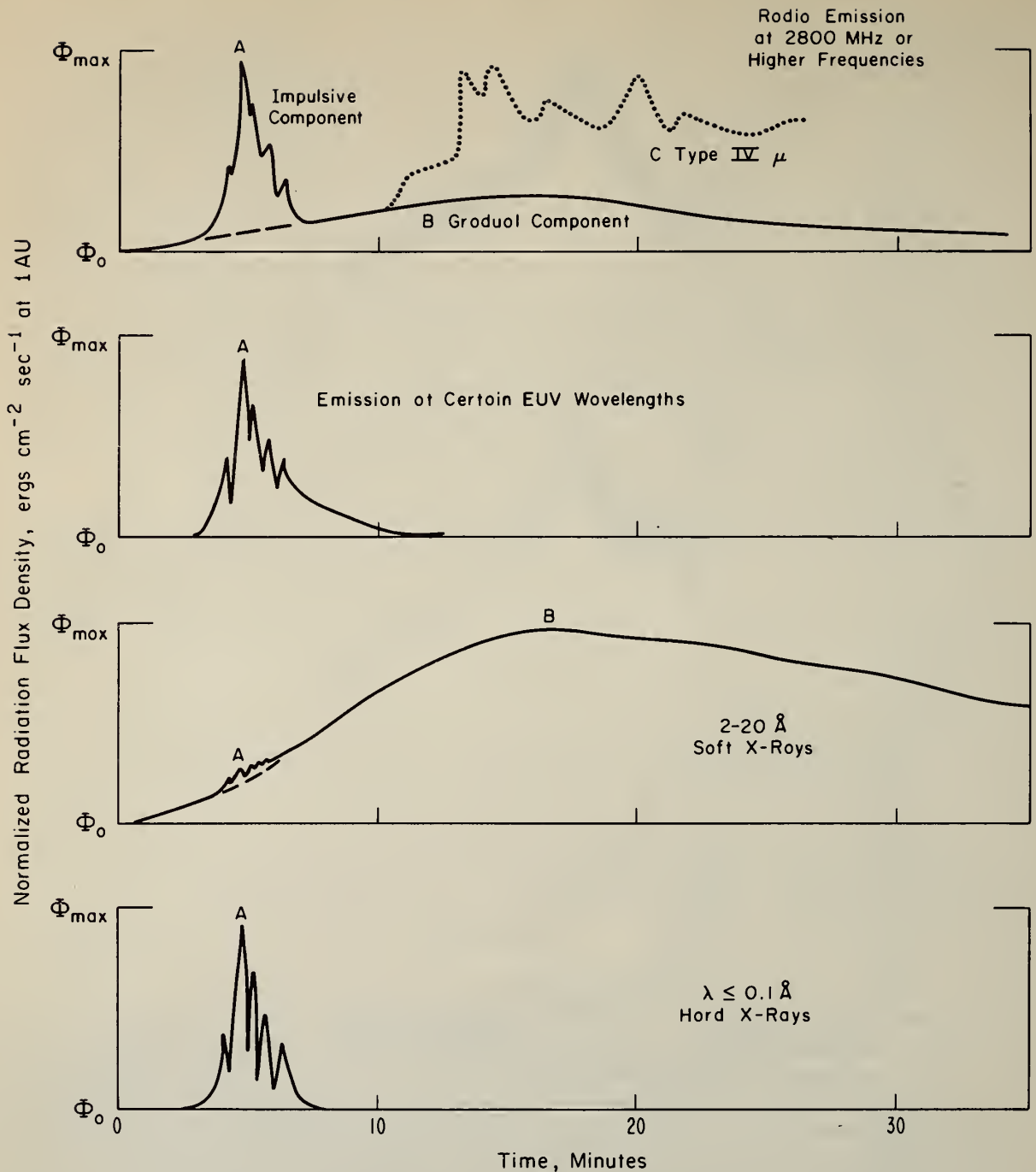


Figure 14. Illustration of components of flare radiation. The impulsive component A occurs concurrently at centimeter wavelengths, hard X-rays, certain EUV wavelengths, certain spatial portions of H $\alpha$  flares, and occasionally in white light. The gradual or slow component, B occurs with slightly different time dependence in soft X-rays, certain other EUV wavelengths, most of the H $\alpha$  flare, and centimeter wavelengths where it is sometimes called a postburst increase. The Type IV Component, C, occurs mainly at radio wavelengths.

by the slow component (Donnelly 1969b). Although the slow component (B) in soft X-rays is quite different from the impulsive component (A) observed by SFD's, the two components are related. For example, A normally occurs during the rise of B.

Numerous soft X-ray flares observed by Mr. R. Kreplin of the U.S. Naval Research Laboratories with SOLRAD satellites (listed in Solar Geophysical Data) that were large enough to produce D-region types of SID's (SWF, SPA, SCNA, etc.,  $\Delta\phi(1-8\text{\AA}) \geq 10^{-3}$  ergs  $\text{cm}^{-2}\text{sec}^{-1}$ ) were not accompanied by EUV flashes large enough to produce SFD's ( $\Delta\phi(1-1030\text{\AA}) \geq 10^{-2}$  ergs  $\text{cm}^{-2}\text{sec}^{-1}$ , with a rise time  $\leq 1$  min). However, no SFD events have been found that definitely were not accompanied by a soft X-ray enhancement. In other words, often component A and B both occur, B may occur without A, but I have found no evidence that A occurs without B. This may be the result of high sensitivity in the satellite measurements of soft X-rays (B) compared to the measurements made of the A component (satellite hard X-ray and EUV measurements, SFDs and ground based microwave measurements). The distribution of the time and wavelength integrated flux of component A relative to that of component B should be studied.

### 5.3 Ultraviolet Flashes (1030-3000 Å)

Few satellite observations of ultraviolet enhancements at wavelengths  $> 1030\text{\AA}$  have been made except at wavelengths near H $\gamma$  Lyman  $\alpha$  1215.7Å. Observations of Lyman  $\alpha$  usually show only small percentage enhancements ( $< 20\%$ ) even for flares of H $\alpha$  importance 3 (Hallam, 1964, Hall and Hinteregger, 1969). Such enhancements are still relatively large in ergs  $\text{cm}^{-2}\text{sec}^{-1}$  compared to the energy flux enhancements at  $\leq 1030\text{\AA}$  because of the large non-flare energy flux in Lyman  $\alpha$ ; consequently, the value  $R\phi$  in table 2 is quite large for Lyman  $\alpha$ . The  $R\phi$  results for Lyman  $\alpha$  vary from one flare to another from 25% to 250%, perhaps because of experimental difficulties in observing the Lyman  $\alpha$  flare. However, SOLRAD-8 satellite measurements of the proton flare of 1525 UT August 28, 1966, in the wavelength intervals 1050-1350Å and 1225-1350Å have been interpreted by Grebenkemper (1969) and McClinton (1968) (Friedman, 1969), as being caused mainly by a continuum enhancement and not by a Lyman  $\alpha$  enhancement, because of the large ratio of  $\frac{\Delta\phi_{\text{max}}(1225-1350\text{\AA})}{\Delta\phi_{\text{max}}(1050-1350\text{\AA})} > 1/3$  (Grebenkemper, 1969). Consequently, the wavelength dependence of 1030-1350Å impulsive flare radiation should be measured and studied further in order to resolve the true nature and intensity of this radiation. The time dependence of both Hall and Hinteregger's (1969) observations of flares in this range and the NRL results for the August 28, 1966 proton flare agrees well with the corresponding EUV flash deduced from SFD data. No satellite measurements of flare radiation in the 1350-3000 Å range have yet been reported to my knowledge; I understand however, that Nimbus 3 made solar flux measurements in the 1100-3000 Å range after April 14, 1969 (Heath, 1969).

### 5.4 White Light Flares

McIntosh and Donnelly (1970) studied white light flare patrol films of Sacramento Peak Observatory at times of SFD's when  $\Delta\phi_{\text{max}}(10-1030\text{\AA}) \geq 2.0$  ergs  $\text{cm}^{-2}\text{sec}^{-1}$  at 1 AU and found the following:

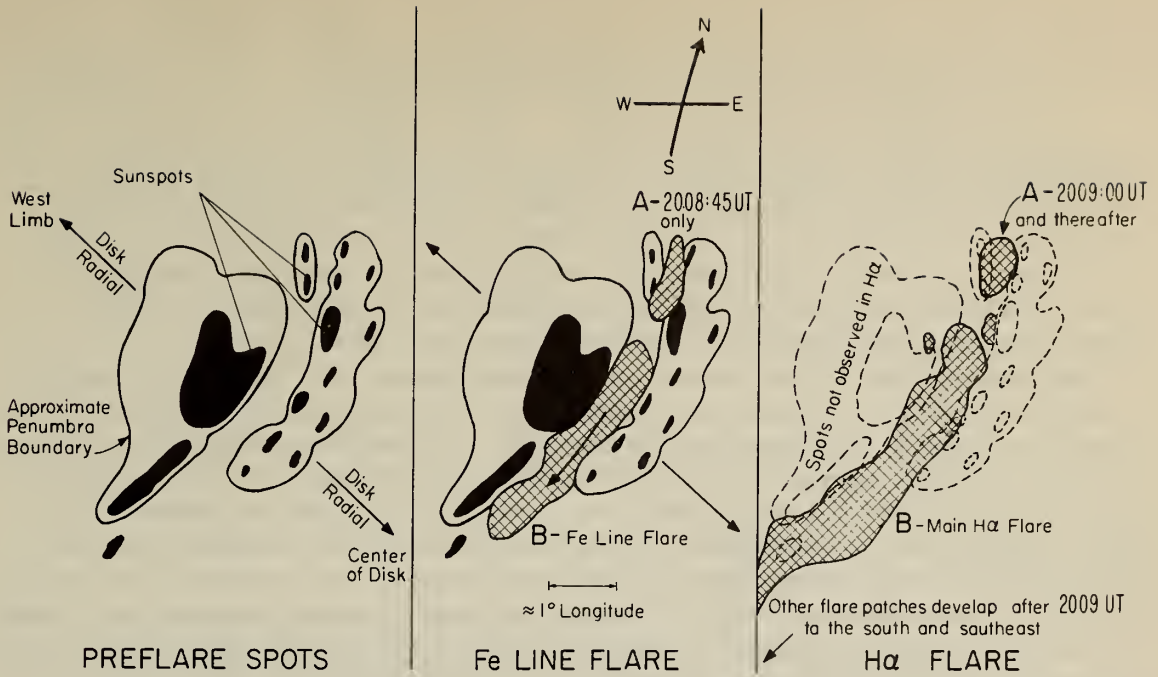
- (1) For the five such cases when white light patrol films were available, three were definitely white light flares and the other two were suggestive of faint white light emission but the seeing was too poor to be certain.
- (2) The white light flash (3500-6500Å) and EUV flash (10-1030Å) were roughly comparable in timing and flux enhancement.
- (3) The white light emission areas and, hence, probably also the EUV emission cores, varied from about 2 to 15 arc seconds in diameter.
- (4) The white light emission cores and, hence, probably the EUV emission cores, lay adjacent to the penumbra of strong sunspots, sometimes covering small umbrae, but never over the larger and very strong spots. These cores occurred in two or more places located near and on either side of a longitudinal neutral line in the magnetic field. This line lay between the leader sunspot of a relatively young sunspot group and the follower of an older group to the west of the line, with the separation between groups being less than one heliographic degree.

Considering the success of the above study, it may be possible to find more small white light flares by checking SFD's when  $\Delta\phi(10-1030 \text{ \AA}) \geq 1/2 \text{ erg cm}^{-2}\text{sec}^{-1}$  at 1 AU, especially since white light flares are more easily seen for flares at large central meridian distances (CMD) while the EUV emission is relatively weak for large CMD. Further quantitative study of white light flare emission should be made because such observations could provide excellent information on the size and location of the source region of the most energetic portion of flares. High time-resolution white light measurements should be made (~ 1 frame per sec); such a high film speed could be automatically triggered at times of large impulsive flares by either SFD or microwave radio measurements.

#### 5.5 Low-Chromosphere Optical Line Emission

Unfortunately, white light flare emission is observable only for very large flares; McIntosh and Donnelly (1970) estimate about 5-6 events per year during the present solar maximum. Optical observations other than white light provide good observations of the impulsive portion of flares smaller than white light flares. Several flares observed by Lockheed observatory (Ramsey et al., 1968) at  $5324 \pm 0.15\text{\AA}$  in an FeI line, which is a low chromosphere line, were studied with respect to the associated SFD. At that wavelength, sunspots and penumbra are visible, which makes it easy to determine the location of the flare emission relative to the sunspots and magnetic fields of the active region. Unfortunately, the flare emission at this wavelength is usually quite faint and moderately energetic flares are still required for quantitative study. Furthermore, good seeing is essential. Unfortunately, the particular flares studied, which were selected because the SFD data were of sufficiently good quality, were cases of fair to poor seeing.

Figure 15 shows the best example studied. Based on the size of the EUV flux enhancement deduced from SFD data, McIntosh and Donnelly (1970) suspect this event to be a white light flare. Although a white light flare patrol film exists for this event, it has not yet been available for study to determine whether a white light flare occurred. The 5324 Å flare observations studied may be partly continuum emission, rather than just Fe line emission. Figure 15 shows a sketch of the preflare



\* Times of Lockheed Observations

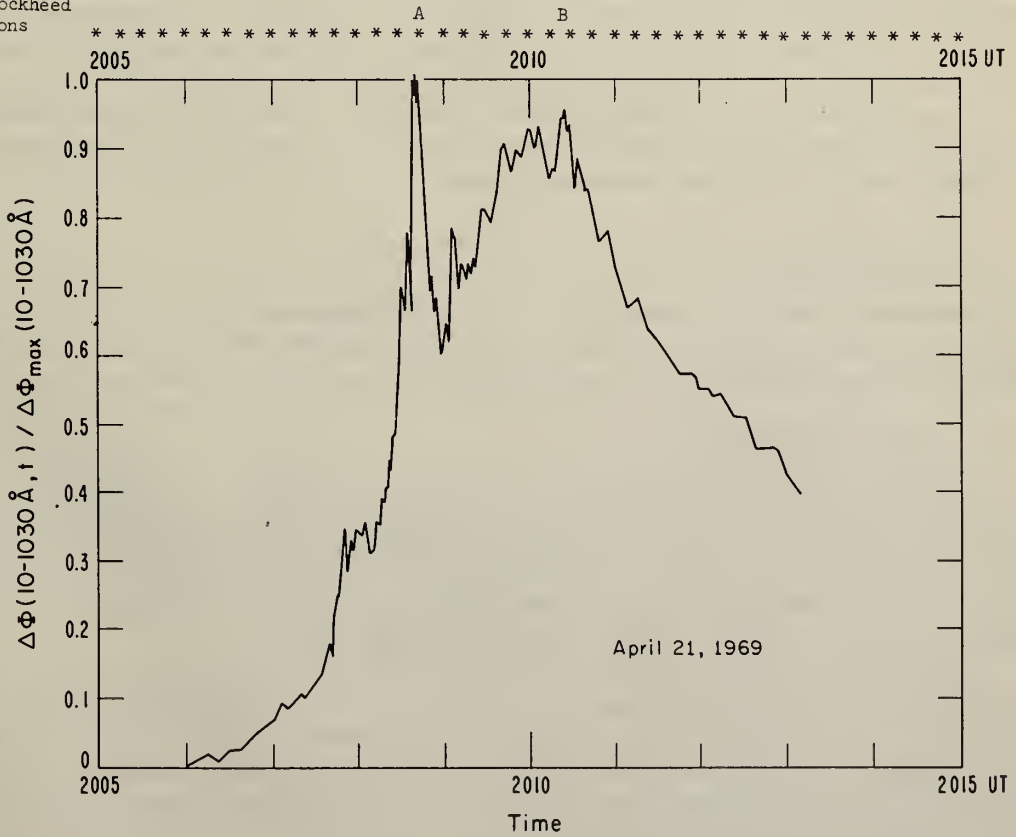


Figure 15. EUV burst, 5324Å Fe emission and H $\alpha$  flare of 2010 UT April 21, 1969.

sunspots based on the Fe line (5324 Å) observations and Boulder sunspot drawings. Detailed features may well be in error, including extraneous or missing small spots; but the overall structure is the important feature here. The main component of the 5324 Å flare (B) rose, peaked at about 2010-2011 UT and then decayed in good time agreement with the overall 10-1030 Å flux enhancement. The main emission region in B slowly progressed with time in the direction of the arrow shown in figure 15.

The main feature of this figure is component A, which appeared abruptly at 2008:45 UT, at the time of the spike in the 10-1030 Å flux enhancement, and then disappeared (although its decay may have appeared to be faster than reality because poor seeing set in). The Lockheed large-scale H $\alpha$  observations of this active region and flare showed more of a step function at location A delayed by one frame (15 sec) after the EUV burst. Before 2008:45 UT there was essentially no H $\alpha$  flare emission in region A. At 2008:45, there were slight indications of flare emission. At 2009:00 UT, a very bright core of H $\alpha$  emission was present and the H $\alpha$  emission thereafter leveled out at nearly the same high value for several minutes. The delay in H $\alpha$  emission may be a consequence of an initial Doppler shift in the H $\alpha$  emission being outside the narrow bandpass of these center-of-H $\alpha$  observations.

In summary, these observations show an impulsive small core of optical emission, associated with an EUV spike, and its location within the active region. Present results involve too few events and too poor seeing to support extensive conclusions. Such observations with better seeing and spatial resolution for more events could be used for quantitative study of the optical component of the energetic portion of flares and its location within the active region, i. e. the portion that produces hard X-ray bursts, EUV flashes, the initial microwave bursts, and white-light emission in the case of very energetic events.

## 5.6 H $\alpha$ Flares

### 5.6.1 Area Dependence

Chan and Villard (1963) and Agy et al. (1965) showed that H $\alpha$  flares and SFD's (and, hence, EUV flashes) are closely associated and that the association increases with increasing H $\alpha$  importance. The results are summarized in table 6.

### 5.6.2 Intensity Dependence

The association of H $\alpha$  flares with SFD's as a function of H $\alpha$  intensity has not been studied in detail except in conjunction with the study of the explosive phase of H $\alpha$  flares (sec. 5.6.4) where it was found that the brighter the H $\alpha$  flare the higher the percentage association with SFD's or EUV flashes. Detailed study of a few particular flares (sec. 5.6.6) suggests that the portion of H $\alpha$  flares most closely related to SFD's are small impulsive bright kernels.

The brightness of an H $\alpha$  flare generally refers to the brightest portion of the H $\alpha$  flare and is not quite the same as the total H $\alpha$  flux intensity enhancement (ergs cm<sup>-2</sup>sec<sup>-1</sup> at 1 AU). Unfortunately few measurements of the latter have been made. Thomas (1970) has measured the total H $\alpha$  flare flux for three flares. The ratio of peak H $\alpha$  flux to the peak 10-1030 Å flux enhancement based on the SFD data

for these same flares is given in table 2. The H $\alpha$  flare is dominated by the slow component (B, see fig. 14) as is evident from the relative time dependence of SFD's and H $\alpha$  flares described in table 6. Hence, Thomas' H $\alpha$  flux measurements are dominated by the slow component and not the impulsive component related to SFD's; hence, the R $\phi$  result for H $\alpha$  given in table 2 is an upper limit for the R $\phi$ (H $\alpha$ ) for the impulsive component.

### 5.6.3 Sunspot Dependence

Dodson and Hedeman (1970) have studied H $\alpha$  flares of importance  $\geq 2$  from nearly spotless active regions. Of their 83 events, only 21 occurred when SFD observations were made at Boulder. In 7 cases, SFD's were observed, so that 60% of their importance 3 flares were accompanied by SFD's and only 33% of their importance 2 flares. These percentages for flares from spotless regions are noticeably smaller than the results in table 6, but not greatly smaller. The most remarkable result of this study was that none of the seven flares from completely spotless regions (their type A) were accompanied by SFD's or impulsive EUV flashes, while 50% of the events from regions with very small spots (type B) were accompanied by SFD's. This latter percentage is consistent with the results in table 6. These results suggest that SFD's or EUV flashes do not occur with flares in completely spotless regions, at least small spots are required. More events should be studied for further verification.

Another parameter, besides brightness, which probably influences the relationship between H $\alpha$  flares and SFD's (or EUV flashes) and which has not been adequately studied is the impulsiveness of the H $\alpha$  rise time. However, the study discussed in the next section is probably a more fundamental study of the dependence on H $\alpha$  impulsiveness than just examining the start-to-maximum time of H $\alpha$  flares.

### 5.6.4 Association of EUV Bursts with the H $\alpha$ Explosive Phase

Moreton (1964) has defined the explosive phase of the H $\alpha$  flare as "the short period, commonly less than 30 seconds, during which time part or all of the flare borders undergo accelerated expansion" ( $\sim 100$  km/sec). During some explosive H $\alpha$  flares, traveling disturbances propagate away from the flare across the solar disk causing disturbances in quiescent solar prominences; sometimes matter appears to be blown off the sun; but in many cases, such associated effects are not observed. The explosive phase sometimes occurs when the H $\alpha$  flare is well developed, when a portion of the H $\alpha$  flare boundary suddenly expands; but for most of the events studied in the present paper, the explosive phase occurred during the flash phase or the rapid portion of the rise in H $\alpha$  intensity.

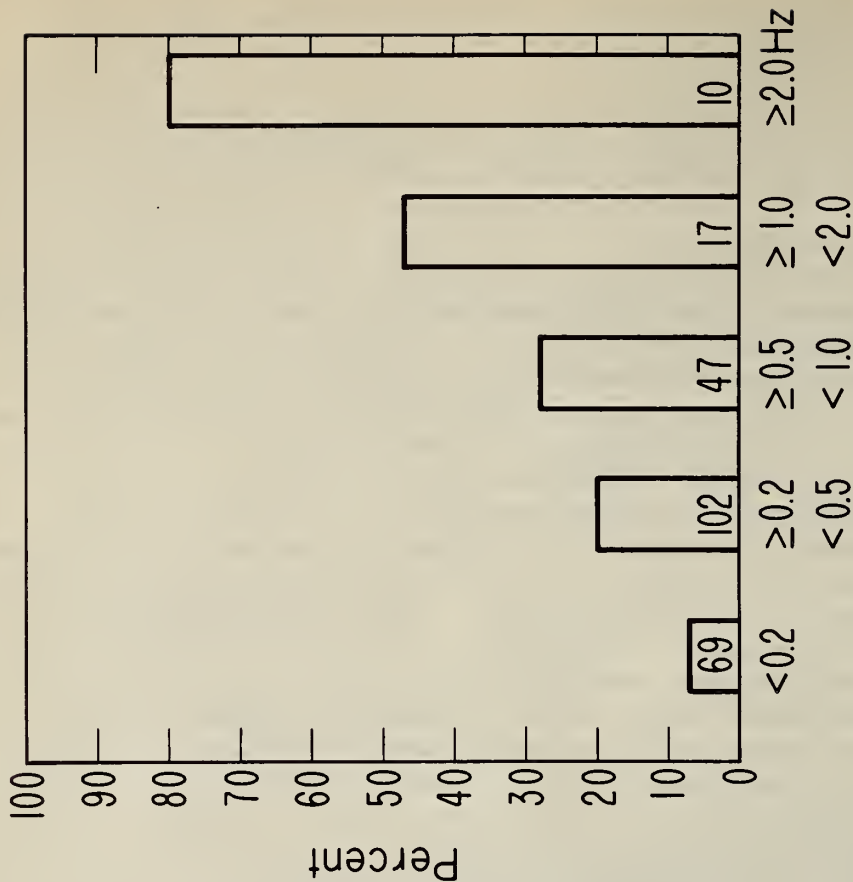
The explosive-phase classifications used in the present paper were made by the Lockheed Observatory staff\* using single-frame projection of 35 mm H $\alpha$  flare patrol films. Table 7 shows a strong association of SFD's with explosive phase flares. In

\* Explosive-phase data were provided through the courtesy of Mr. Harry Ramsey of the Lockheed Observatory.

# Number of SFD's Accompanied by Explosive-Phase Flares

Table 7. Contingency Table for SFD's and H $\alpha$  Flares with an Explosive-Phase.

	Explosive Phase	No Explosive Phase	Totals
SFD	54 (12)	191 (233)	245 SFD's
No SFD	48 (90)	1830 (1790)	1878
Totals	102 Explosive-Phase Flares	2021	2123 H $\alpha$ Flares



## SFD PEAK FREQUENCY DEVIATION

Figure 16. The dependence of the association of SFD's with explosive-phase H $\alpha$  flash on the intensity of the SFD. The number at the bottom of each histogram bar denotes the number of events involved.

the chi-squared test,  $\chi^2 = 43$  (table 7) compared to  $\chi^2 = 2.8$  for 95% confidence; so these two phenomena are clearly not independent. During the 1960-1964 period studied, the Lockheed Observatory classified intensity on a scale from 1 to 4, class 1 being faint and class 4 meaning very bright. The numbers in parentheses would be the expected number of events if EUV bursts and the explosive expansion of the H $\alpha$  flare area were unrelated. Figure 16 shows that this association is proportional to the EUV burst intensity. Figure 17 shows the association is stronger with either increasing H $\alpha$  flare area or brightness. The dependence on brightness is particularly evident from the fact that, of the 45 events of associated SFD's and H $\alpha$  flares of intensity class 3, 10 were subflares and 9 of these were classified as explosive. A previous study (Davies and Donnelly, 1966) using start times for the explosive phase scaled visually from patrol films found that on the average SFD's started 1 1/2 minutes earlier than the explosive phase; however, start times remeasured photometrically by Angle (1968, 1969) were essentially the same on the average as the SFD start time.

The association of EUV bursts and explosive expansion of H $\alpha$  area seems close enough that it is interesting to examine the cases in which they are not associated. Most of these are cases of small SFD's and subflares where the associated H $\alpha$  effects were too small to classify as "explosive." Many of the flares without an "explosive-phase" classification rated a "rapid rise" notation by the observer. A study was made of complex time-structured SFD's and the corresponding H $\alpha$  flare patrol films to determine whether each peak in the EUV burst was associated with a particular explosive portion of the H $\alpha$  flare. This study was inconclusive because the H $\alpha$  flares were very complicated and the time resolution was too low to provide a precise link with the SFD structure.

A second study involved single-peaked SFD's of moderate size unaccompanied by an "explosive phase" in the H $\alpha$  flare. Figure 18 is an example of one of these events.\* To my untrained eye there was no explosive expansion of H $\alpha$  flare area at the time of the SFD; but the sensitive photometer detected a very bright and impulsive core in the H $\alpha$  emission at one end of the flare over the edge of a sunspot. Figure 18 shows that the core was essentially time coincident with the EUV burst. Because the preflare plage and the overall flare area were so bright, there was no "apparent" explosive expansion of H $\alpha$  flare area. These impulsive kernels seem more fundamentally related to EUV bursts. If these kernels occur where the preflare emission is of fairly low intensity, the flare will probably be classified as having an explosive-phase; if it occurs where the H $\alpha$  emission is already quite bright for usual flare-patrol film exposures, the flare may not be classified as having an "explosive phase." These impulsive kernels are discussed in more detail in section 5.6.6.

#### 5.6.5 Dependence on Location of the H $\alpha$ Flare

##### 5.6.5.a Dependence of Occurrence on Central Meridian Distance

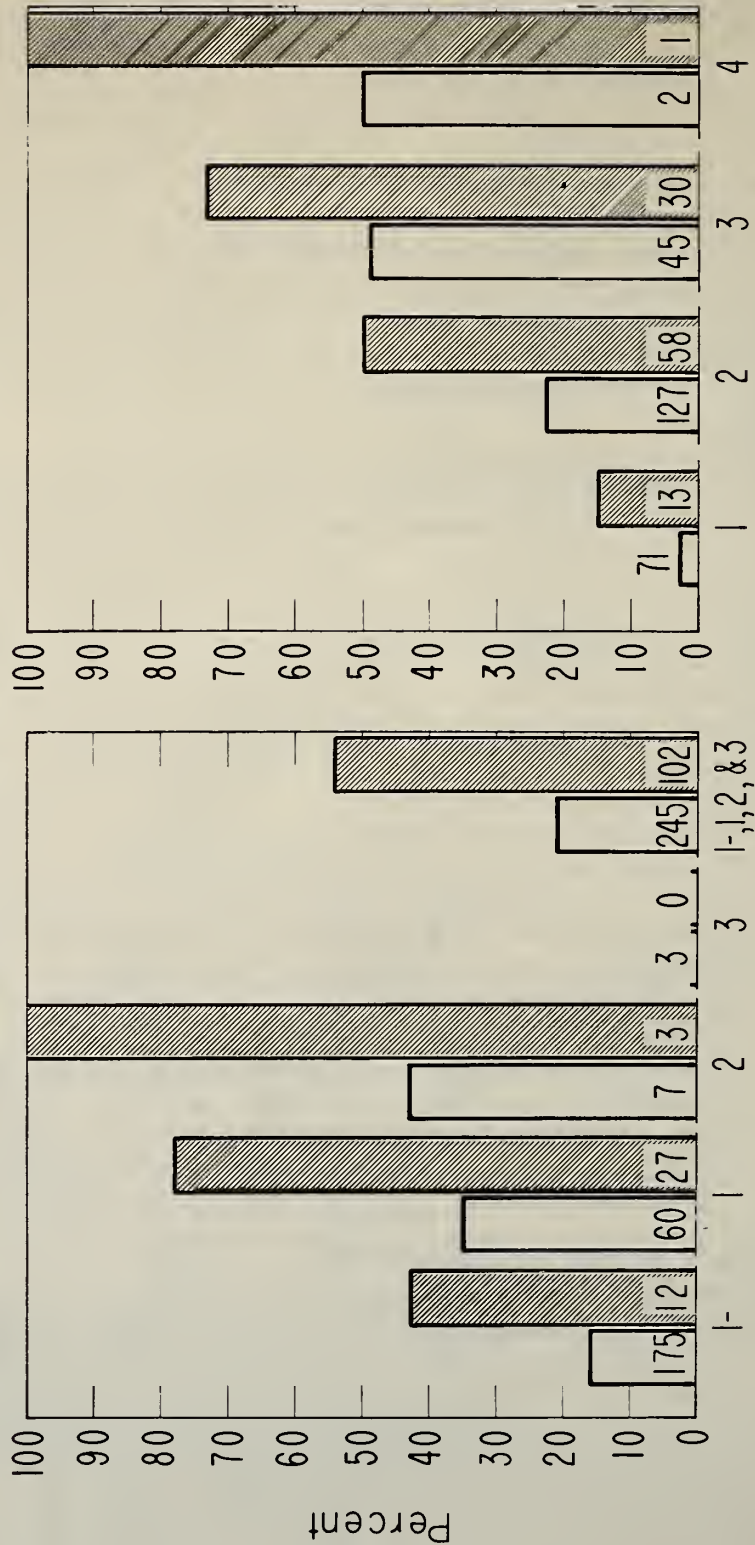
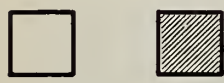
Figures 19 to 23 show the occurrence of H $\alpha$  flares, SFD events, and the percentage of all H $\alpha$  flares with SFD's grouped in 5° intervals. Each CMD interval includes the angle at the higher end of its range and excludes the angle at its lower end.

---

\* The H $\alpha$  photometry for this event was conducted at McMath-Hulbert Observatory through the courtesy and aid of Miss E. Ruth Hedeman.

Number of SFD's Accompanied by Explosive-Phase Flares  
 Total Number of SFD's

Number of Explosive-Phase Flares Accompanied by SFD's  
 Total Number of Explosive-Phase Flares



(a) H $\alpha$  FLARE IMPORTANCE (b) H $\alpha$  FLARE INTENSITY

Figure 17. The association of SFD's and H $\alpha$  explosive-phase flares as a function of H $\alpha$  flare importance and brightness. The number at the bottom of the histogram bars denotes the number of events involved.

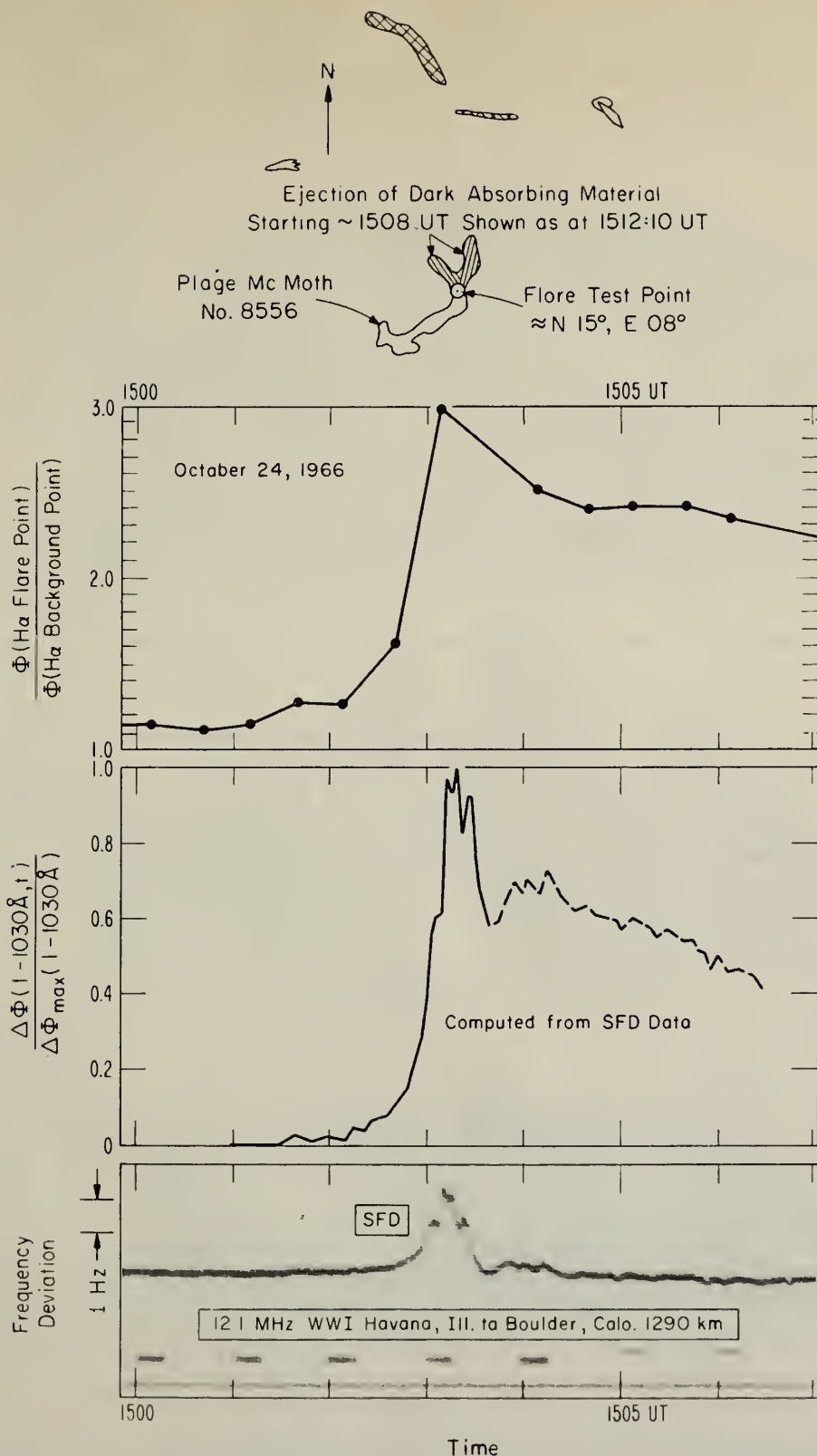


Figure 18. Association of an EUV burst with a small bright Ha kernel.

Events at  $0^\circ$  were alternately added to the  $0-5^\circ$  West and the  $0-5^\circ$  East range. The range marked  $85-90^\circ$  really means  $\text{CMD} > 85^\circ$ .

The number of  $\text{H}\alpha$  flares peaks sharply at  $\text{CMD} > 85^\circ$ , probably because we're seeing many flares where the center of the emitting area is located beyond the limb so that the effective CMD range is greater than  $5^\circ$ . The number of  $\text{H}\alpha$  flares with SFD events decreases toward the limb with a weak peak at the limb, much weaker than the large peak for all  $\text{H}\alpha$  flares. Consequently, the percentage of  $\text{H}\alpha$  flares with SFD's or EUV flashes peaks at  $\text{CMD} \leq 5^\circ$  and decreases appreciably for large CMD for both the east and west limbs. This result is evident for each year studied as well as for all five years and also for  $\text{H}\alpha$  flares excluding subflares. Data for 1964 and 1965 are not shown separately, because the number of events was too small to show significant results. Several of the secondary peaks at intermediate CMD values, e.g.,  $60-65^\circ$  East, which is particularly evident in the percentage figure for 1967, are largely due to several flare-prolific active regions and are probably not indicative of a preference of EUV emission from those locations.

The observed CMD dependence could be caused by a bias in  $\text{H}\alpha$  flare observations for near-limb flares, a decrease in EUV emission with increasing CMD, or both. The bias in seeing  $\text{H}\alpha$  flares centered beyond the limb, discussed above, probably preferentially selects large flares; therefore, since large  $\text{H}\alpha$  flares are statistically more frequently accompanied by SFD's than small  $\text{H}\alpha$  flares, this type of bias should result in the percentage of  $\text{H}\alpha$  flares with SFD's increasing at the limb. This may explain why the percentage of  $\text{H}\alpha$  flares with SFD's for  $\text{CMD} > 85^\circ$  is comparable to that for  $80^\circ < \text{CMD} \leq 85^\circ$  rather than being less, but this effect is opposite that required to explain the near-limb results compared to the center-of-disk results. There are undoubtedly other biases in  $\text{H}\alpha$  flare observations that are not accounted for by present correction factors, e.g., the background  $\text{H}\alpha$  emission decreases with increasing CMD thereby, perhaps, making small faint flares easier to detect. The  $\text{H}\alpha$  flare area observed near the center of the disk is the area projected on the solar surface, but flares observed at the limb must depend partly upon the radial extent of the  $\text{H}\alpha$  flare. For further discussion of problems in the CMD dependence, see Smith and Smith (1963). Studies of soft X-ray emission from flares (Thomas, 1970, Dodson and Hedeman, 1964) suggest that the importance of  $\text{H}\alpha$  flares near the limb tends to be underestimated. Considering the statistically increasing association of SFD's and  $\text{H}\alpha$  flares with increasing  $\text{H}\alpha$  importance, the bias in the CMD dependence of  $\text{H}\alpha$  flares is probably not the main cause of the CMD dependence of the percentage of  $\text{H}\alpha$  flares with SFD's. Consequently, the relative strength of impulsive EUV emission from flares probably decreases with increasing CMD, particularly near the limb.

#### 5.6.5.b Peculiar Long-Duration Events

During the past ten years of SFD observations, a number of events stand out as being rather unusual compared to the average characteristics of SFD's, e.g., events with very extensive fine structure (see sec. 4.5). Another type of peculiar event that has an unusually long duration of the frequency deviation exceeding the preflare

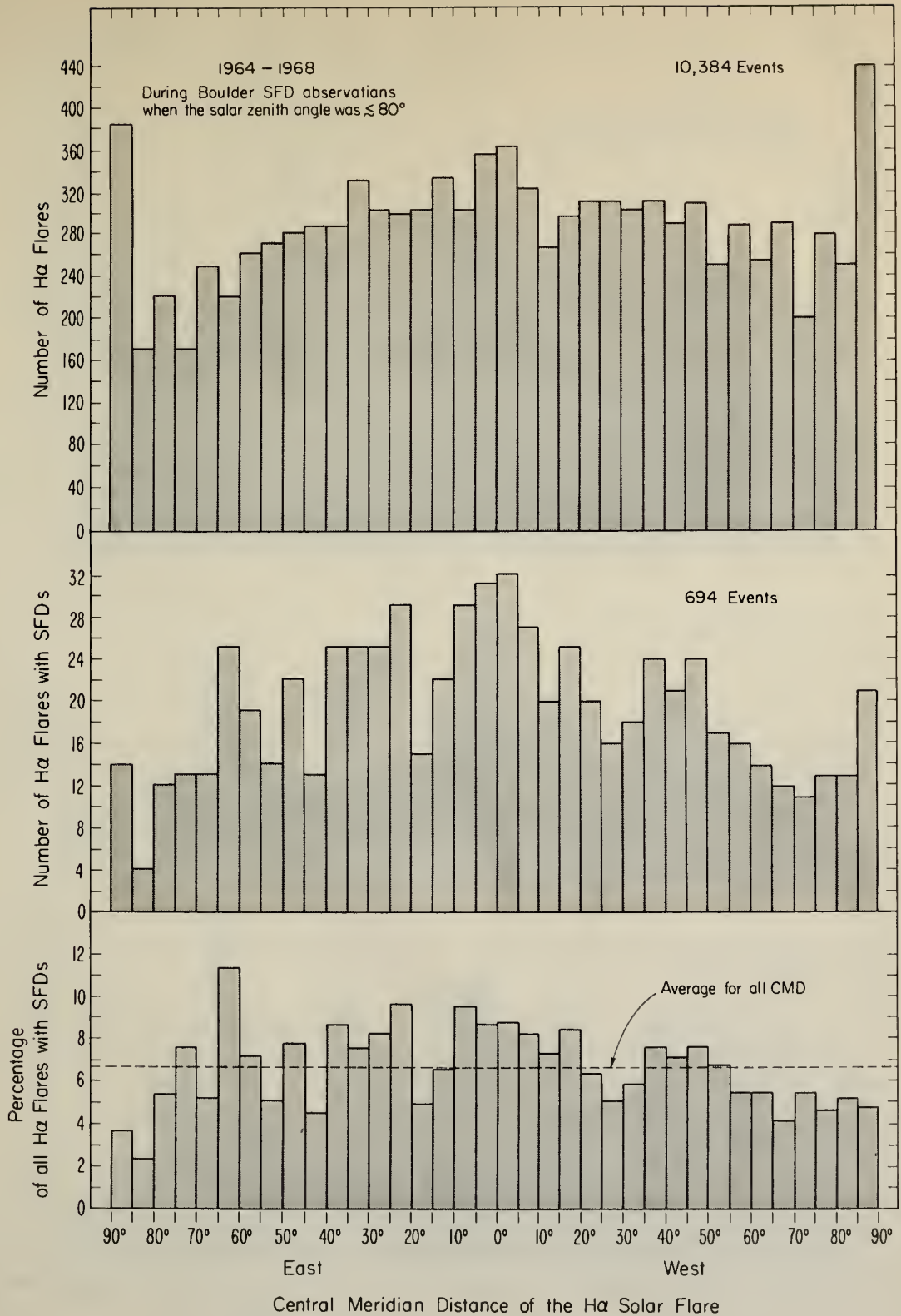


Figure 19. Dependence of EUV flashes on the central meridian distance of the associated H $\alpha$  flare for 1964-1968 for all H $\alpha$  flare classifications.

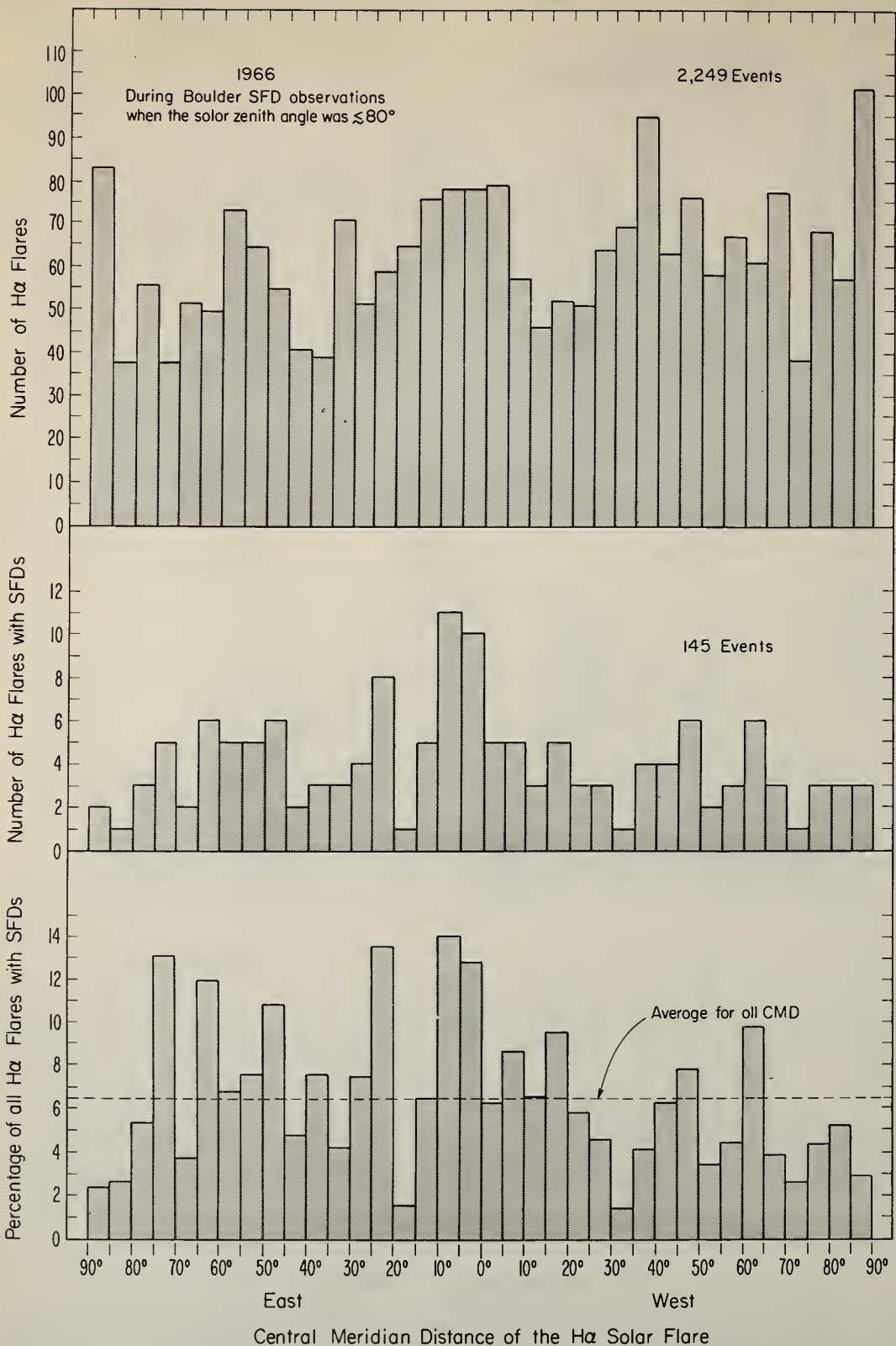


Figure 20. Dependence of EUV flashes on the central meridian distance of the associated H $\alpha$  flare for 1966 for all H $\alpha$  flare classifications.

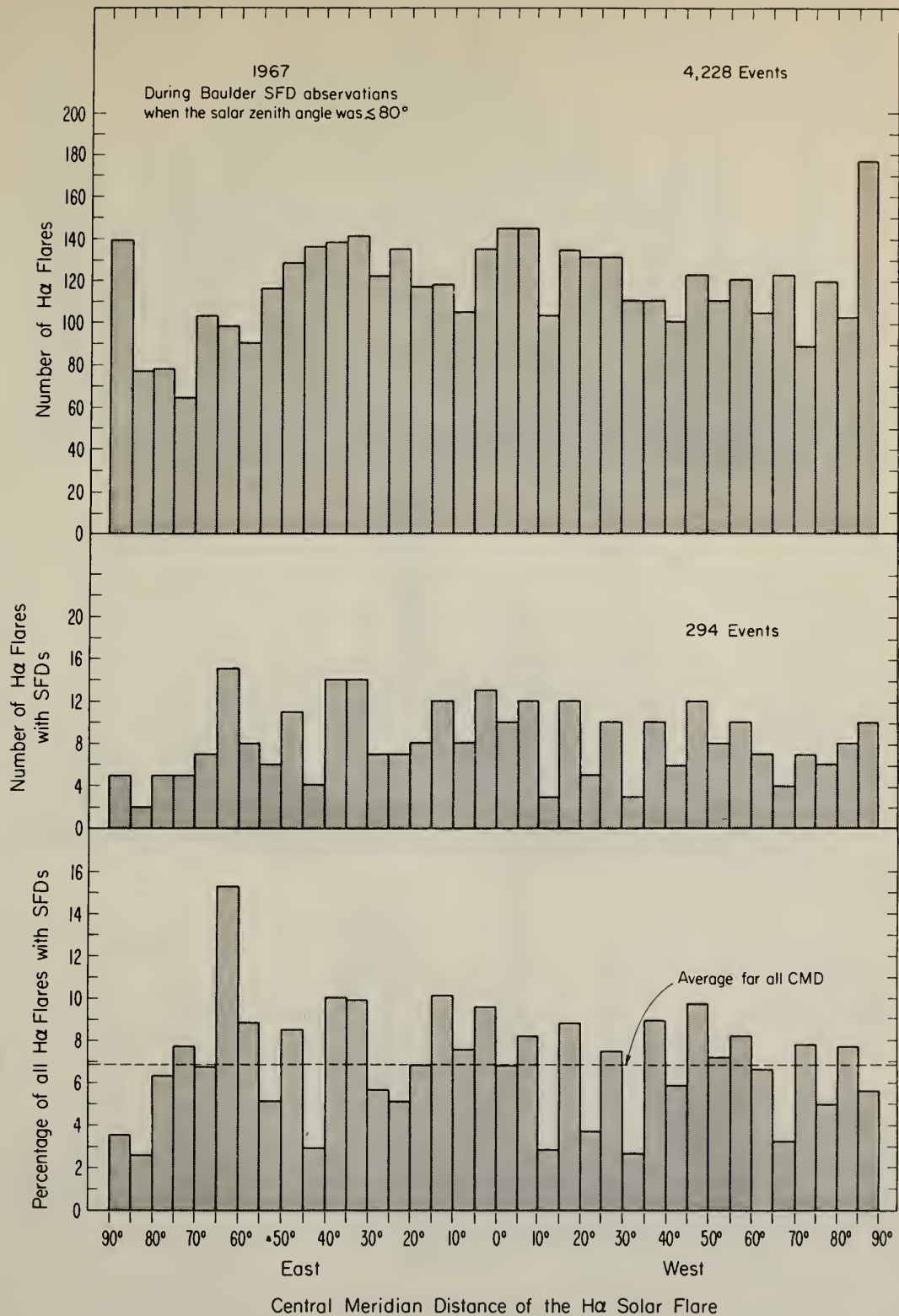


Figure 21. Dependence of EUV flashes on the central meridian distance of the associated H $\alpha$  flare for 1967 for all H $\alpha$  flare classifications.

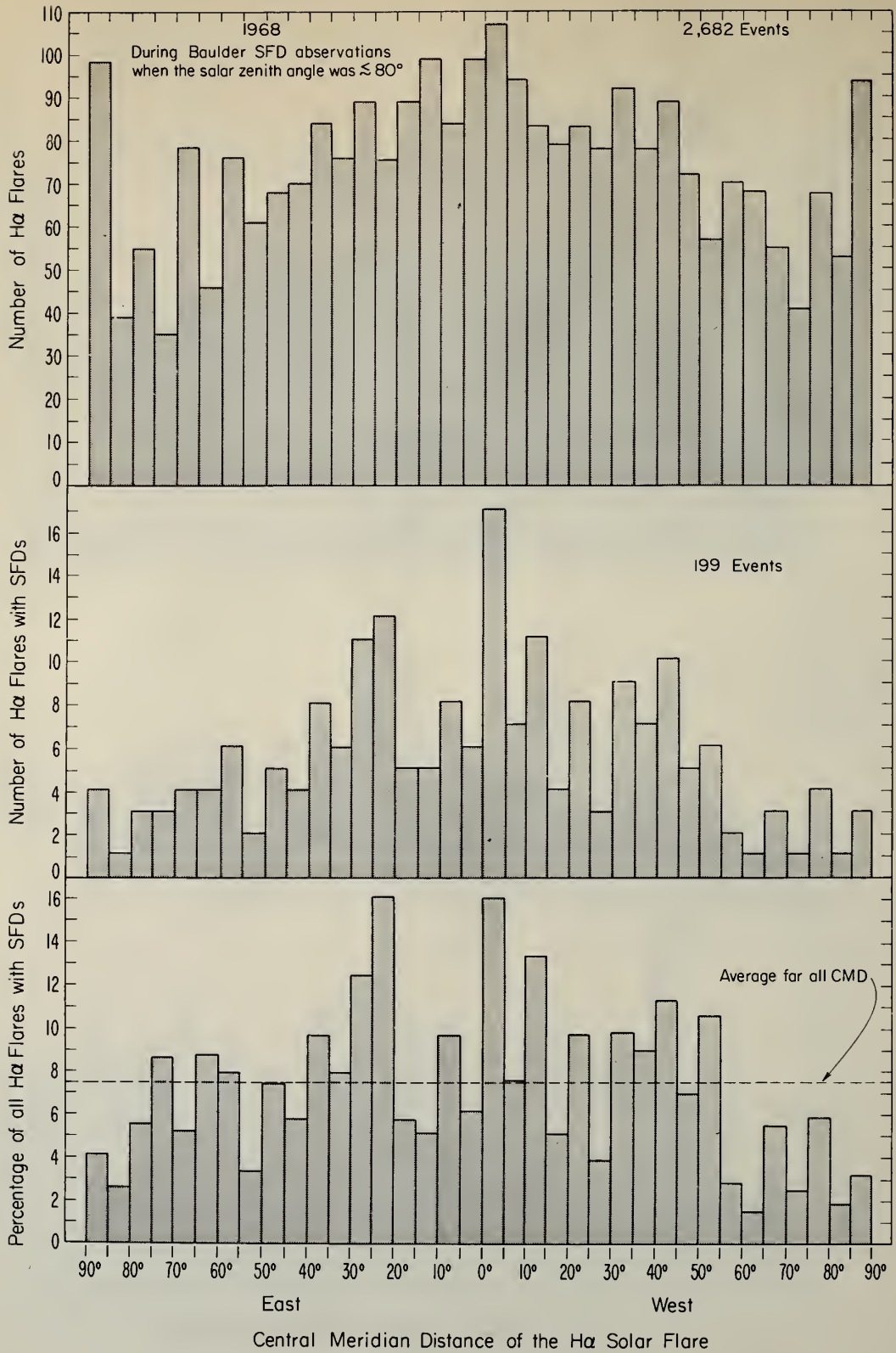


Figure 22. Dependence of EUV flashes on the central meridian distance of the associated H $\alpha$  flare for 1968 for all H $\alpha$  flare classifications.

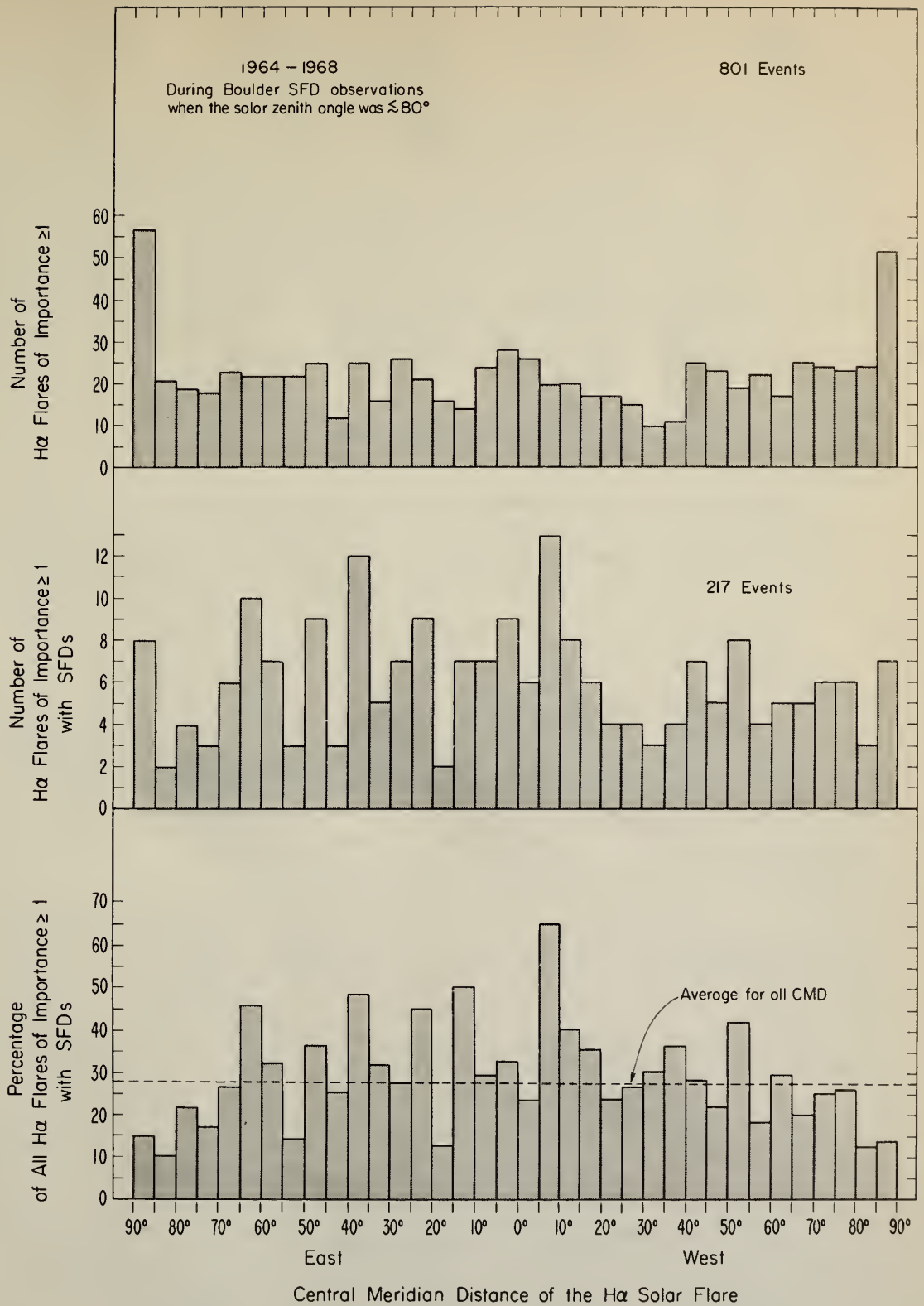


Figure 23. Dependence of EUV flashes on the central meridian distance of the associated H $\alpha$  flare for 1964-1968 for H $\alpha$  flares of importance  $\geq 1$ .

Table 8. Long Duration Events

SFD (Time UT)										K $\alpha$ Flare (Time UT)						
Date	Start	Max	Main Zero Crossing	End	*1 $\gamma$	*2	*3	*4 $X$	*5	*6 $X$	Start	Max	End	Imp.	Lat.	Long.
09/10/61	1953	1953	2025	----	0.3	10.000 WWV	38	127	43°		1950	2010	2052	1	11°N	85°E
07/07/66	0025.0	0027.2	0044.8	0126	3.0	10.000 WWV	20	7	80°		0023	0036	0140U	2B	35°N	47°W
10/13/66	1334.0	1343.7	1346.1	1353	0.3	8.900 WWI	12	40	81°		1330	1341	1410	1N	22°N	58°E
12/09/66	1756.0	1800.0	1806.0	1816	0.9	4.000 KKE42	12	13	64°		1755	1805	1825U	2B	21°N	50°E
03/22/67	0026.0	0031.2	0044.2	0055	0.3	5.100 KKE42	18	61	84°		0025	0033	0120D	3B	25°N	68°E
04/14/67	1705.3	1708.7	1712.1	1718.4	0.5	13.000 WWI	6.8	14	36°		1703	1715	1734	2N	25°N	71°W
04/26/67	2121.9	2126.8	2129.0	2144	0.6	11.100 WWI	7.1	12	47°		2115	2138	2250	1B	19°S	89°E
06/01/67	1918.1	1922.5	1924.8	1929	0.6	9.900 WWI	6.7	11.2	21°		1913	1922	1934	SN	24°N	26°E
08/04/67	1514.0	1516.6	1526.5	1539.4	0.7	11.100 WWI	12.5	18	47°		1512	1515	1533	SN	21°N	72°E
08/18/67	2120.0	2131.4	2136.5	2144.2	0.6	9.900 WWI	17	28	48°		1902	2138	2156	1N	25°N	91°E
10/23/68	1936.6	1940.8	1943.0	1949	0.3	11.100 WWI	6.4	21	54°		1939	1941	1958	SN	18°S	61°E
03/01/69	2139.8	2140.9	2148.3	2205.0	1.0	13.000 WWI	8.5	8.5	65°		2140	2139	2204	1N	08°N	89°W
03/27/69	1323.0	1329.5	1341.3	1410.0	0.7	8.900 WWI	18	26	75°		1323	1341	1424	2B	21°N	69°W
05/17/69	1922.4	1925.1	1934.2	2005.0	0.6	11.100 WWI	11.8	20	24°		1923	1931	1947	SB	11°N	90°E
05/29/69	1937.2	1942.0	1948.5	2000.3	1.8	11.100 WWI	11.3	6.3	24°		1939	1944	2010	1B	10°N	76°W
08/21/69	1411.6	1413.7	1417.3	1431.0	0.6	8.900 WWI	5.7	9.5	63°		1410	1415	1440	1B	10°N	90°E
02/11/70	2106.8	2113.6	2122.5	2140.0	0.7	13.000 WWI	16	22	66°		2110E	2122	2200D	2B	19°N	12°W

\*1  $\Delta f_{max}$  (Hz)      \*2  $f_o$  (MHz)      \*3 Transmitter Station Call Letters      \*4  $\Delta t_{so}$  (min)      \*5  $\Delta t_{so}/\Delta f_{max}$  or X/Y      \*6 Solar Zenith Angle

values is illustrated in figure 24. The value of X is unusually large relative to Y. Furthermore, the fine structure occurs early during the event and the latter portion of the positive frequency deviation is unusually free from fine structure. (Another example of a long-duration event is the event of March 1, 1969, discussed in sec. 5.1 and shown in fig. 13).

A special study was made of these long-duration events. Boulder SFD data from March 1966, through May, 1970, and published figures of SFD's from October 1960 through March, 1966, (Agy et al., 1965, Baker, 1965) were searched for such events using the following criteria:

- (1)  $X/Y > 5 \text{ min Hz}^{-1}$
- (2)  $X \geq 5 \text{ min}$
- (3)  $Y \geq 0.3 \text{ Hz}$
- (4) Fine structure does not dominate during the latter portion of the period of positive frequency deviation.
- (5) Negligible frequency deviation from nonflare-induced ionospheric disturbances.
- (6) SFD observed on a propagation path reflected in the F-region and not at the bottom of the E layer or from Sporadic E.
- (7) The H $\alpha$  flare associated with the SFD could be unambiguously identified.

Criterion 3, which insures that the SFD was large enough to be accurately scaled, disqualified about 40% of all SFD's. Criterion 2, which insures the event is of long duration, disqualified another 40% of the SFD's. Criteria 1, 4, 5, 6 and 7 disqualified nearly all the rest of Boulder SFD's except those listed in table 8. Criterion 1 insures that the event has long duration relative to the size of the event, criterion 4 insures that it is not simply a long-duration impulsive event (e.g., the July 8, 1968 event, see sec. 6), and criterion 5 disqualifies noisy SFD's. Criterion 6 is necessary because SFD's observed on propagation paths reflected from the bottom of the E layer are produced mainly by soft X-rays, which have relatively slow enhancements during flares, such that these SFD's often satisfy criteria 1-5, even when the SFD's for the same event for F-region propagation paths are very impulsive. One might suspect that the above criteria may be simply selecting weak events, i.e., selecting  $\Delta f$  small enough that the first criterion is satisfied. However, peak frequency deviation and duration are roughly correlated so that if one decreases the EUV flare emission he would usually have to also decrease the duration of that emission.

Among the seventeen events in table 8, there are some that look distinctly different from the event in figure 24, yet they still satisfy the above seven criteria. These events have essentially no impulsive structure, even at their beginning, and their  $\Delta f(t)$  trace becomes very faint because of high ionospheric absorption of our probing radio waves induced by the associated soft X-ray flare. Such behavior is typical (and much more frequent) of SFD's observed on radio paths reflected from the bottom of E-layer, so a careful study of the preflare propagation paths and fuzziness and wiggleness of the preflare frequency deviations (F-region  $\Delta f(t)$  traces are distinctly more fuzzy and wiggly than bottom of the E-layer or Es traces) had to be made to properly identify these events. These events suggest that more such long duration events exist than are indicated by table 8 because, if the absorption was too great and the SFD trace was lost, the X value could not be determined and the event was

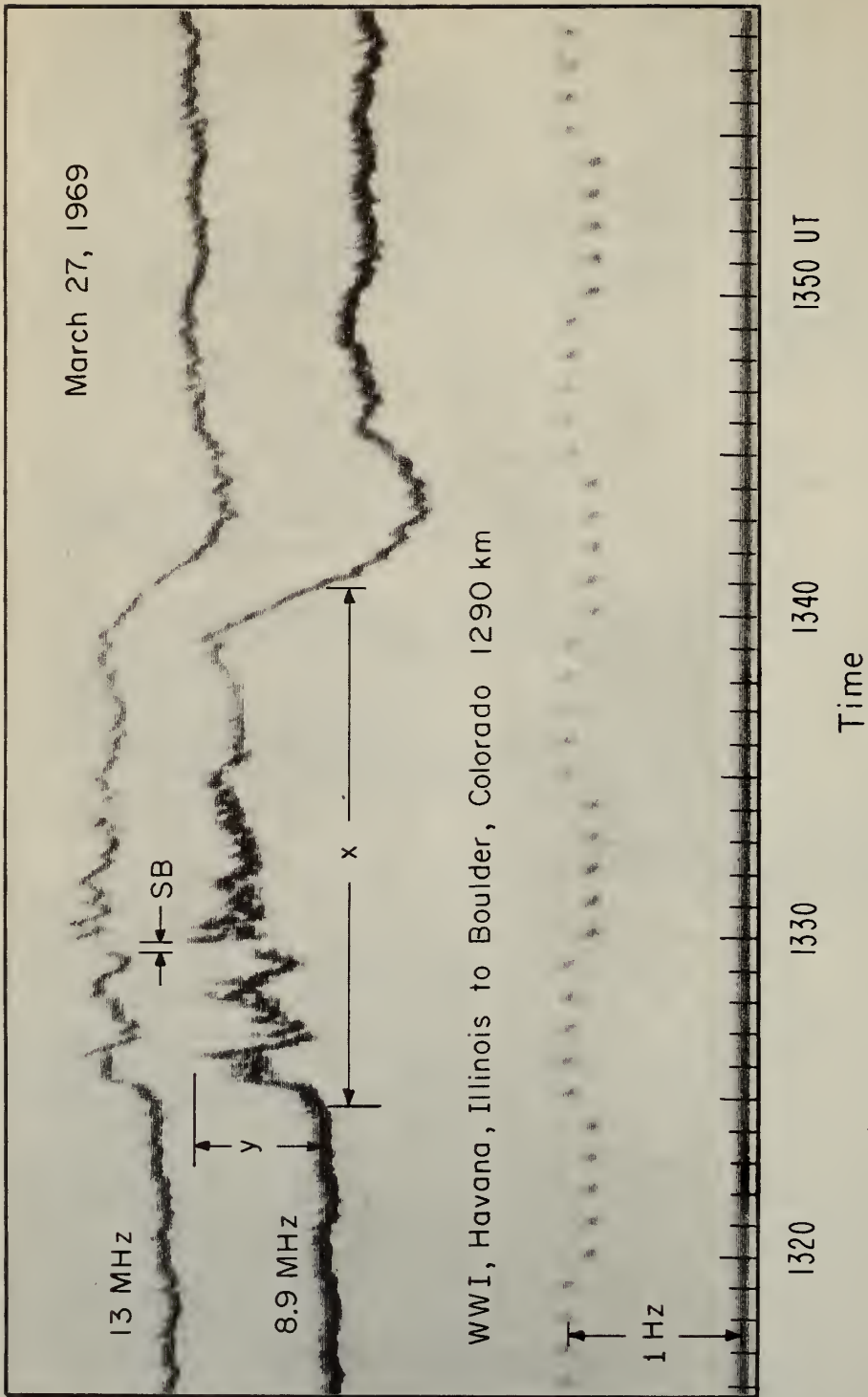


Figure 24. An example of an SFD with an unusually long duration of positive frequency deviation. SB denotes the station-identification break.

disqualified. Furthermore, because of their slowness and lack of sizeable frequency deviations, such events could easily have been ignored and not listed when the original data were processed to detect SFD's. One of the best examples of this type of event is the SFD of September 10, 1961, shown in figures 33 and 34, pp 52-5, of Baker (1965).

Nine of the seventeen events (53%) were at central meridian distances greater than  $70^\circ$ , while for all SFD's observed in Boulder only about 15% are at  $CMD > 70^\circ$ . Considering the CMD dependence discussed in the previous section, a possible qualitative explanation of these peculiar long-duration events is as follows: The impulsive EUV radiation from source regions at relatively low heights suffer considerable absorption by the surrounding cool atmosphere in the active region and surrounding solar atmosphere, especially for the line of sight for flares near the solar limb. Slow radiations including soft X-rays and certain EUV lines are emitted from relatively high source regions and suffer negligible absorption compared to the impulsive EUV emissions. Because the impulsive emissions are relatively weak, the peak frequency deviation ( $Y$ ) is fairly small and the frequency deviations are impulsive mainly early in the event. Because the slow emissions are large and unattenuated, the duration of  $\Delta f \geq 0$  ( $X$ ) is anomalously large. If the same flare occurred near the center of the disk so that the EUV source were observed looking through the overlying ionized flare region, negligible absorption of the EUV flash would occur and a very large impulsive SFD would be observed. The recovery from the EUV flash would quickly drive  $\Delta f$  below zero even through the slow emissions were the same as for the near-limb case. Hence, the same flare at the center of the disk would have a much larger  $Y$  and smaller  $X$ .

An alternative explanation is that the emission of the impulsive component of these flares was relatively weak. However, events like that of March 1, 1969, (discussed in sec. 5.1) exhibit large impulsive microwave and hard X-ray bursts which show that the impulsive component of these flares was quite large.

The flares in table 8 at  $CMD < 70^\circ$  have a slight tendency toward large solar zenith angles ( $\chi$ ) which has a similar effect of attenuating the impulsive EUV emission relative to the slow emission in the ionosphere. This is because the latter emission is large in the 1-100 Å range which is more penetrating than the 100-800 Å range. The validity of this effect can be checked by studying SFD's observed at two locations where large solar zenith angles are involved at one location and fairly small angles at the other.

Some of the events neither fit the large CMD or  $\chi$  explanations, e.g., those of June 1, 1967 and February 11, 1970. They can perhaps still be explained by the same basic mechanism, i.e. by relatively high absorption of the impulsive EUV emission by the solar atmosphere along the line of sight through the active region. For example, filaments or prominences may act as an absorbing screen. However, Boulder H $\alpha$  observations for the active regions involved show no large filaments near the flare and no unusual limb prominence at either limb passage. Perhaps these two cases are better explained by the alternative explanation, i.e. the impulsive component of these flares was relatively weak.

Note that the flare of 0030 UT March 22, 1967, is one of the events listed in table 8. This event is the one for which the largest EUV enhancements observed by

satellite experiments has been reported in the literature (Hall and Hinteregger, 1969). It is also the one on which many of the entries in table 2 are based (the ones with 1's in the column for number of events observed). The present study suggests that the observed impulsive EUV flux may have been smaller relative to the slow emissions than for most flares. The main influence this may have had on the results in table 2 would be to reduce the  $R_f$ ,  $\phi_f$ , and  $R\phi$  values for certain wavelengths if these wavelengths encounter greater absorption in the solar atmosphere compared to other wavelengths. For example, the radiation at wavelengths within the hydrogen continuum probably encounters more absorption than the flare radiation at wavelengths just above this continuum.

#### 5.6.5.c Limb Flares

Besides the above studies of the CMD dependence of EUV flashes, a special study of large limb flares was made. Solar Geophysical Data was searched for importance 2 H $\alpha$  flares located at CMD  $\geq 80^\circ$  from October 1960 through June 1970, during Boulder SFD observations when the solar zenith angle was  $\leq 80^\circ$ . Only sixteen such flares were found and only four (25%) were accompanied by SFD's; whereas, from table 6, we would expect eight to have SFD's. Furthermore, the four SFD's were quite small. The SFD data were checked at the time of the other twelve events. Large absorption (SWF) was evident, which implies a large soft X-ray enhancement; but there was no evidence of a frequency deviation or EUV flash. These results also support the idea that the impulsive EUV emission of flares is relatively weak for limb flares; unfortunately the number of events involved is undesirably small, which may be partially a consequence of a tendency to underrate limb flares (Sawyer, 1967).

#### 5.6.6 Bright Impulsive H $\alpha$ Kernels

Several high quality photographs of impulsive bright kernels observed at the center of H $\alpha$  have appeared in the literature. Some particularly good ones are shown by Tallant (1970, fig. 1) with a video scan across the main kernel for the flares of 1859 and 2003 UT, March 20, 1966 and 1510 UT, March 21, 1966. The SFD's for the March 20th events are shown in figure 39 in appendix A. Films of the H $\alpha$  flare patrol show that the kernel measured by the video scan at 1859 UT flashed starting with the SFD spike at 1858. Similarly the kernel selected for the video scan at 2003 UT flashed at the same time as the SFD. The size of these kernels depends upon the intensity level used to define its boundary; the brightest part appears to be less than 10 arc-sec in diameter ( $< 7 \times 10^3$  km). Vorpahl and Zirin (1970) have reported that a hard X-ray pulse at about 2358 UT, September 11, 1968, was associated with the impulsive formation of a brilliant H $\alpha$  kernel in the H $\alpha$  flare. Their hard X-ray spike and brilliant H $\alpha$  kernel were concurrent with a small spike SFD. The kernel for the flare of October 24, 1966, shown in figure 18 was only several arc sec. in diameter. The cross section (parallel to the photosphere) of a EUV source region is therefore estimated to be about  $3 \times 10^{17}$  cm<sup>2</sup>. Large flares appear to consist of a number of such kernels. These kernels do not always appear to be round, sometimes they look like very small arches low down near the edge of spots.

Broadband  $H\alpha$  observations or observations in lines weaker than  $H\alpha$  (see sec. 5.5) appear to me to be more suitable for studying the optical kernels of flares than the center of  $H\alpha$ , because only the brightest portion of flares appear and because the sunspots are more clearly visible so that one can better locate the position of the flare kernels with respect to the sunspots.

The kernels are usually located at the edge of spots (see also sec. 5.4, 5.5, and 5.6.4), but no quantitative study of their location has been made. Their relation to Rust's (1969) magnetic anomalies has not been determined. Such anomalies would mean the existence of magnetic flux tubes having anomalously low rates of convergence toward the photosphere compared to surrounding tubes that converge into the main spot; hence, these tubes may permit dumping of energetic electrons into low density regions, namely the hot kernels, more so than most magnetic tubes through the flare region.

In section 4.5, the hypothesis was suggested that flares with quasi-periodicity in the time structure of hard X-ray, EUV and centimeter-wavelength radio emissions were cases where a series of flare kernels at different locations occurred in a nearly periodic time sequence. Janssens and White (1970) have published filtergrams spanning  $H\alpha \pm 4.1\text{\AA}$  with a scanning rate of  $0.295\text{\AA}$  and about 2 sec in time between frames for the quasi-periodic flare of August 8, 1968. Their selected published frames are not at precisely the right time to determine whether new spatially-separate emission regions are appearing in time with each major spike in the hard X-ray, EUV, or centimeter-wavelength radio emission with the possible exception of the one at 1816.6 UT, which is accompanied by several new small emission regions at  $H\alpha + 3\text{\AA}$  shown in their figure 1, frame 18.

Observations of  $H\alpha$  for the flare of 1620 UT June 11, 1969, which were made at 5 sec intervals at Sacramento Peak Observatory and provided for study through the courtesy of Mr. Howard Demastus, were studied to check our hypothesis of  $H\alpha$  kernels separated in time of occurrence and spatial location being associated with the EUV fine structure. This event was the highly structured one discussed in section 4.5 and shown in figure 10. The pulses in this event are quite distinct and separated enough in time compared to  $H\alpha$  photographic observations that if the above hypothesis were correct, we would expect to see small bright  $H\alpha$  kernels popping off one at a time at different locations at the time of each EUV pulse. This was not the case; hence, this hypothesis is inadequate for explaining some quasi-periodic EUV bursts. The  $H\alpha$  observations included an off-band sweep so that the bright  $H\alpha$  cores were easily seen. Several small cores were present but were not very impulsive. The impulsive portion of the  $H\alpha$  flare spread along a tear-drop shaped arch where the pointed tail of the tear-drop pointed into the major sunspot of the flare region. The impulsive flare emission started at the blunt end of the "tear-drop" arch, then shot along one side of it toward the spot, then along the other side, etc. Hence, there were impulsive  $H\alpha$  emissions; but separate bright cores could not be identified with each EUV pulse.

In summary, impulsive H $\alpha$  emissions are observed in association with EUV flashes. Sometimes these H $\alpha$  emissions appear as explosive expansions of the H $\alpha$  flare area (the explosive phase, see sec. 5.6.4) sometimes as impulsive stationary bright kernels, and sometimes as bright rapidly-spreading arch structures. Apparently no one simple spatial structure will suffice to explain the impulsive H $\alpha$  emissions associated with EUV flashes. Perhaps a reasonably small set of basic types of structures will suffice. Further study of the impulsive optical-emission regions associated with EUV flashes or hard X-ray bursts should be made, including classifying the types of source regions and quantitatively studying the relationship between each type and the sunspots and magnetic field of the flaring active region.

### 5.7 Relation to Surges, Sprays and Eruptive Prominences

A surge is a stream of chromospheric gas that shoots upward from an active region along the magnetic field lines, slows to a peak extension, dims, and may fall back along the field lines. A spray shoots out more rapidly, seemingly breaking the bonds of the active region magnetic fields and escaping off into space. Eruptive prominences involve pre-existing prominences that start ascending slowly, usually in arch form, and then accelerate to high velocities at a later phase some ten to twenty minutes later. Sprays reach velocities of 1000 km sec<sup>-1</sup> in about 3 minutes while eruptive prominences do so in about 30 minutes (Valnicek, 1964). These three phenomena, surges, sprays and eruptive prominences, appear as bright emissions when seen on the limb and sometimes as dark material when observed in H $\alpha$  on the solar disk.

The sprays and surges studied were those tabulated by Smith (1968), Zirin and Werner (1967), and Zirin (1969). Table 9 shows the association of SFD's with surges and sprays when the latter events were observed during daylight at Boulder and SFD observations were being made. An SFD was assumed to be associated if its start time or end time was within 10 minutes of the spray or surge start-of-ejection time.

Table 9. Association of SFD's with Surges and Sprays

Number of Surges	Number of Sprays	
3	13	Events Accompanied by SFD's
37	17	Events Without SFD's
40	30	Total Number of Events

There appears to be little relationship between surges and SFD's. When the events are associated, the SFD's were very small; and the timing of the events are in poor agreement with a tendency for the surge to follow the SFD. These results imply there is little or no 1-1030 $\text{\AA}$  radiation enhancement associated with the surges studied compared to 10<sup>-2</sup> ergs cm<sup>-2</sup> sec<sup>-1</sup> above the earth's atmosphere. If one looks at the H $\alpha$  sun, very small surges are rather common. The above comparison does not take into account how large the surges are; unfortunately, surges are not routinely classified by size. The above study is believed to be dominated by small surges.

For all the SFD's for which the author has studied the H $\alpha$  flare patrol films, few were accompanied by surges, and in those cases the surge occurred after the SFD.

The association between sprays and SFD's is fair according to table 9, i.e., 43% of sprays are accompanied by SFD's. Furthermore, the spray start-of-ejection time agrees with the start time of the SFD to within less than one minute on the average. Smith (1968) points out that some sprays are related to the explosive-phase of flares. Smith further argues that sprays and the explosive-phase are not always part of the same phenomena, i.e., that some explosive flares are not accompanied by sprays and vice versa. In section 5.6.4, we have seen that SFD's, or flashes of EUV emission, are closely connected with the explosive phase of H $\alpha$  flares. In sections 5.1 and 5.6.5, we reported that EUV bursts from limb flares are anomalously low in intensity or that SFD's are relatively insensitive to limb flares. Conversely, sprays are most easily observed at the limb. Therefore, the association of sprays and EUV bursts is probably higher than indicated above, i.e., the opposing "seeing" bias of sprays and SFD's probably cause the apparent association to be weaker than their real association.

Eruptive prominences are very weakly associated with SFD's. Again, eruptive prominences are mainly limb events and SFD's are relatively insensitive to limb flares. Furthermore, prominence eruptions are relatively slow events compared to the time scales of SFD's, and SFD's are quite insensitive to slow events. For disk events, e.g., the filament ejection of 1830 UT, September 3, 1962 (Nolan et al. p 20, 1970), the corresponding SFD is concurrent with the associated impulsive H $\alpha$  flare and appears less directly related to the filament ejection. The slowly rising loop structures observed after the flash phase of some large flares are also weakly associated with SFD's.

Reeves et al. (1970) have reported on OSO-6 EUV observations of a limb surge on September 15, 1969, which shows that with the spatial resolution and sensitivity to small EUV fluxes presently achievable in satellite experiments, EUV surges can be observed. However, considering the slowness of surges and the minimum 10-1030 $\text{\AA}$  flux enhancement detectable by SFD observations ( $\sim 10^{-2}$  ergs  $\text{cm}^{-2}$   $\text{sec}^{-1}$  at 1 AU), the 10-1030 $\text{\AA}$  emission from surges is not observed in SFD data.

### 5.8 Microwave Bursts

Strauss et al. (1969), Basu and Chowdhury (1968), and Chan and Villard (1963), denoted respectively by S, BC and CV below, have studied the relationship between tabulated SFD and microwave radio bursts; their results are as follows:

- (1) Radio bursts at frequencies below 500 MHz and gradual rise and fall events at higher frequencies are poorly correlated with SFD's (CV).
- (2) Impulsive radio bursts of frequencies above 500 MHz are fairly well correlated in occurrence with SFD's. More than 30% of SFD's are accompanied by radio bursts (S, BC, and CV) and about 46% of impulsive 2800 MHz bursts are accompanied by SFD's (CV).
- (3) The correlation of occurrence of SFD's and microwave bursts increases with the peak amplitude of the radio burst (BC, CV, S).
- (4) The correlation of occurrence increases with increasing frequency of the radio burst observation for radio frequencies above 600 MHz to a fairly flat peak at about 5 GHz (S).
- (5) The start times of SFD's and impulsive radio bursts at frequencies greater than 600 MHz are correlated; most events having a difference in start times less than 2 min (BC, S).

- (6) Solar radio bursts at 4995 MHz (in radio flux units) and SFD's (in Hz) follow practically the same inverse square intensity distribution law (S).
- (7) The correlation of occurrence of SFD's and microwave bursts depends on the spectrum of the radio burst. The correlation is small for radio bursts with spectra that decrease with frequency above 600 MHz; fairly large for radio bursts with spectra that increase with frequency in the 600-8800 MHz range, and largest for radio bursts with spectra that peak in the 600-8800 MHz range (S).

Studies of the detailed time dependence of the 10-1030Å flux enhancement deduced from SFD's in comparison to that of microwave bursts (e.g. Donnelly, 1968c) often (but not always) exhibit similar (but not identical) fine time structures during the SFD or during the early portion of the radio burst. The agreement in fine structure generally improves with increasing frequency of the radio burst observation and the transition from dissimilar to similar time structure usually occurs in the 2-5 GHz range, depending on the particular event involved.

Richards (1970) studied the time dependence of EUV bursts observed by Hall and Hinteregger (1969) in comparison with microwave bursts. He found good agreement in start times and times for the first peak of EUV flares and centimeter wavelength radio bursts, but later peaks did not match up well. He also found that after the initial peak, the EUV bursts generally exhibited smoother structure and longer decay times than the radio bursts. More EUV measurements of flares with high time resolution should be made and studied quantitatively in comparison to radio bursts.

The peak intensity of the 10-1030Å flux enhancements deduced from SFD data for the same events studied in comparison to hard X-ray bursts by Kane and Donnelly (1970) were also studied in comparison to the associated microwave bursts. The average ratio of microwave flux ( $\text{ergs cm}^{-2}\text{sec}^{-1}$ ) in the 3-10 cm wavelength range to the 10-1030Å flux enhancement deduced from SFD's is about  $2 \times 10^{-8}$  at the time of the impulsive peak of the 10-1030Å enhancement (see table 2). The regression diagrams in figures 25-30 exhibit an amount of scatter similar to that of the corresponding diagrams of hard X-ray peak flux versus peak radio flux and, for frequencies  $\geq 2695$  MHz, similar to that of the diagram of hard X-ray flux versus 10-1030Å flux enhancement (Kane and Donnelly, 1970). The 606 MHz and 1415 MHz peak fluxes are poorly correlated with the 10-1030Å flux enhancements; the two types of data are poorly fit by a linear relation. The correlation coefficient jumps to about 0.8 as the radio burst frequency increases to 2695 MHz and then levels out and remains high as the frequency increases to 10 GHz. Similarly, a linear relation fits the peak radio flux and 10-1030Å flux enhancement fairly well at frequencies of 2695 MHz and higher. There is slight evidence of a dependence of the ratio of radio flux to 10-1030Å flux enhancement on the central meridian distance (CMD) of the associated H $\alpha$  flare, i.e. a relatively large ratio for limb flares compared to disk flares. However, any such CMD dependence is far less evident than the CMD dependence of the ratio of the hard X-ray flux to 10-1030Å flux found by Kane and Donnelly (1970). There are only 46 events involved in figure 27. Radio flux measurements are available for far more events than hard X-ray measurements are available. Further study should be made of the relation between microwave radio bursts and 10-1030Å flux enhancements as a function of radio frequency, radio spectra, and CMD of the associated H $\alpha$  flare.

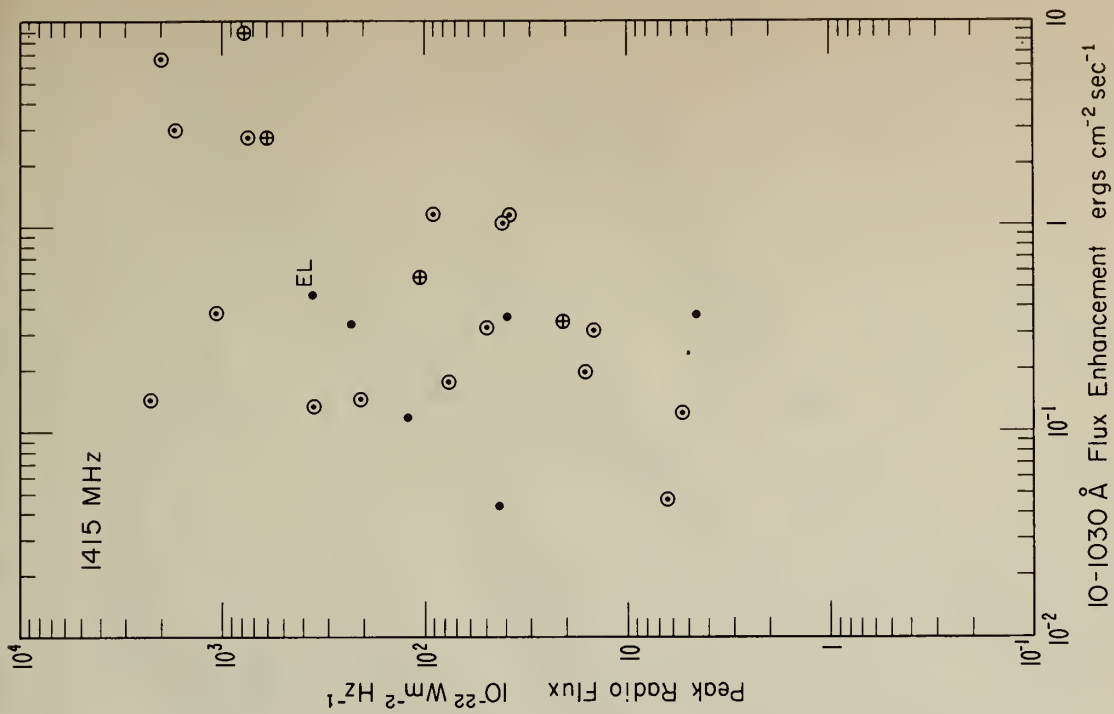


Figure 25. Peak 606 MHz emission versus peak 10-1030 Å flux enhancement.

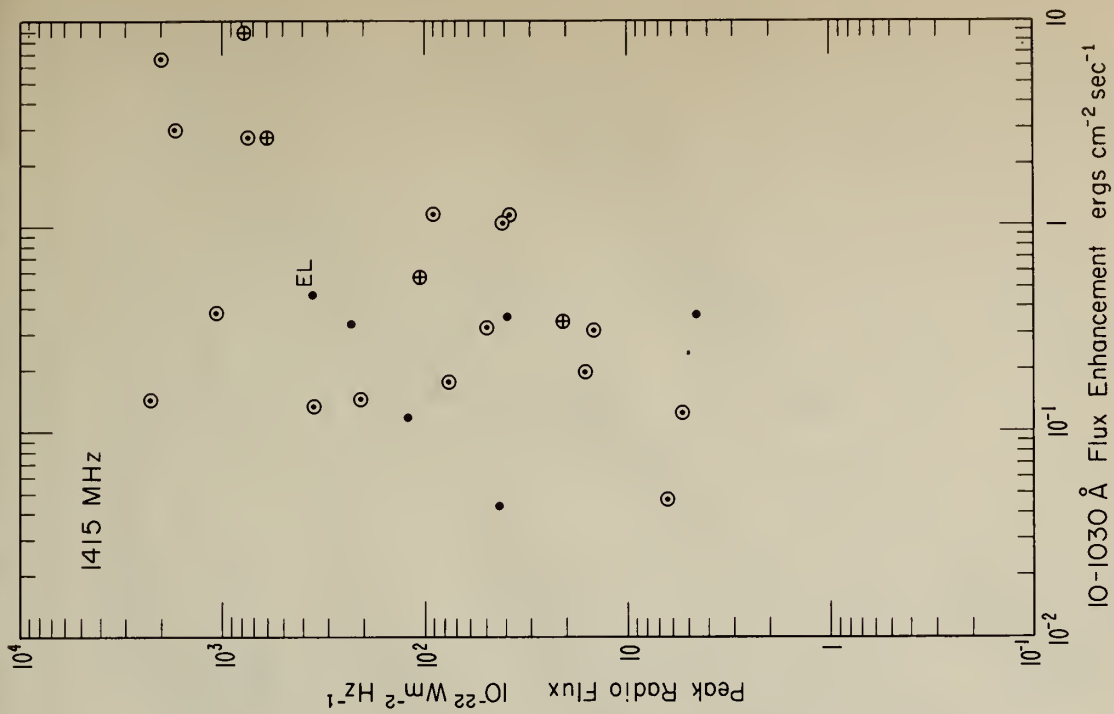


Figure 26. Peak 1415 MHz emission versus peak 10-1030 Å flux enhancement.

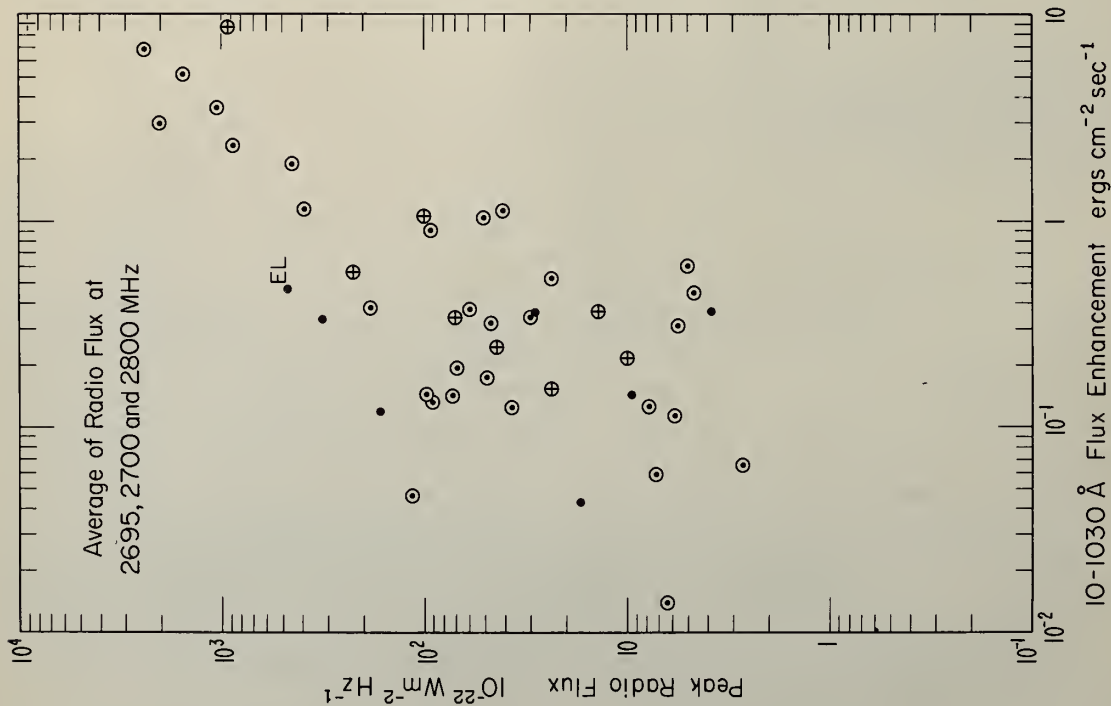


Figure 27. The average of peak radio emissions observed at 2695, 2700, and 2800 MHz versus peak 10-1030 Å flux enhancements.

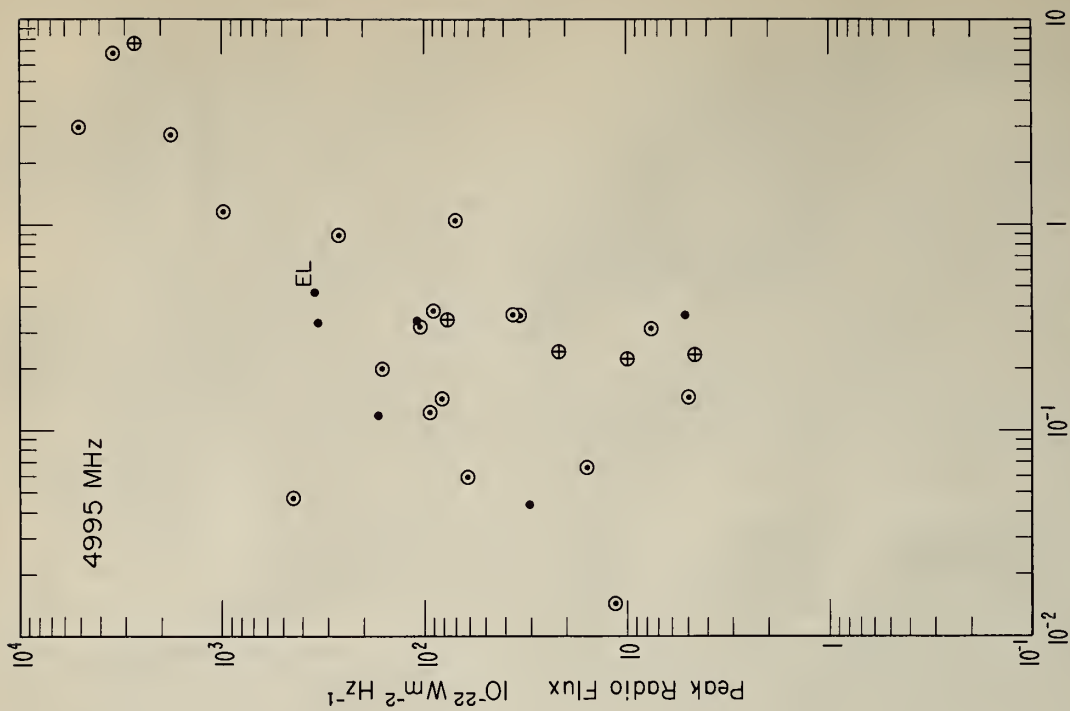


Figure 28. Peak 4995 MHz emission versus peak 10-1030 Å flux enhancement.

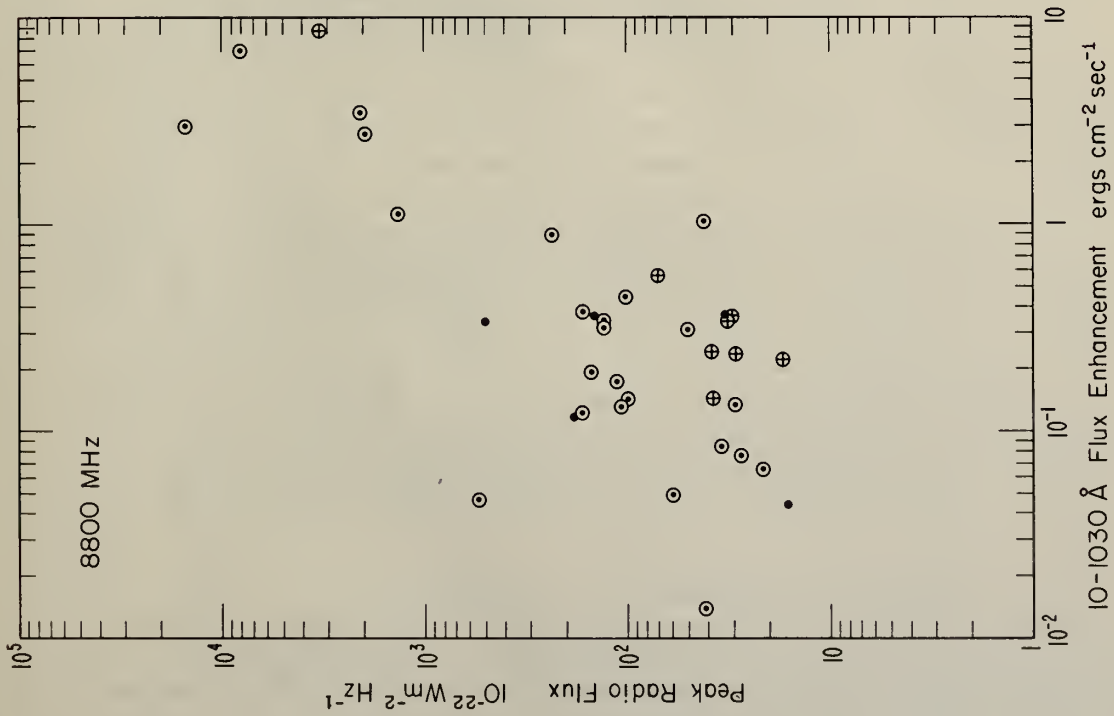


Figure 29. Peak 8800 MHz emission versus peak 10-1030 Å flux enhancement.

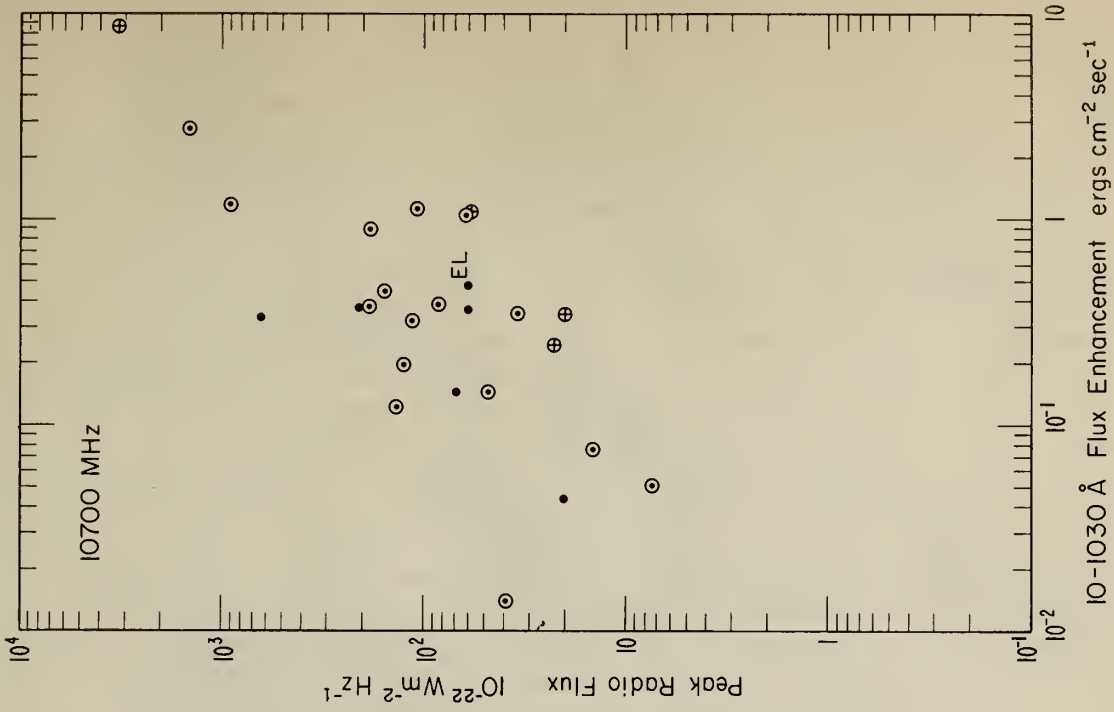


Figure 30. Peak 10700 MHz emission versus peak 10-1030 Å flux enhancement.

## 6. SFD'S FOR FAMOUS FLARES

Over the past several years, a number of solar flares and their interplanetary and terrestrial effects have been studied by numerous scientists in many different disciplines. In this section, we present previously unpublished SFD observations of some of these famous events. Table 10 lists references to other studies of the same flares. The peak EUV flux enhancement for these events is given in table 4 in section 4.2. All the SFD's in table 10 are very large events.

Figure 31 illustrates a type of distortion in the shape of  $\Delta f(t)$  for certain transmission frequencies that occurs in such large events, namely, the ratio  $\Delta f(t, 5.1 \text{ MHz})/\Delta f(t, 9.9 \text{ MHz})$  decreases with time during the event. The 5.1 MHz observations involve a near-vertical path while the 8.9, 9.9 and 11.1 MHz observations involve a 1290 km oblique path. This distortion is caused by the height of reflection for 5.1 MHz lowering considerably (10's of km) during the flare because the flare-induced electron-density enhancement in the E and F1 regions is comparable to the preflare electron density. Lowering the height of reflection reduces the SFD's sensitivity to EUV radiation. The distortion is much greater for 4 MHz. The oblique paths are much less distorted, partly because their height of reflection lies above most of the flare-induced ionization enhancement at a height where the percentage increase in ionization is relatively small, and partly because changes in the equivalent vertical incidence frequency minimize the change in height of reflection. As the electron density increases, the height of reflection decreases but the ray-path take-off angle of elevation and equivalent vertical-incidence frequency ( $f_v$ ) increase for these oblique paths reflected in the F2 region of the ionosphere. Increasing  $f_v$  partially compensates for the increasing electron density resulting in a smaller decrease in the height of reflection than for a vertical path having the same frequency as the preflare value of  $f_v$ .

The July 8, 1968 SFD in figure 33 is a good example of an SFD with much fine structure. All the SFD's discussed in this section were part of the fine time-structure study of section 4.5. The three SFD records in figure 34b are almost identical even though their propagation paths are different, which shows how self consistent the SFD data are for small changes in transmission frequency or path length. The pre-flare ionosphere near Boulder was relatively quiet for this event, it is not unusual for small SFD's observed on near vertical paths to suffer distortions from ionospheric variations unrelated to flares. Oblique paths are less influenced by local ionospheric irregularities and are therefore less influenced by these distortions. However, the oblique records for the April 21, 1969 SFD in figure 35 suffer a related type of distortion in that the traces are fuzzy. The ionosphere at the midpoint of the Illinois to Boulder path was apparently disturbed while the ionosphere over Boulder was relatively calm, an unusual situation. The fuzziness of the oblique trace is believed to be a consequence of an averaging process of local irregularities near the midpoint of the propagation path for the small bundle of rays received in Boulder.

## 7. CONCLUSIONS, RECOMMENDATIONS, AND SPECULATIONS

Observations of SFD's have provided considerable information about EUV flashes of solar flares. We have learned (sec. 5.1 and 5.8) that EUV flashes are closely related to hard X-ray bursts and 3 cm radio bursts; the quantitative relation between the EUV, radio, and hard X-ray energy fluxes has been determined (to within about

Table 10. Famous Events

Date	Approximate SFD Peak Time UT	References to Studies of SFD's	References to other studies of the same flare or the associated geophysical effects
07/07/66	0027	Donnelly (1968b, 1969e)	Stickland (1969) and references therein, and Richmond (1970).
08/28/66	1527	Donnelly (1968a, c)	Svestka and Simon (1969) and references therein, and Richmond (1970).
05/21/67	1924	Figures 31 and 32 of this report.	Garriott et al. (1967, 1969), Angle (1969), Malville and Tandberg-Hanssen (1969), McIntosh and Donnelly (1970), and Richmond (1970).
05/23/67	1838	Donnelly (1969d)	Lincoln (1969) and references therein. Malville and Tandberg-Hanssen (1969), McIntosh and Donnelly (1970), Richmond (1970) and Garriott et al. (1967, 1969).
05/23/67	1938	Donnelly (1969d)	Lincoln (1969) and references therein, Malville and Tandberg-Hanssen (1969), and Garriott et al. (1967).
07/08/68	1710	Figure 33 of this report.	Fortini and Torelli (1970), and Richmond (1970).
08/08/68	1816	Donnelly (1969c)	Parks and Winckler (1969a, b), Janssens and White (1970).
03/12/69	1740	Figure 34 of this report, McIntosh and Donnelly (1970), Solheim (1970).	McIntosh and Donnelly (1970).
04/21/69	2009	Figure 35 of this report, Solheim (1970).	

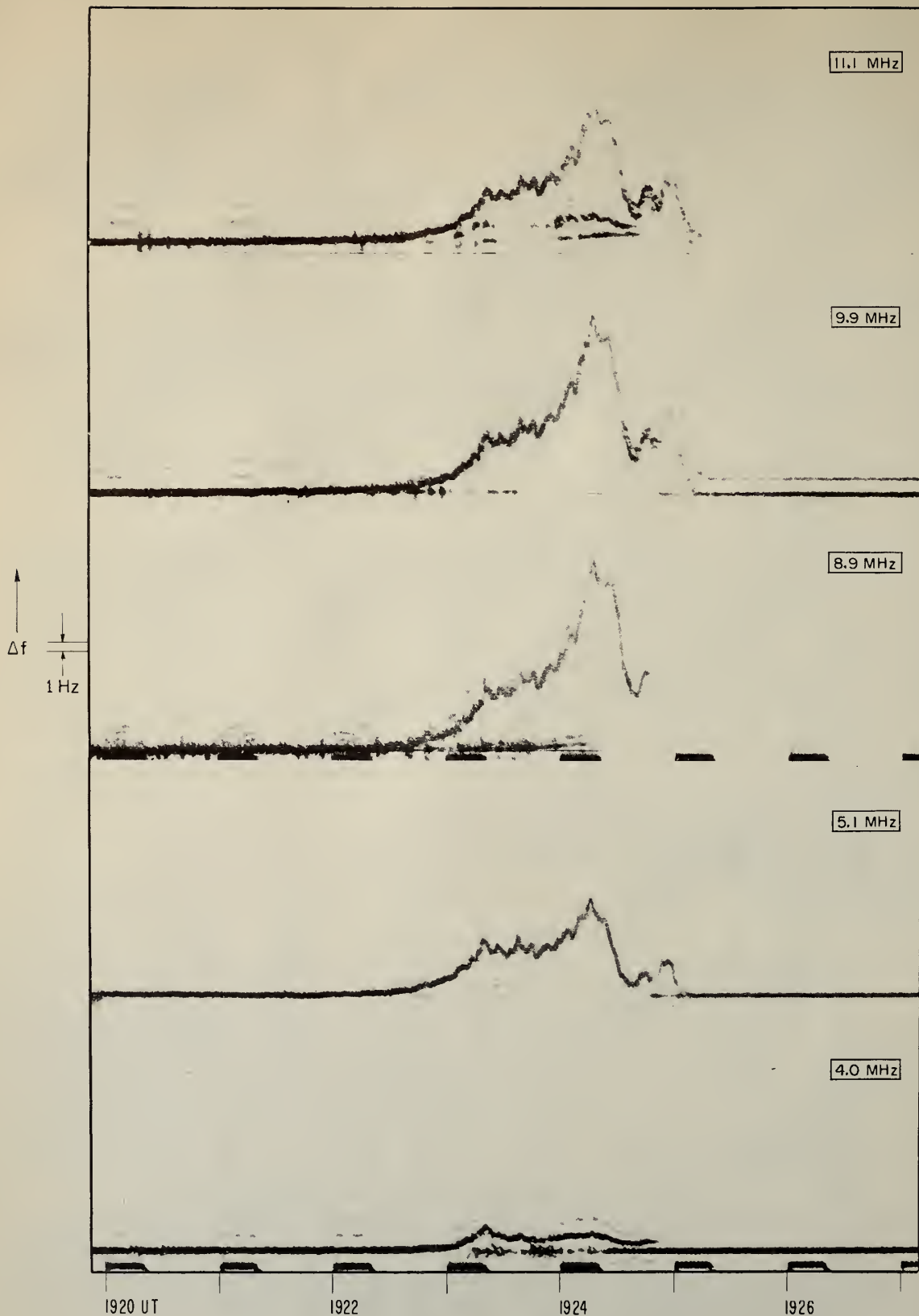


Figure 31. Boulder SFD observations for the flare of 1924 UT May 21, 1967.

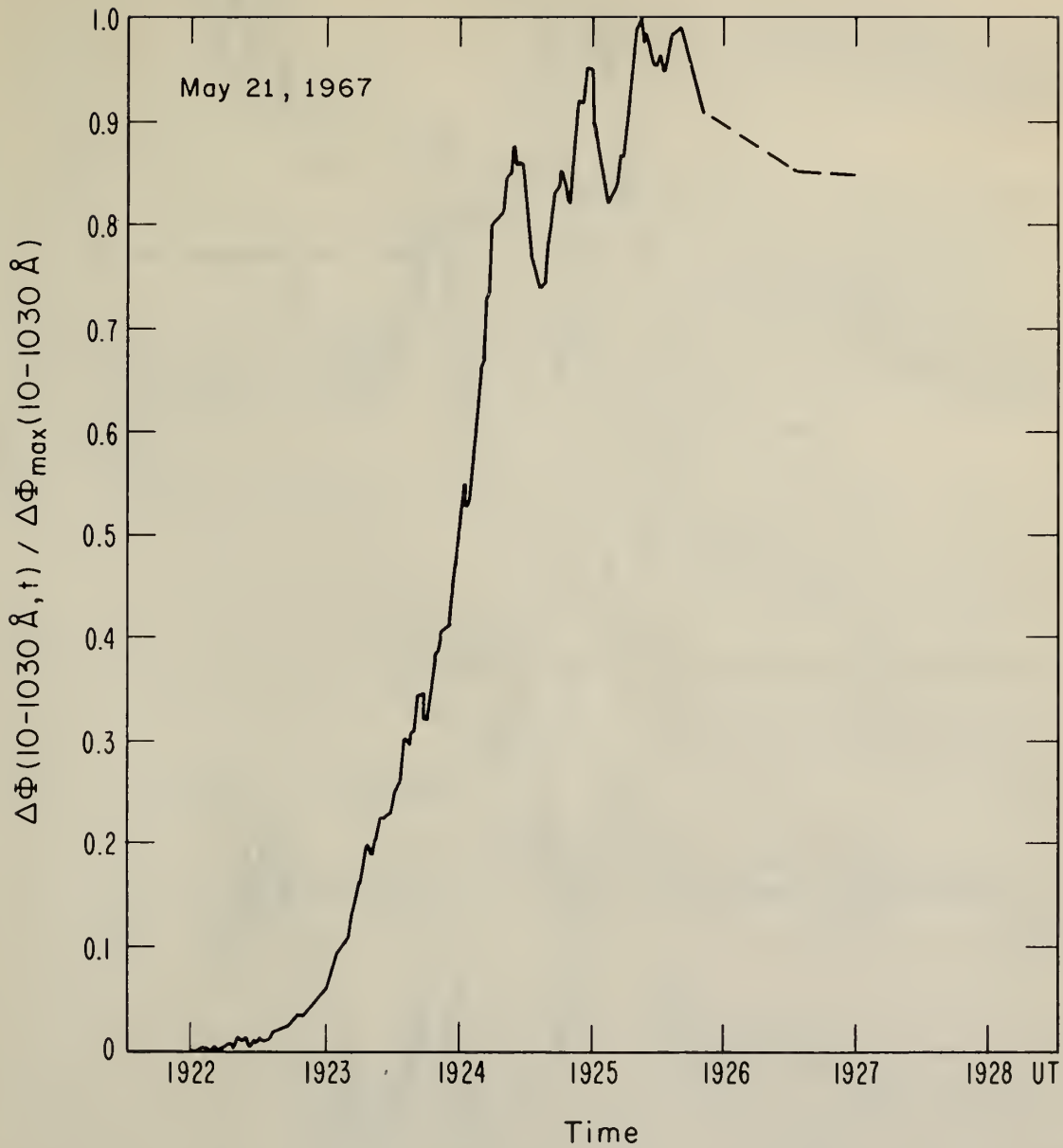


Figure 32. Normalized 10-1030 $\overset{\circ}{\text{A}}$  flux enhancement as a function of time for the flare of 1924 UT May 21, 1967.

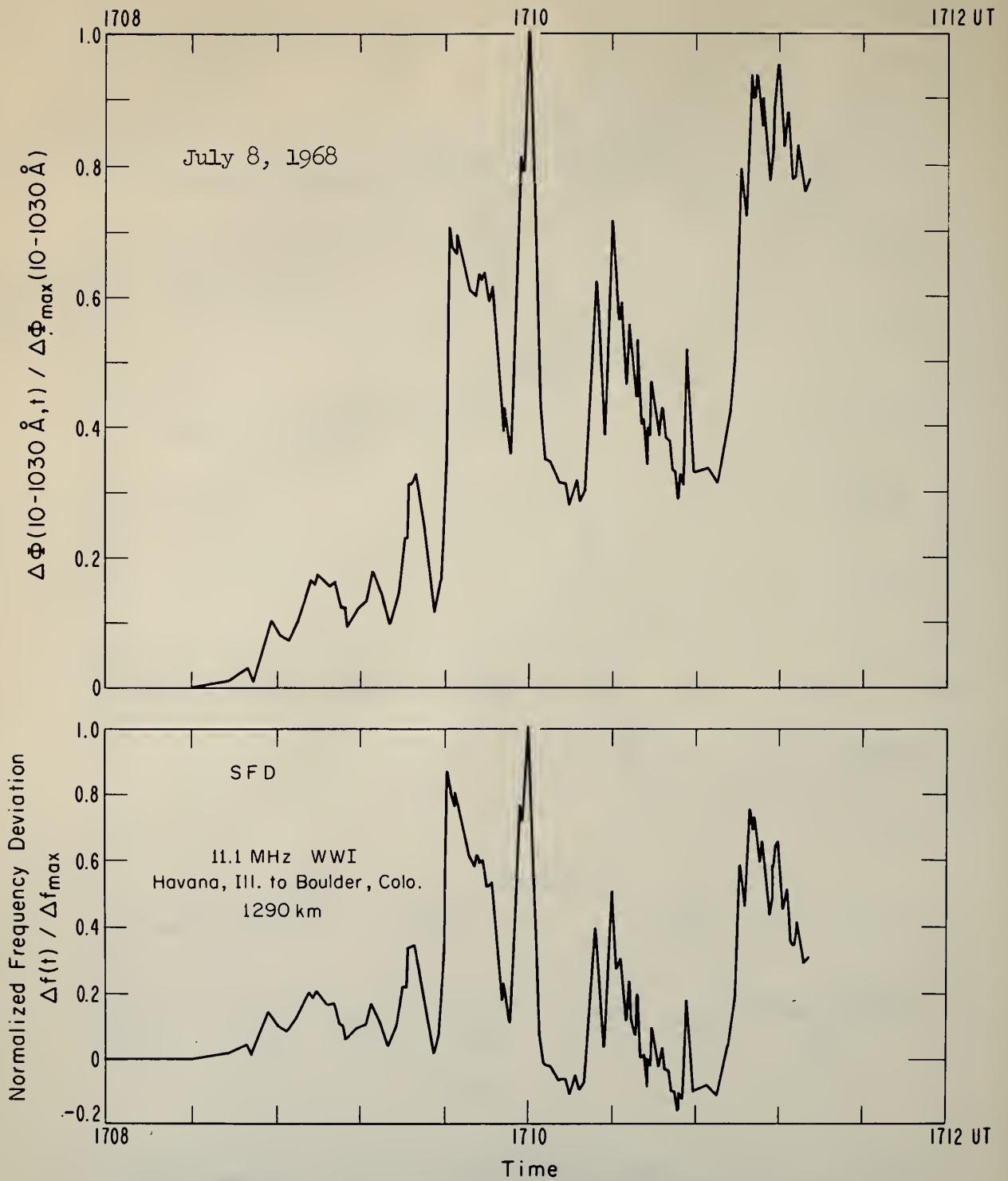


Figure 33. SFD and 10-1030 $\text{\AA}$  flux enhancement as a function of time for the flare of 1710 UT July 8, 1968.

March 12, 1969

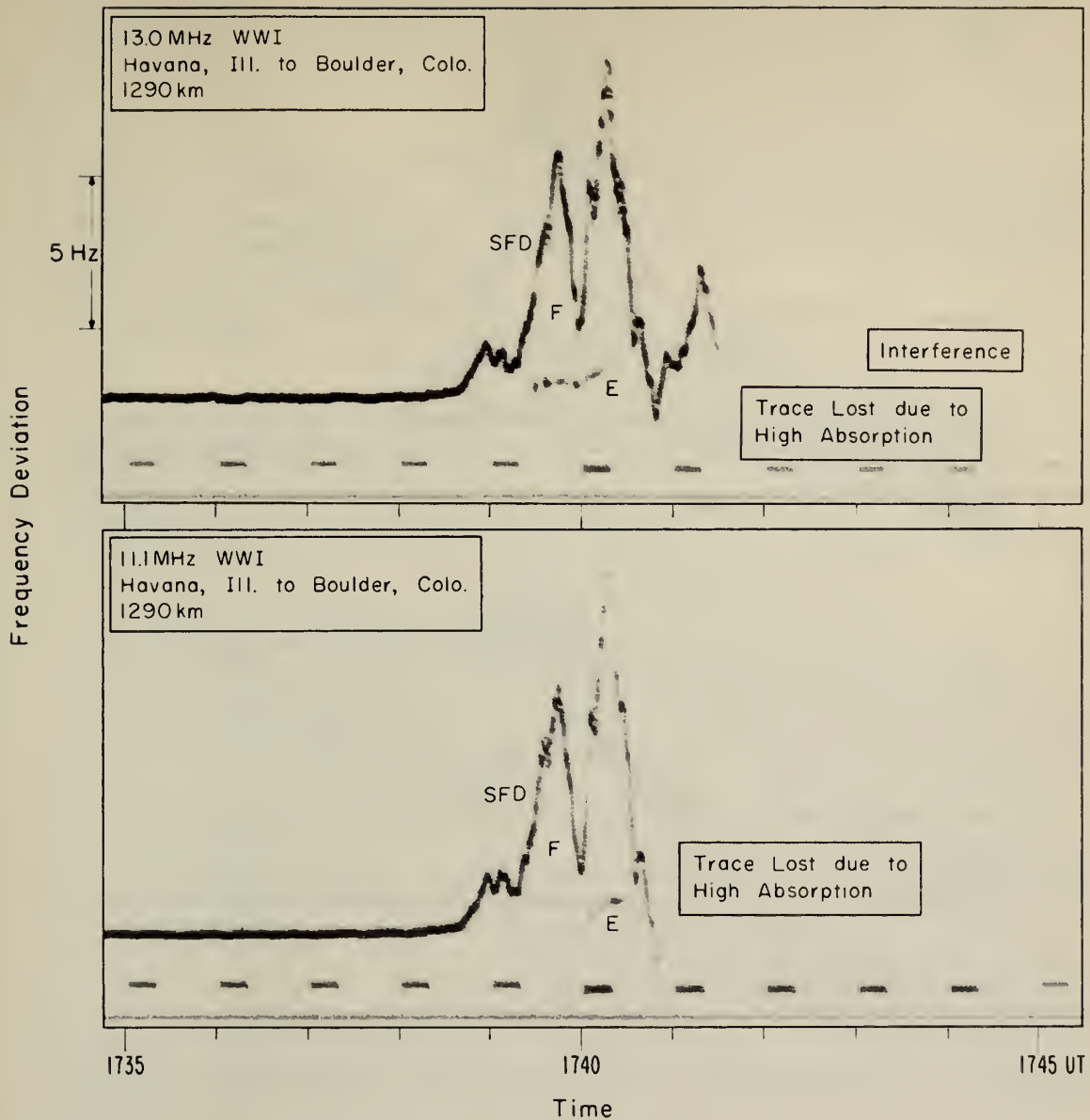


Figure 34. Boulder SFD observations for the flare of 1740 UT March 12, 1969 (a) Oblique-Path Observations  $WD(10-1020\text{\AA}, t)$  for this event is presented in McIntosh and Donnelly (1970).

March 12, 1969

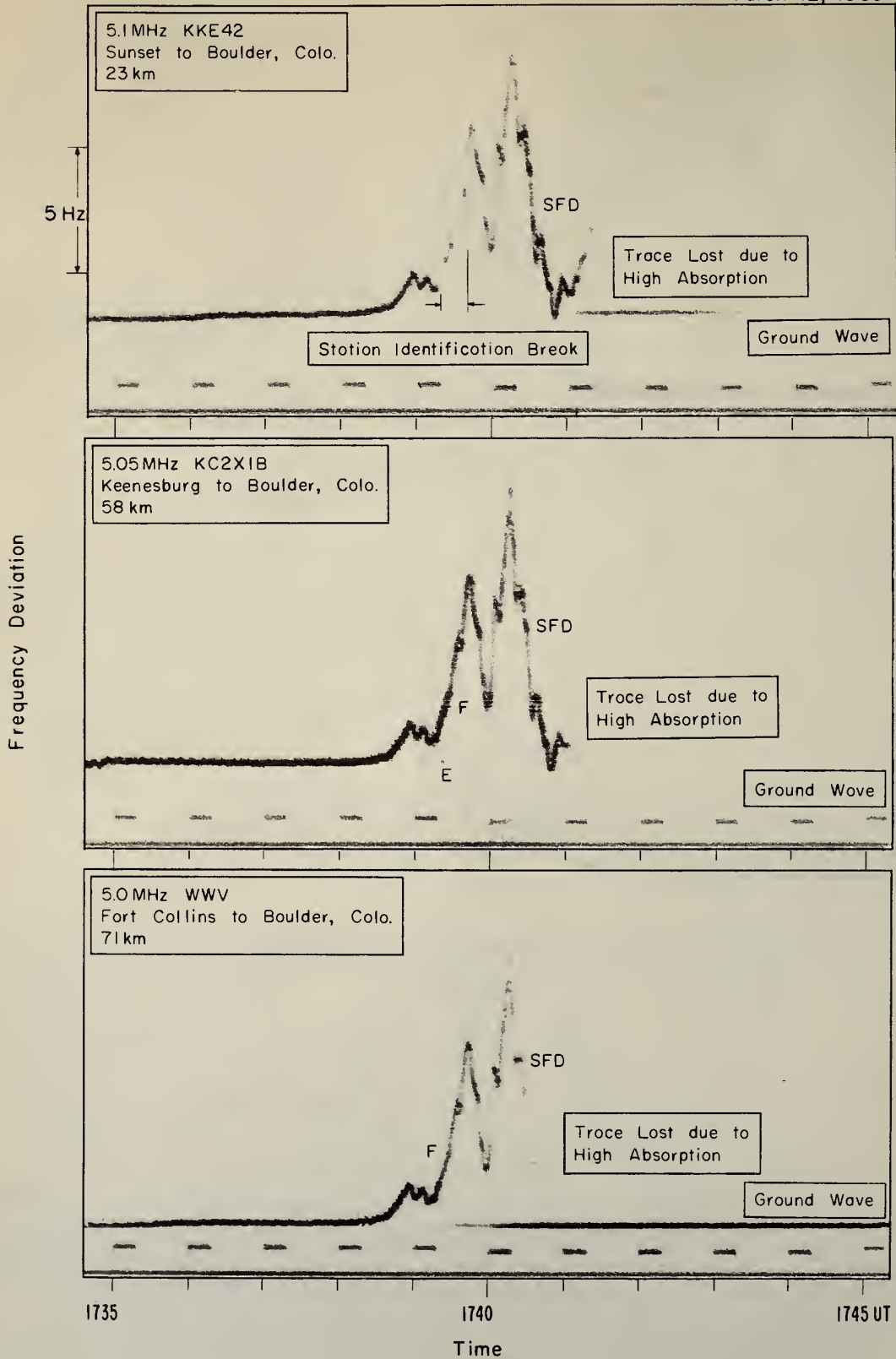


Figure 34. (b) Near Vertical-Incidence Observations.

April 21, 1969

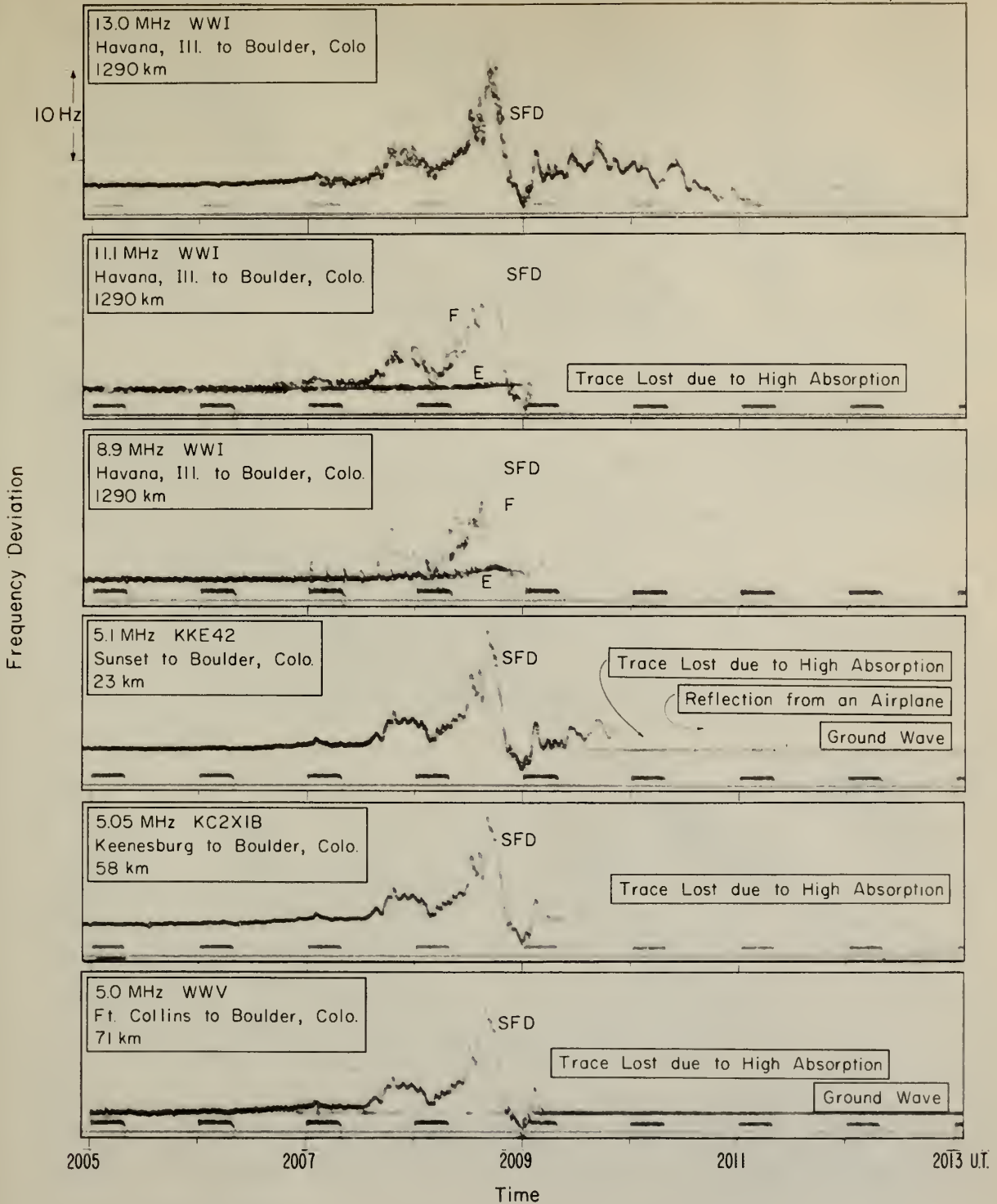


Figure 35. Boulder SFD observations for the flare of 2009 UT April 21, 1969  $\Delta\Phi(10-1030A, t)$  for this event is discussed in section 5.6.6.

the absolute accuracy of the 10-1030Å flux enhancements deduced from SFD data, namely a factor of 4). Large EUV flashes are closely related in time and occurrence with white-light flare emission and the relative energy fluxes of these emissions are roughly comparable (sec. 5.4). Figure 14 summarizes our present picture of the time relation of EUV flashes with respect to other flare radiations, which is essentially that of DeJager (1964).

Some information of the spectrum of the 10-1030Å flashes has been learned from comparisons of SFD data with satellite EUV measurements. These results (sec. 3) indicate that line emission from the more abundant solar constituents (H, He, C and O) contribute significantly to the 10-1030Å flashes; but we do not know yet whether continuum emission other than radiative recombination continua contributes significantly to 10-1030Å flashes. Further information on the spectrum of the 10-1030Å flash will require more satellite observations with high wavelength resolution.

Data on SFD have shown that the relative intensity of EUV flashes varies with the central meridian distance of the associated H $\alpha$  flare location (sec. 5.1, and 5.6.5). Also the EUV flash appears to be associated with small impulsive portions of the H $\alpha$  flare that are quite bright and usually located near the edge of sunspots (sec. 5.6.6, see also sec. 5.4 and 5.5).

Recommendations for further study of SFD's have been made throughout the text; however, further experimental advances of our knowledge of EUV flashes from solar flares will probably depend upon satellite measurements, since any experimental advances will probably require high wavelength and/or spatial resolution as well as high time resolution. Measurements of SFD should, nevertheless, still be quite helpful into the next solar cycle because their high time resolution of 10-1030Å flashes should inexpensively provide useful information which is supplementary to satellite measurements with high wavelength or spatial resolution, since such measurements usually result in low time resolution compared to the fine structure of EUV flashes (see sec. 4.5).

Believing that the interaction of experiment and theory are vital for the vigorous growth of our knowledge, what is probably needed more than refinements of present EUV satellite experiments is more theoretical work to explain present observations and to determine which experiments will be decisive in evaluating alternative theoretical explanations. Figure 14 is a first step toward a theoretical examination of the complex phenomena of solar flares, namely separating the phenomena into parts. It is quite an insufficient breakdown since it doesn't include the all important particle radiation, but it is probably sufficient for theoretical examination of EUV flashes. Our second step, and a logical extension of the study of the experimental results of SFD's, is to try to develop a theoretical model for the source region of the impulsive EUV emissions.

A model for the EUV emissions must include impulsive line emission like those that have been observed (see table 2). It must explain the following:

- (1) the observed detailed time agreement between the EUV flash and hard X-ray bursts and their energy flux ratios (sec. 5.1),
- (2) the similar time dependence of white light emission with comparable energy flux (sec. 5.4),

- (3) the similar time dependence of microwave flashes, their energy flux ratios, and dependence on microwave spectrum (sec. 5.8),
- (4) the EUV flash dependence on the central meridian distance of the flare (sec. 5.1, 5.6.5), and
- (5) the smallness and location of the associated H $\alpha$  impulsive kernels, an extensive task!

Fortunately, much work has been done in attempts to explain the relation between the hard X-ray burst and centimeter radio burst (e.g., Takakura, 1969). Hence our attempts at a model for the EUV source will build on these works.

Four models for the impulsive EUV source region (component A) are proposed for consideration. They are illustrated in figure 36. Detailed arguments for or against these models will be the subject of a later report. Model A has been proposed by Kane and Donnelly (1970) to explain the relationship between hard X-ray bursts and EUV flashes. In this model, the over-all time dependence of the impulsive burst, including its decay, reflects the time dependence of the unknown mechanism that energizes the particles. Each energetic electron quickly loses its energy in a time short compared to the duration of the impulsive burst.

Model B is similar to A except that the mechanism that creates the energetic electrons operates during the rise of the hard X-ray burst and the decay is controlled by the electron loss from the trapping region. The average electron stays at a high energy until appropriately deflected so that it escapes the magnetic bottle and rapidly loses its energy in the dense chromosphere.

Model C employs a continuum emission mechanism for the EUV emission. Bhatia and Tandon (1970) have suggested synchrotron emission as the cause of the EUV emission. This does not necessarily conflict with Hall and Hinteregger's (1969) observations of line emission contributing to the EUV flash because this continuum emission would excite the underlying or surrounding chromosphere, which would subsequently emit EUV line emission.

Model D is an attempt to connect with Nakagawa and Hyder's (1969) flare model wherein infalling material sets up a shock wave that hits the lower chromosphere. I favor model A but all four models should be considered further. An explanation of the EUV emission is not too important a goal in itself; but, if only one suitable explanation can be found, then in effect, we will have better defined the characteristics of the energetic particles involved in this portion of the flare. This in turn better defines what the particle acceleration mechanisms within the flare are required to do. The physical processes involved in accelerating particles and the mechanism that triggers the acceleration are major goals of solar flare research.

The EUV flash should provide important restraints on the physical processes involved in the impulsive component of flares because the EUV energy flux is so large, at least with respect to hard X-ray or microwave radio emission (see table 2). However, the total energy radiated in the EUV flash is not too large compared to the  $10^{32}$  ergs estimated for the total energy of the largest flares. Assuming  $10 \text{ ergs cm}^{-2} \text{ sec}^{-1}$  at 1 AU for the 10-1030 $\text{\AA}$  wavelength range for the largest EUV flashes (see table 4), assuming a  $10^3$  sec duration (see fig. 9), and assuming uniform EUV

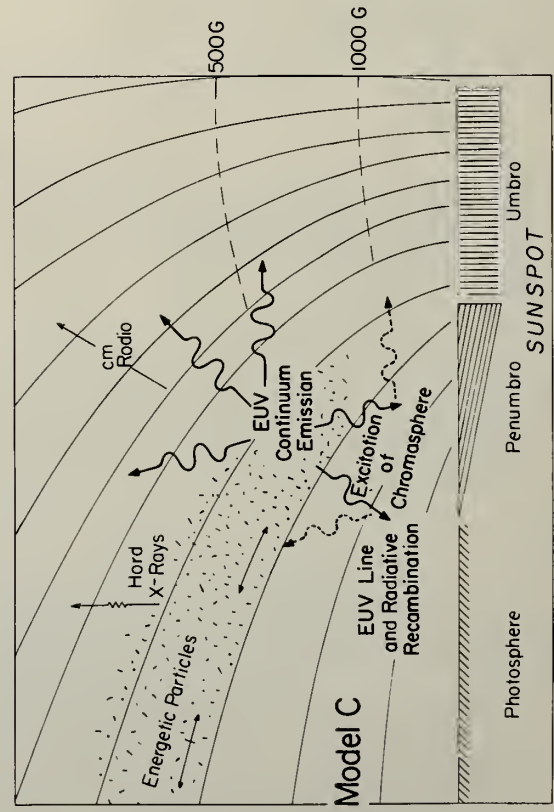
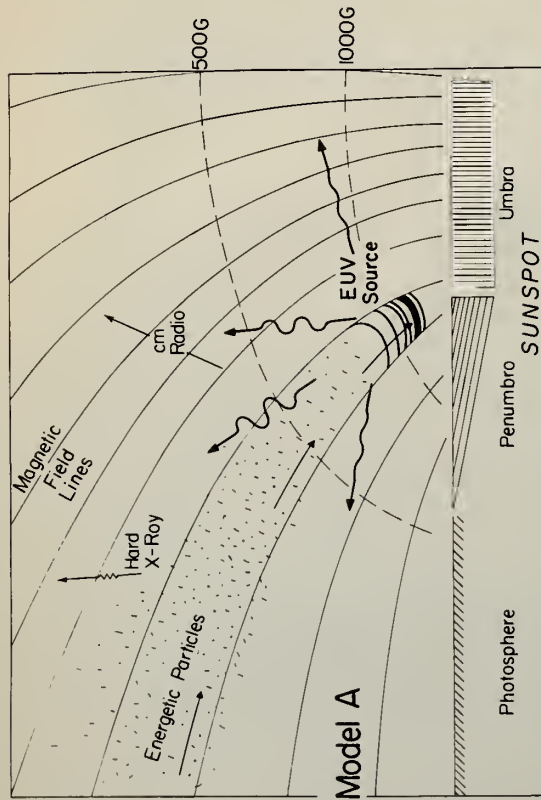
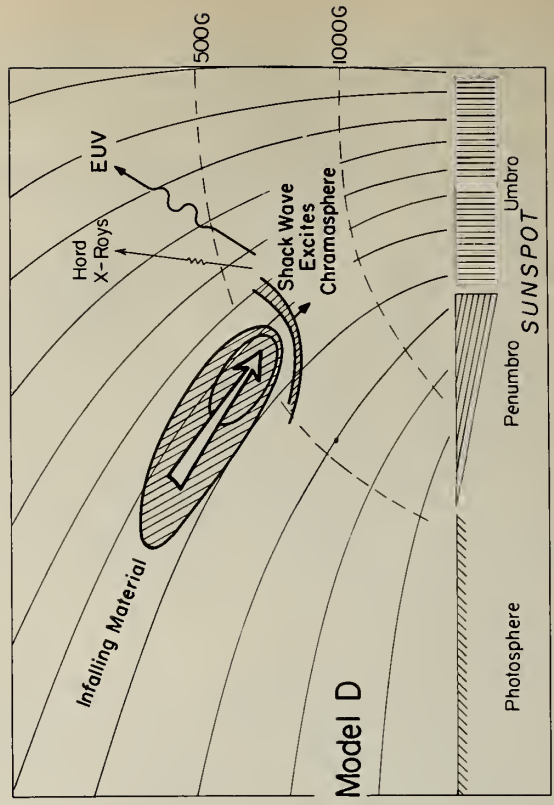
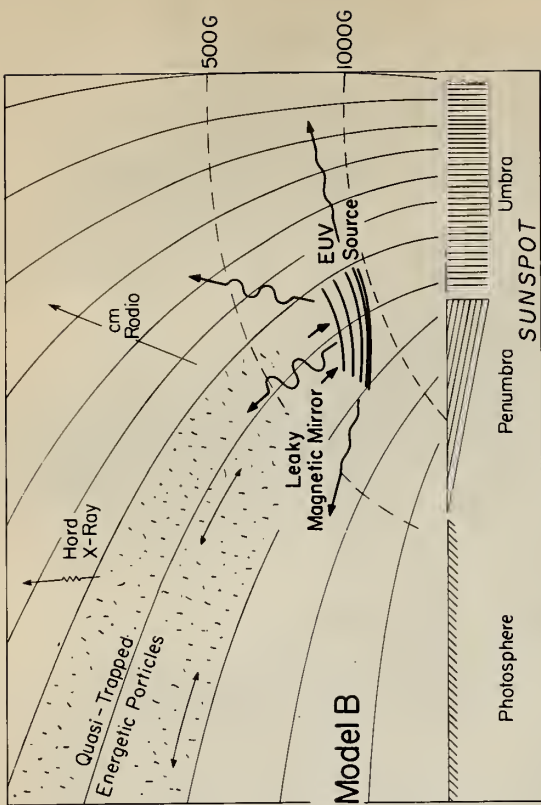


Figure 36. Models for the impulsive EUV flash

emission over a hemisphere, the total energy radiated in the 10-1030Å flash is only  $\leq 10^{31}$  ergs. However, the estimates of  $10^{32}$  ergs for the total flare energy probably relate primarily to the slow component of flares; and the energy of the EUV emission may be a major portion of the impulsive component of flares.

#### 8. ACKNOWLEDGEMENTS

I am grateful to Dr. Kenneth Davies of NOAA, who is the main person responsible for ten years of good SFD measurements being made at Boulder. I would like to thank Mr. John E. Jones, who improved the instrumentation for Boulder SFD measurements, which resulted in particularly high quality SFD measurements from late 1966 through 1968. I am also thankful to Mr. Dennis Anderson, Mr. Henry Mai, and Mr. Dale Springer, who helped with the data analysis during the last three years of SFD observations. I am (wholeheartedly) thankful for the financial support for part of this work, particularly that reported in sections 5.5, 5.6.5, and 5.6.6, from the NASA Marshall Space Flight Center under Government Order No. H-42710-A. Finally, I would again like to thank Dr. L. A. Hall of Air Force Cambridge Research Laboratories, who has provided unpublished information of his EUV measurement from OSO-3 and rocket flights, which have been very important in furthering our knowledge of SFD's.

## 9. REFERENCES

- Agy, V., D. M. Baker, and R. M. Jones (1965), Studies of solar flare effects and other ionospheric disturbances with a high frequency Doppler technique, NBS Tech. Note No. 306 (U.S. Government Printing Office, Washington, D. C.).
- Angle, K. L. (1968), Characteristics of the explosive phase of flares, *Astron. J.* 73, S53.
- Angle, K. L. (1969), Ionospheric effects of solar flares, M. S. Thesis, Dept. of Meteorology, University of California, Los Angeles.
- Baker, D. M. (1965), An atlas of solar flare effects in the ionosphere observed with a high-frequency Doppler technique September 1960-December 1962, NBS Tech. Note No. 326 (U.S. Government Printing Office, Washington, D. C.).
- Baker, D. M., N. Chang, K. Davies, R. F. Donnelly and J. E. Jones (1968), A review of some ionospheric studies based on a high-frequency Doppler technique, ESSA Tech. Rept. ERL 78-SDL 1 (U.S. Government Printing Office, Washington, D. C.).
- Basu, S., and S. R. Chowdhury (1969), Correlation of sudden frequency deviations with solar microwave bursts, *J. Geophys. Res.* 74, 4175-4177.
- Bennett, J. A. (1967), The calculation of Doppler shifts due to a changing ionosphere, *J. Atmosph. Terr. Phys.* 29, 887-891.
- Bhatia, V. B. and J. N. Tandon (1970), Extreme ultraviolet radiation from solar flares, Sci. Rept. No. PL-480-3, Dept. of Physics and Astrophys., University of Delhi, Delhi, India.
- Chan, K. L. and O. G. Villard Jr. (1963), Sudden frequency deviations induced by solar flares, *J. Geophys. Res.* 68, 3197-3224.
- Davies, K. (1965), Ionospheric Radio Propagation, NBS Monograph 80 (U.S. Government Printing Office, Washington, D. C.); (1966) (Dover Publications Inc., New York); (1966) (Corona Press, Tokyo, Japan, in Japanese).
- Davies, K., and R. F. Donnelly (1966), An ionospheric phenomenon associated with explosive solar flares, *J. Geophys. Res.* 71, 2843-2845.
- DeJager, C. (1964), Solar ultraviolet and X-ray radiation, *Research in Geophysics, 1, Sun, Upper, Atmosphere, and Space*, ed. H. Odishaw, (MIT Press, Cambridge, Mass.) 1-42.
- Dodson, H. W., and E. R. Hedeman (1964), Problems of differentiation of flares with respect to geophysical effects, *Planet. Space Sci.* 12, 393-418.
- Dodson, H. W., and E. R. Hedeman (1970), Major H $\alpha$  flares in Centers of Activity with very small or no spots, *Solar Phys.* 13, 401-419.
- Donnelly, R. F. (1967), An investigation of sudden frequency deviations due to the immediate ionospheric effects of solar flares, ESSA Tech. Rept. IER 19-ITSA 19 (U.S. Government Printing Office, Washington, D. C.).
- Donnelly, R. F. (1968a), An analysis of sudden ionospheric disturbances associated with the proton flare of 1522 UT, August 28, 1966, ESSA Tech. Rept. ERL 92-SDL 6 (U.S. Government Printing Office, Washington, D. C.).
- Donnelly, R. F. (1968b), An analysis of sudden ionospheric disturbances associated with the proton flare of 0026 UT, July 7, 1966, ESSA Tech. Rept. ERL 86-SDL 3 (U.S. Government Printing Office, Washington, D. C.).
- Donnelly, R. F. (1968c), The X-ray and extreme ultraviolet radiation of the August 28, 1966 proton flare as deduced from sudden ionospheric disturbance data, *Solar Phys.* 5, 123-126.

- Donnelly, R. F. (1968d), Early detection of a solar flare: a study of X-ray, extreme ultraviolet, H-alpha, and solar radio emission from solar flares, ESSA Tech. Rept. ERL 81-SDL 2 (U.S. Government Printing Office, Washington, D. C.).
- Donnelly, R. F. (1969a), Contribution of X-ray and extreme ultraviolet radiation of solar flares to sudden frequency deviations, ESSA Tech. Rept. ERL 95-SDL 7 (U.S. Government Printing Office, Washington, D. C.).
- Donnelly, R. F. (1969b), Contribution of X-ray and EUV bursts of solar flares to sudden frequency deviations, J. Geophys. Res. 74, 1873-1877.
- Donnelly, R. F. (1969c), Energetic X-ray and extreme-ultraviolet flashes of solar flares, Astrophys. J. 158, L165-L167.
- Donnelly, R. F. (1969d), The 10-1030<sup>o</sup>Å flux for the flares of May 23, 1967, as deduced from SFD data: preliminary results, Data on solar event of May 23, 1967 and its geophysical effects, Rept. UAG-5, World Data Center A, Boulder, Colo. (U.S. Government Printing Office, Washington, D. C.).
- Donnelly, R. F. (1969e), The X-ray and extreme ultraviolet radiation of the July 7, 1966, proton flare as deduced from SID data, Paper 32, Annals of the IQSY 3, The Proton Flare Project (The July 1966 Event), (MIT Press, Cambridge, Mass.), 204-208.
- Drake, J. F. (1969), Characteristics of 2-12<sup>o</sup>Å solar X-ray flares, University of Iowa Tech. Rept. No. 69-41.
- Fortini, T., and M. Torelli (1970), The flares of July 6 and 8, 1968, Solar Phys. 11, 425-433.
- Friedman, H. (1969), X-ray observations of solar flares, Solar Flares and Space Research ed. C. DeJager and Z. Svestka (North-Holland Publ. Co., Amsterdam) 87-94.
- Frost, K. J. (1969), Rapid fine structure in a burst of hard solar X-rays observed by OSO-5, Astrophys. J. 158, L159-L163.
- Garriott, O. K., A. V. DaRosa, M. J. Davis, and O. G. Villard, Jr. (1967), Solar flare effects in the ionosphere, J. Geophys Res. 72, 6099-6103.
- Garriott, O. K., A. V. DaRosa, M. J. Davis, L. S. Wagner, and G. D. Thome (1969), Enhancement of ionizing radiation during a solar flare, Solar Physics 8, 226-239.
- Grebenkemper, C. J. (1969), U.S. Naval Res. Lab., Washington, D.C., private communication.
- Hall, L. A. (1969), Air Force Cambridge Res. Lab., Bedford, Mass., private communication of their EUV flux measurements presented by H. Hinteregger at the IAGA Meeting, Sept. 1969, Madrid, Spain.
- Hall, L. A., and H. E. Hinteregger (1969). Solar EUV enhancements associated with flares, Solar Flares and Space Research, ed. C. DeJager and Z. Svestka (North-Holland Publ. Co., Amsterdam) 81-86.
- Hall, L. A., J. E. Higgins, C. W. Chagnon and H. E. Hinteregger (1969), Solar-cycle variation of extreme ultraviolet radiation, J. Geophys. Res. 74, 4181-4183.
- Hallam, K. L. (1964), Solar flares in the light of hydrogen Lyman-Alpha, AAS-NASA Symposium on the Physics of Solar Flares, NASA SP-50, ed. W. N. Hess (U.S. Government Printing Office, Washington, D. C.) 63-64.
- Heath, D. F. (1969), NASA Goddard Space Flight Center, Greenbelt, Maryland, private communication.
- Hinteregger, H. E., and L. A. Hall (1969), Solar extreme ultraviolet emissions in the range 260-1300Å observed from OSO III, Solar Phys. 6, 175-182.

- Janssens, T. J., and K. P. White, III (1970), Description of mass motions and brightenings in a class 2b flare, August 8, 1968, *Solar Phys.* 11, 299-309.
- Jones, R. M. (1966), A three-dimensional ray tracing computer program, ESSA Tech. Rept. IER 17-ITSA 17 (U.S. Government Printing Office, Washington, D. C.).
- Kane, S. R., and K. A. Anderson (1970), Spectral characteristics of impulsive solar flare X-rays  $\geq 10$  keV, submitted to *Astrophys. J.*
- Kane, S. R., and R. F. Donnelly (1970), Impulsive hard X-ray and ultraviolet emission during solar flares, submitted to *Astrophys. J.*
- Lincoln, J. V. (1969), Compiler, Data on solar event of May 23, 1967 and its geophysical effects, Rept. UAG-5, World Data Center A, Boulder, Colo. (U.S. Government Printing Office, Washington, D. C.).
- Malville, J. M., and E. Tandberg-Hanssen (1969), Magnetic fields in flares and active prominences I: The flares in active region McMath no. 8818, May 21 and 23, 1967, *Solar Phys.* 6, 278-289.
- McClinton, A. T., Jr. (1968), White light flares, NRL Space Research Seminar (U. S. Naval Research Lab., Washington, D. C.), 63.
- McIntosh, P. S., and R. F. Donnelly (1970), Relationships among white light flares, magnetic fields, and EUV bursts, to be submitted to *Solar Phys.*
- Moreton, G. E. (1964), The association of bremsstrahlung X-rays with explosive flares, AAS-NASA Symposium on the Physics of Solar Flares, NASA SP-50, ed. W. N. Hess (U. S. Government Printing Office, Washington, D. C.) 209-212.
- Nakagawa, Y., and C. L. Hyder (1969), Response of the transition region to infalling material associated with solar flares, Chromosphere-Corona Transition Region, NCAR High Altitude Observatory, Boulder, Colo., 231-241.
- Nolan, B., S. Smith and H. Ramsey (1970), Solar Filtergrams of the Lockheed Observatory, Lockheed Solar Observatory, Burbank, Calif.
- Ohshio, M., R. Maeda, and H. Sakagami (1966), Height distribution of local photo-ionization efficiency, *Japan Radio Res. Labs. J.* 13, 245-577.
- Parks, G. K. and J. R. Winckler (1969a), Sixteen-second periodic pulsations observed in the correlated microwave and energetic X-ray emission from a solar flare, *Astrophys. J.* 155, L117-L120.
- Parks, G. K. and J. R. Winckler (1969b), 16-second periodic modulations observed in hard solar X-rays, (abstract) *Trans. Am. Geophys. Union* 50, paper STS13, 299.
- Ramsey, H. E., S. F. Smith, and K. L. Angle (1968), High resolution solar photography, Lockheed Missiles and Space Co., Tech. Rept. LMSC-68 1495.
- Reeves, E. M., A. K. Dupree, L. Goldberg, M. Huber, R. W. Noyes, W. H. Parkinson, and G. L. Withbroe (1970), Observations of active regions of solar flares in the extreme ultraviolet, paper S4-2, presented at The International Symposium on Solar-Terrestrial Physics, Leningrad, U.S.S.R.
- Richards, D. W. (1970), Sudden frequency deviations, solar extreme ultraviolet bursts and solar radio bursts, unpublished preliminary report Air Force Cambridge Research Laboratories, Bedford, Mass.
- Richmond, A. D. (1970), Geomagnetic crochets and ionospheric tidal winds, PhD thesis and Sci. Rept. 1 of NSF Grants GA 1453 and GA 18132, Dept. of Meteorology, University of California, Los Angeles.
- Rust, D. M. (1968), Chromospheric explosions and satellite sunspots, Structure and Development of Solar Active Regions, ed. K. O. Kippenheuer (D. Riedel Publ. Co., Dordrecht, Holland), 77-84.

- Sawyer, C. (1967), Correcting solar-flare data, *Astrophys. J.* 147, 1135-52.
- Smith, E.V.P. (1968), Flare sprays, Mass Motions in Solar Flares and Related Phenomena, Nobel Sympos. 9, ed. Y. Ohman (Wiley Interscience Div., John Wiley and Sons, Inc., New York) 137-153.
- Smith, H. J., and E.V.P. Smith (1963), *Solar Flares*, (MacMillan Co., New York).
- Solheim, F. (1970), Ph.D. Candidate, Dept. of Physics and Astrophysics, University of Colorado, Boulder, private communication.
- Stickland, A. C. (1969), general editor, *Annals of the IQSY 3*, The Proton Flare Project (The July 1966 Event) (MIT Press).
- Strauss, F. M., M. D. Papagiannis, and J. Aarons (1969), The relation of sudden frequency deviations to the spectrum and other characteristics of solar microwave bursts, *J. Atmosph. Terr. Phys.* 31, 1241-1249.
- Svestka, Z., and P. Simon (1969), Proton flare project, 1966, *Solar Phys.* 10, 3-59.
- Takakura, T. (1969), Interpretation of time characteristics of solar X-ray bursts referring to associated microwave bursts, *Solar Phys.* 6, 133-150.
- Tallant, P. E. (1970), A solar flare videometer, *Solar Phys.* 11, 263-275.
- Thomas, R. J. (1970), Solar soft X-radiation, Ph.D. Thesis and final rept of ORA Project 05567, Dept. of Astronomy, University of Michigan, Ann Arbor.
- Valnicek, B. (1964), *Bull. Astron. Inst. Czech.* 15, 207.
- Vorpahl, J., and H. Zirin (1970), Identification of the hard X-ray pulse in the flare of September 11-12, 1968, *Solar Phys.* 11, 285-290.
- Wright, J. W. (1967), Ionospheric electron-density profiles with continuous gradients and underlying ionization corrections. III. Practical procedures and some instructive examples, *Radio Sci* 2, (New Series), 1159-1168.
- Zirin, H. (1969), Some interesting events observed in detail with the Caltech Photoheliograph 24 August 1967-9 September 1969, unpublished.
- Zirin, H., and S. Werner (1967), Detailed analysis of flares, magnetic fields and activity in the sunspot group of Sept. 13-26, 1963, *Solar Phys.* 1, 66-100.

## APPENDIX A

### 1. Procedures for Analyzing SFD Data to Deduce the 10-1030Å<sup>o</sup> Flux Enhancement: Brief Descriptions

#### Method 1

##### Assumption of EUV Flash Spectrum

- (a) Use preflare ionograms, taken near the midpoint of the propagation paths employed to detect the SFD, with Newbern Smith transmission-curves (see Davies, 1965, pp 165-73) to estimate the preflare propagation paths.
- (b) Compute the electron density as a function of true height from the ionogram data (see Wright, 1967).
- (c) Compute the preflare propagation paths in detail using a ray tracing program (see Jones, 1966).
- (d) If preflare satellite measurements of the 1-1030Å<sup>o</sup> flux as a function of wavelength are available, compute the preflare rate of production of ionization as a function of height using the most recent model atmosphere appropriate for the preflare level of solar activity, e.g. the CIRA 1965 model atmospheres. Comparing the preflare rate of production of ionization with the measured electron density as a function of height, determine the electron loss rates as a function of height. If no such satellite measurements are available either use recent laboratory measurements of the reaction rates for the reactions involved or assume a model for the effective recombination coefficient as a function of height (see Donnelly 1968b, pp 36-8). This step is a major source of error in estimating the 10-1030Å<sup>o</sup> flux, particularly for the decay stage of any event or for slow events.
- (e) Assume a spectrum for the 1-1030Å<sup>o</sup> flash based on past satellite measurements (see table 2).
- (f) Assume a total 1-1030Å<sup>o</sup> flux based on simpler methods described below.
- (g) Assume a first estimate of the radiation time dependence based on the simpler method 3 described below.
- (h) Compute the rate of production of ionization as a function of height and time using the standard production equations, recent values for absorption and ionization cross sections, and a model atmosphere suitable for the preflare level of solar activity (see Ohshio et al., 1966).
- (i) Compute the time-rate-of-change of electron density  $\frac{dN}{dt}(h)$  and the electron density enhancement  $\Delta N(h)$  as a function of time and height using the results in (b), (d) and (h) above.
- (j) Compute the frequency deviation as a function of time for each of the propagation paths used for SFD observations starting with the results in (c). Use the ray tracing program by Jones (1966), which evaluates the most general formula for frequency deviations (Bennett, 1967).
- (k) Based on the intensity of the computed frequency deviations compared to the SFD observations, particularly during the early portion of the event to its peak, iteratively adjust (repeating h-1) the total 1-1030Å<sup>o</sup> flux to obtain a suitable fit between the computed frequency deviations and the observations.

(1) Based on the relative time dependence of the computed frequency deviations compared to the observations, iteratively adjust the time dependence of the 1-1030Å radiation until a suitable fit is achieved.

For large flares, a two component spectrum, where one set of wavelengths has a slow time dependence and the other an impulsive time dependence, may be necessary to obtain a satisfactory fit with observations. This method has the advantage of improved accuracy but has the disadvantages of a large amount of analysis time and large expense, mainly from the numerous ray tracing calculations.

### Method 2

Assumption of Height Dependence of the Rate of Production of Electrons.

This method is very similar to method 1 above. It has been described in detail elsewhere (Donnelly, 1968a) and will not be described here. Method 1 has the advantage over Method 2 that a variety of spectra can be assumed and processed simultaneously, providing an evaluation of the sensitivity of the  $\Delta\phi(1-1030\text{Å})$  results to the spectrum assumption. The computer programs presently used for methods 1 and 2 consist of one or more programs for each step; they have not yet been reorganized for operational use.

Methods 3-5 below are all intended for quick, inexpensive, rough estimates of  $\Delta\phi(10-1030\text{Å})$ . They make use of a frequent situation, illustrated in figure 37, where the electron-loss time constant ( $\tau = 1/2\alpha_{\text{eff}}N_0$ ) is nearly constant over the 110-200 km height range. The model for  $\alpha_{\text{eff}}(h)$  used is that used by Donnelly (1969a).  $N_0(h)$  is the preflare electron density. They also assume that  $\Delta q$ , the flare-induced enhancement of the rate of production of electrons, is negligible below about 100 km, approximately constant from 110 to about 200 km altitude, and then decreases with height fairly rapidly so that

$$\int_{100\text{km}}^{\infty} \Delta q(h) dh \approx \int_{100\text{km}}^{200\text{km}} \Delta q(h) dh = \bar{\Delta q} \times 10^7 \text{ cm}^{-2} \quad (1)$$

Also

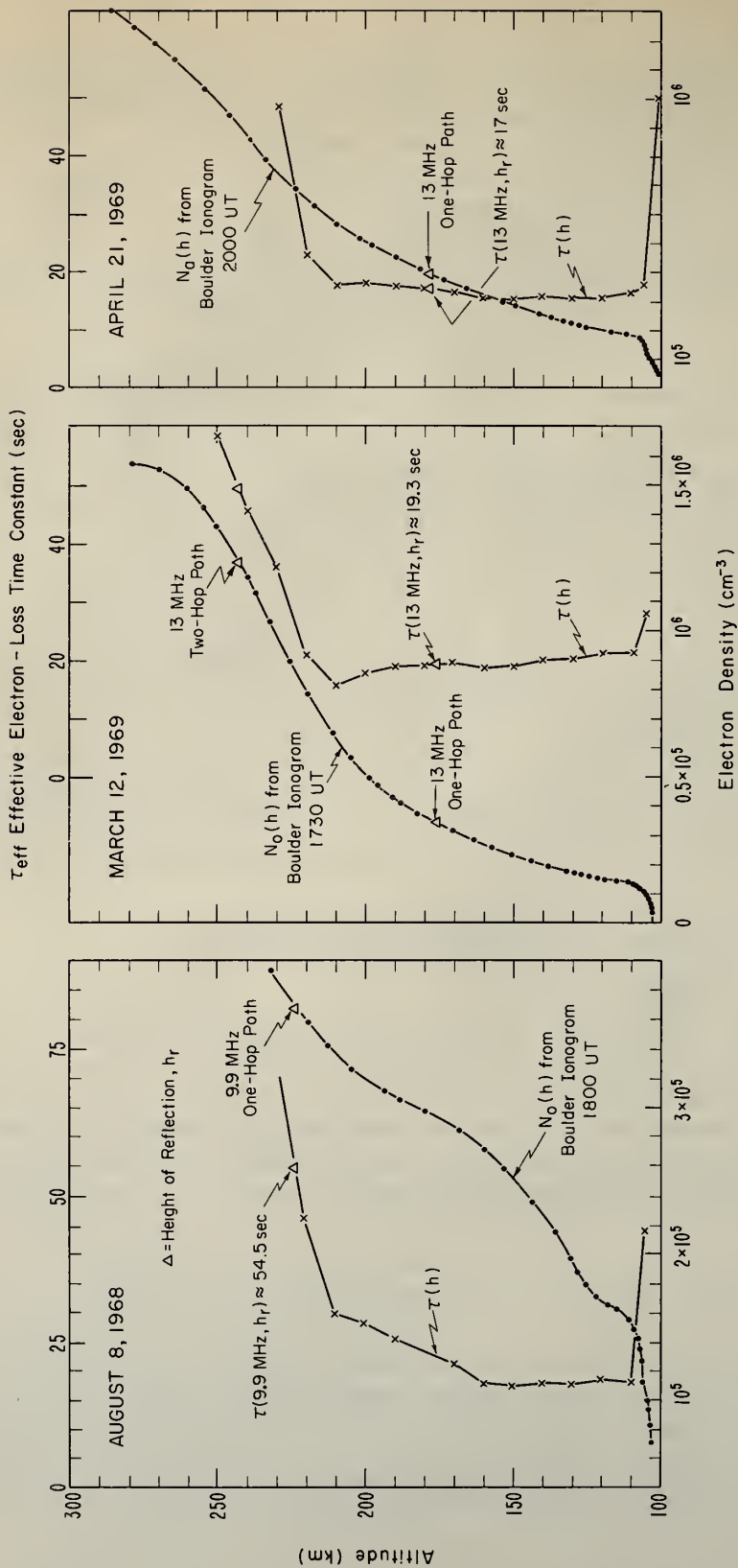
$$\int_{100\text{km}}^{\infty} \Delta q(h) dh \approx \cos(\chi) \int_{10\text{Å}}^{1030\text{Å}} \eta_e(\lambda) \Delta\phi(\lambda) d\lambda \approx \bar{\eta}_e \cos(\chi) \Delta\phi(10-1030\text{Å}), \quad (2)$$

where  $\chi$  is the solar zenith angle,  $\eta_e$  is the ionization efficiency in electrons produced per erg of radiation at wavelength  $\lambda$ ,  $\Delta\phi$  is the flare radiation enhancement in  $\text{ergs cm}^{-2} \text{sec}^{-1} \text{Å}^{-1}$  at 1 AU,  $\Delta\phi(10-1030\text{Å})$  is the net radiation enhancement in the 10-1030Å range in  $\text{ergs cm}^{-2} \text{sec}^{-1}$  at 1 AU, where

$$\Delta\phi(10-1030\text{Å}) = \int_{10\text{Å}}^{1030\text{Å}} \Delta\phi(\lambda) d\lambda, \text{ and } \bar{\eta}_e = \left[ \int_{10\text{Å}}^{1030\text{Å}} \eta_e \Delta\phi d\lambda \right] / \Delta\phi(10-1030\text{Å}). \quad (3)$$

Since  $\Delta q(h)$  and  $\tau(h)$  are assumed approximately constant in the 110-200 km altitude range, then as long as the nonlinear loss term is negligible in the electron continuity equation, namely

$$\frac{d\Delta N}{dt} = \Delta q - \frac{\Delta N}{\tau} - \alpha_{\text{eff}}(h) (\Delta N)^2$$



Propagation Paths: WWI Havana, Illinois to Boulder, Colorado - 1290 km

Figure 37. Examples of electron density and loss time constant as a function of height.

then  $\Delta N$  and  $\frac{d\Delta N}{dt}$  will also be nearly constant over that height range. In that case, the frequency deviation formula developed by Agy et al. (1965) applies for a propagation path reflected near 200 km or below;

$$\Delta f_o = \frac{k}{f_v c} \frac{dN}{dt} (h_r - h_o), \quad (4)$$

where  $k = 8.06 \times 10^7 \text{ Hz}^2 \text{ cm}^3$ ,  $f_v$  is the equivalent vertical-incidence frequency,  $c$  is the speed of light,  $h_r$  is the virtual height of reflection, and  $h_o \approx 100 \text{ km}$  in this case. From (1), (2), and (4)

$$\begin{aligned} \Delta\phi(10-1030\text{\AA}, t) &\approx \frac{c}{k} \frac{\sec\chi}{h_r - h_o} \frac{f_v}{\bar{n}_e} 10^7 \left( \Delta f(t) + \frac{1}{\tau} \int_0^t \Delta f(u) du \right) \\ &\approx a \frac{f_v \sec\chi}{h_r - h_o} \left( \Delta f(t) + \frac{1}{\tau} \int_0^t \Delta f(u) du \right) \end{aligned} \quad (5)$$

where  $a \approx 2.44 \times 10^{-6} \text{ Hz}^{-2} \text{ km ergs cm}^{-2} \text{ sec}^{-1}$ .

Note that in figure 37, the height of reflection for 9.9 MHz for the flare on August 8, 1968, is well above the region where  $\tau$  is approximately constant; so (5) would not apply for that event. All the cases shown in figure 37 correspond to large EUV bursts and the nonlinear loss term is not completely negligible. Equation (5) is then used by adding the nonlinear term weighted at the height of reflection of the probing radio wave, namely

$$\Delta\phi(10-1030\text{\AA}) \approx a \frac{f_v \sec\chi}{(h_r - h_o)} \left[ \Delta f_o(t) + \frac{1}{\tau} \int_0^t \Delta f_o(u) du + \alpha_{\text{eff}}(h_r) \left( \int_0^t \Delta f_o(u) du \right)^2 \right]. \quad (6)$$

(The weighting at the height of reflection is used because much of the observed frequency deviation comes from near the height of reflection where the effect of  $dN/dt$  is greatly magnified by deviative effects, i.e. by a  $\frac{1}{\mu}$  multiplying term where  $\mu$  is the phase refractive index).

### Method 3

Assumption of  $\Delta q$  and  $\tau$  constant with height.

- (a) and (b) same as for Method 1. Determine  $h_r$  and  $f_v$ .
- (c) Assume the effective recombination coefficient as a function of height (see Donnelly, 1968b, pp 36-8).
- (d) Compute the electron-loss time constant as a function of height. If  $\tau$  is approximately constant in the 100-200 km, proceed with (e). If no paths are reflected on the  $\tau$  curve where  $\tau \approx$  constant, this method does not apply.
- (e) Determine the true heights of reflection by determining the height at which the electron density corresponds to a plasma frequency equal to  $f_v$ . For a path with  $h_r \approx 200 \text{ km}$ , scale  $\Delta f(t)$  in detail.
- (f) Compute the solar zenith angle.
- (g) Evaluate (6).

### Method 4

#### Six Point Method

This method is the same as method 3 except it is used to compute only the maximum value of  $\Delta\phi(10-1030\text{\AA})$  rather than its detailed time dependence. Approximation of  $\Delta f(t)$  by five straight lines defined by six points. The number of points is of course, arbitrary, but in practice six points have been found to be a good compromise for almost all SFD's. The first point is the start, one is the  $\Delta f$  peak,

and the sixth is that where  $\Delta f$  equals zero at the start of its negative decay stage.

#### Method 5

Rough Estimate of  $\Delta\phi_{\max}^{\circ}(10-1030\text{\AA})$

- (a) Same as Method 1, and use data for  $f_{\nu} \approx 5$  MHz.
- (b) Estimate the solar zenith angle from nomographs,  $R_{\chi} = \cos\chi$ .
- (c) Estimate  $\tau_{\text{eff}}$  in the 110-200 km altitude range assuming  $\alpha_{\text{eff}} = 10^{-7} \text{cm}^3 \text{sec}^{-1}$  and computing  $N_o$  for a plasma frequency equal foE, the E layer critical frequency.
- (d) Approximate  $\Delta f(t)$  by a linear rise to the peak value, measure the corresponding start-to-maximum time ( $t_p$ ) and the peak frequency deviation.
- (e) Determine  $R_t$  from a nomograph, where  $R_t$  in this case is given by (Donnelly, 1969a, p. 41)

$$R_t \approx \frac{\tau_{\text{eff}}}{t_p} (1 - e^{-t_p/\tau_{\text{eff}}}) \quad (7)$$

- (f) Compute  $\Delta\phi_{\max}^{\circ}(10-1030\text{\AA})$  as follows:

$$\Delta\phi_{\max}^{\circ}(10-1030\text{\AA}) \approx \frac{\phi f(10-1030\text{\AA}) \Delta f_{\max}}{m R_t R_{\chi}} \quad (8)$$

, where m is the number of hops in the propagation path and  $\phi f(10-1030\text{\AA}) = 0.08$ .

Methods 3 and 4 give results for  $\Delta\phi_{\max}$  for the same event that agree closely. These results also agree closely with results obtained by methods 1 or 2 for the same event for the few cases when these more precise but cumbersome methods were employed. Method 5 has been found to give only order of magnitude results and to be inapplicable to slow or highly structured events.

## 2. Sensitivity of Frequency Deviations to Solar Bursts

The frequency deviation ( $\Delta f$ ) produced by bursts of ionizing radiations from solar flares may be expressed by a function F that operates on the radiation enhancement  $\Delta\phi(\lambda, t)$  ( $\text{ergs cm}^{-2} \text{sec}^{-1} \text{\AA}^{-1}$  at 1 AU)

$$\Delta f = F(\lambda, \chi, t, f_{\nu}, \Delta\phi) \quad \text{Hz} \quad (9)$$

In general, F is a nonlinear operator that is a function of the wavelength  $\lambda$  of the ionizing radiation, the solar zenith angle  $\chi$ , time t during the event, the hour of day, season, etc., the equivalent vertical incidence frequency  $f_{\nu}$  of the SFD probing radio wave, and other ionospheric disturbances as well as on  $\Delta\phi(\lambda, t)$ . In effect, everytime method 1 above is applied, F is numerically determined for the particular event studied. For the purposes of qualitatively understanding the characteristics of SFD's as a detector of solar flare radiations, some simplifying but reasonable assumptions will be made below in order to develop analytic expressions that permit insight into the physical processes that influence SFD's.

Assuming that the nonlinear electron loss term is small compared to the linear term in (3), then (9) can be written as a linear integral operation as follows:

$$\Delta f = \int_0^{\lambda_i} S_g(\lambda, \chi, t, f_{\nu}) \Delta\phi(\lambda, t) d\lambda, \quad (10)$$

where  $S_g$  is a general sensitivity function ( $\text{Hz erg}^{-1} \text{cm}^2 \text{sec}$ ), and  $\lambda_i$  is the longest wavelength of radiation capable of producing ionization, which is less than 1030 $\text{\AA}$  for all major constituents of the upper atmosphere. For impulsive radiations and an electron loss time constant that is approximately constant over most heights of interest, then

$$S_g(\lambda, \chi, t, f_{\nu}) \approx S(\lambda, f_{\nu}) R_{\chi} R_t \quad (11)$$

(see Donnelly, 1969a, pp 40-42), i.e.,  $S_g$  is separable into functions of  $\chi$ , t, and

$$R_{\chi} = \cos \chi, \text{ and} \quad (12)$$

$\lambda$  with  $f_v$ , where

$$R_t = 1 - \frac{\Delta \phi(t) * e^{-t/\tau_{eff}}}{\tau_{eff} \Delta \phi(t)}, \text{ where } * \text{ denotes convolution.} \quad (13)$$

These results are not exactly true in the real ionosphere, however equations (11-13), can be used keeping in mind that the proper  $S(\lambda, f_v)$  function should still have some dependence on  $\chi$  and  $t$ . In other words, the  $R_{\chi}$  and  $R_t$  terms account for most of the dependence on  $\chi$  and  $t$  respectively, but  $S(\lambda, f_v)$  will still have some residual dependence on  $\chi$  and  $t$ . Equation (10) then becomes:

$$\Delta f = R_{\chi} R_t \int_0^{1030\text{\AA}} S(\lambda, f_v) \Delta \phi(\lambda) d\lambda \quad (14)$$

$$\Delta f_o (f_v = 5\text{MHz}) = R_{\chi} R_t \frac{\Delta \phi_f(1-1030\text{\AA})}{\phi_f(1-1030\text{\AA})} \quad (15)$$

where the subscripts "o" and "f" refer to observed and solar flare, respectively, then from (14)

$$\phi_f(1-1030\text{\AA}) = \left[ \frac{\int_0^{1030\text{\AA}} S(\lambda, f_v = 5\text{MHz}) \Delta \phi_f(\lambda) d\lambda}{\int_0^{1030\text{\AA}} \Delta \phi_f(\lambda) d\lambda} \right]^{-1} \quad (16)$$

Since  $\phi_f(1-1030\text{\AA}) \approx 0.08$  (sec. 3), the average value of  $S(\lambda, 5\text{MHz})$  over the 1-1030 $\text{\AA}$  range should be about 12.5 if  $\Delta \phi_f$  were nearly uniform over this wavelength range.

For radio waves reflected at heights of 200 km and higher, and for wavelengths  $\lambda \leq 100\text{\AA}$  and for most wavelengths in the 796-1030 $\text{\AA}$  range, the production of electrons occurs almost entirely below the height of reflection in the nondeviative region; hence,

$$\Delta f = \frac{k}{f_v c} \int_0^{h_E} \frac{dN}{dt} dh \approx \frac{k}{f_v c} R_t \int_0^{\infty} \Delta q dh \approx \frac{k R_t}{f_v c} R_{\chi} \int_0^{1030\text{\AA}} \eta_e \Delta \phi(\lambda) d\lambda \quad (17)$$

Therefore, for  $10\text{\AA} \leq \lambda \leq 100\text{\AA}$  and  $796\text{\AA} < \lambda < 1030\text{\AA}$ ,

$$S(\lambda, f_v) \approx \frac{k \eta_e(\lambda)}{f_v c} = b \frac{\lambda \eta_{eff}}{f_v} \quad (18)$$

where  $b = 1.36 \times 10^5 \text{ Hz}^2 \text{ erg}^{-1} \text{ cm}^2 \text{ sec} \text{\AA}$ ,  $\lambda$  is the wavelength in  $\text{\AA}$ ,  $\eta_e$  is the ionization efficiency in electron-ion pairs per erg while  $\eta_{eff}$  is the ionization efficiency in electron-ion pairs per photon, and  $f_v$  is the equivalent vertical-incidence frequency in Hz.

The  $\eta_{eff}$  term in (18) deceptively appears simple, particularly for wavelengths in the 796-1030 $\text{\AA}$  range. The ionization efficiency for each of the individual constituents of the upper atmosphere are approximately known, but the effective ionization efficiency for the mixture of these constituents in the upper atmosphere is not a simple function of the ionization efficiencies of the constituents, particularly at wavelengths above 796 $\text{\AA}$  where the major constituent  $N_2$  is a strong absorber without producing ionization, i.e.  $\eta_{N_2} = 0$  for  $\lambda > 796\text{\AA}$ . The  $\eta_{eff}$  values used in evaluating (18) were obtained from detailed computer calculations like those of Ohshio et al. (1966). The results depend on the particular model atmosphere used and somewhat on the solar zenith angle.

For  $\lambda < 10\text{\AA}$ , (18) is inadequate mainly because of the rapid loss of electrons by attachment to form negative ions and by the fact that the free electrons that remain encounter such a high collision frequency because of the dense ambient gas density that they do not interact effectively with the SFD probing radio waves. The value of  $S_{fv}$  accounts for this latter factor (Donnelly, 1968b, p. 26). The negative ion problem can be approximately accounted for by multiplying  $\frac{dN}{dt}$  by the factor  $(1 + N_e/N_I^-)$ , where  $N_e$  is the total electron density and  $N_I^-$  the total negative ion density after equilibrium

for the attachment process has been attained (see Donnelly, 1968b, p 39). This means we are considering only radiation bursts that are slow relative to the attachment time constant, which is consistent with all observations of solar radiations having time constants  $> 1$  sec. Then (18) becomes

$$S(\lambda, f_v) \approx \frac{b}{f_v} \left( \frac{S_{fv}}{1 + N_e/N_i} \right) \lambda \eta_{eff} \quad (19)$$

where

$$\frac{S_{fv}}{1 + N_e/N_i} = \frac{\int_0^{\infty} \frac{S_{fv} \Delta q}{1 + N_e/N_i} dh}{\int_0^{\infty} \Delta q(\lambda, h) dh} \quad (20)$$

For wavelengths  $\lambda \geq 10\text{\AA}$ ,  $(S_{fv}/(1 + N_e/N_i)) \approx 1$ , and this term is not important. For wavelengths  $\lambda \ll 10\text{\AA}$ , it becomes very small and provides a low wavelength cut off for  $S(\lambda, f_v)$ . Also at  $\lambda \ll 10\text{\AA}$ , the ionization efficiency is approximately 35eV per electron-ion-pair. Equation (20) has been evaluated numerically using the model for  $N_e/N_i$  as a function of height used by Donnelly (1968b, p. 40). The results depend on the solar zenith angle, i.e. the term,  $R_\chi = \cos \chi$  does not completely account for the solar zenith angle dependence. The value of (20) is mainly dependent upon how much of the height curve of the rate-of-production of electrons for radiation at wavelength  $\lambda$  lies above about 75 km.

For wavelengths in the 100-796\AA range and for radio waves reflected near 200 km altitude, (18) again becomes inadequate because the height curve of the rate of production of electrons is no longer mainly below the height of reflection. This has two effects, first

$$\int_0^{\infty} \Delta q(h) dh \neq \int_0^{h_r} \Delta q(h) dh,$$

and secondly,  $\Delta q(h_r) \neq 0$ . The first effect tends to reduce  $S(\lambda)$  while the second tends to increase it because of the  $\frac{1}{\mu}$  amplification effects in the deviative region near the height of reflection where the phase refractive index  $\mu \rightarrow 0$ . To account for this, the area  $A$  under the  $\Delta q(h)$  curve is divided into three parts,  $A_1 = \int_{h_r}^{\infty} \Delta q(h) dh$ ,  $A_2 = \Delta q(h_r)(h_r - h_0)$ , where  $h_0$  is at the bottom of the  $\Delta q(h)$  curve where  $\Delta q(h_0) = \Delta q(h_r)$ , and  $A_3 = \int_0^{h_r} \Delta q dh - A_2 = A - A_1 - A_2$ . The frequency deviation produced by  $A_2$  will have the dependence given by (4), and that produced by  $A_1$  is given by (17).

Hence,

$$S(\lambda, f_v) \approx \frac{b \lambda \eta_{eff}}{f_v} \left( \frac{A - A_1 - A_2 + A_2 \frac{h_r - h_0}{h_r - h_0}}{A} \right) \quad (21)$$

Assuming  $\Delta q(h) \approx \Delta q(h_r) e^{-(h-h_r)/H_r}$  for  $h \geq h_r$ , where  $H_r$  is the atmospheric scale height at  $h_r$ , and assuming  $\Delta q_{max} \approx A/(e H_m)$ , where  $H_m$  is the atmospheric scale height at the height of the  $\Delta q$  peak for a particular  $\lambda$  (see Donnelly, 1967, pp 14-18), then

$$S(\lambda, f_v) \approx \frac{b \lambda \eta_{eff}}{f_v} \left( 1 + x \frac{h_r - h_r - (h_0 - h_0) - H_r}{H_0} \right) \quad (22)$$

where  $x = \frac{\Delta q(h_r)}{\Delta q_{max}}$  and  $h_0$  is the virtual height of  $h_0$  ( $h_0 > h_0$ ). Again, the evaluation of (22) was made with computer calculations to determine  $\eta_{eff}$ ,  $x$ , and  $h_0$ ; the results depend upon the solar zenith angle and the particular model atmosphere used. In practice, method 1 described above is as easy to apply as to evaluate  $S(\lambda, f_v)$  from (18), (19) and (21) for a particular event and involves far fewer assumptions, approximations, and restrictions.

Equations (18), (19) and (21) were evaluated for a particular case where  $f_v = 5$  MHz,  $h_r = 200$  km,  $h_0 = 350$  km,  $f_0 = 13$  MHz, and  $\chi = 60^\circ$ , with the CIRA 1965 Mean Model Atmosphere. The absorption cross sections and ionization efficiencies used agree well with those used by Ohshio et al., (1966). The results are shown in figure 1 and in more detail in figure 38 together with  $S(\lambda)$  results for  $f_v = 2$  MHz. The drop-off in  $S(\lambda)$  for

both curves in figure 38 at  $\lambda < 3\text{\AA}$  is caused by the  $\left(\frac{S f_v}{1 + N_e/N_1}\right)$  term. In other words, the electrons produced by radiation at these wavelengths is produced at low heights in the ionosphere where they are quickly lost to form negative ions and restrained by collisions from interacting with our probing radio waves. Only that portion of the  $\Delta q(h)$  curve for these wavelengths which lies above about 75 km contributes much to  $S(\lambda)$ , and as the wavelength decreases this portion decreases. Above  $6\text{\AA}$ ,  $S(\lambda)$  again decreases for  $f_v = 2$  MHz because the portion of  $\Delta q(h)$  that lies above the height of reflection and does not contribute to  $\Delta f(f_v = 2$  MHz) increases. The  $f_v = 2$  MHz path is reflected from the bottom of the E layer where the electron-density height gradient is large, the deviative region is small, and the net  $\frac{1}{\mu}$  magnification is small. The line of  $S(\lambda)$  jumps back up at wavelengths above  $30\text{\AA}$  because the absorption cross section of the major constituent  $N_2$  drops abruptly there (because of its K-shell discontinuity), which drops the  $\Delta q(h)$  curves back down to a low enough altitude to be seen by  $\Delta f(f_v = 2$  MHz). Strictly speaking, some similar minor peaks for  $S(\lambda, f_v = 2$  MHz) occur at certain wavelengths in the 910-1030 $\text{\AA}$  range, but they are of little importance.

The line of  $S(\lambda)$  for  $f_v = 5$  MHz is fairly flat from  $4\text{\AA}$  to  $100\text{\AA}$ . Above  $100\text{\AA}$ , the  $\frac{1}{\mu}$  magnification near the height of reflection is the main cause of increasing  $S(\lambda)$ . Above about  $700\text{\AA}$  there is considerable fine structure in  $S(\lambda)$  (not shown in figs. 1 and 38 but indicated by the wiggly line) caused by the fine structure in the absorption cross sections of the upper atmosphere constituents, particularly in  $N_2$  and  $O_2$ .

The line of  $S(\lambda)$  in figure 38 has several limitations. It is computed assuming the ionospheric response to flare radiations is linear, which limits its use in the  $1/2 - 8\text{\AA}$  range to flux enhancements  $< 10^{-3}$  ergs  $\text{cm}^{-2}\text{sec}^{-1}$ . Many soft X-ray flares exceed that, which is not a problem to SFD studies, even though it invalidates  $S(\lambda)$  at  $\lambda < 8\text{\AA}$ , because very little of an SFD observed on a path reflected in the upper-E or F regions are caused by radiations at  $\lambda < 8\text{\AA}$  (see table 2) and because simultaneous observations on paths reflected off the bottom of the E layer (see fig. 38) provide a measure of the small frequency deviations caused by the radiations at  $\lambda < 8\text{\AA}$ . Also, one function for  $R_t$  for the whole 1-1030 $\text{\AA}$  range, strictly speaking, only applies for about the first 10 sec of an event when  $R_t \approx 1$  at all heights; after that, separate  $R_t$  functions for different height ranges or radiation wavelength ranges would be required. The  $S(\lambda)$  results for  $300\text{\AA} < \lambda < 800\text{\AA}$  depend upon the particular preflare electron-density ( $N_o(h)$ ) used, which influences the  $1/\mu$  magnification. The sharp drop in  $S(\lambda)$  at  $972.5\text{\AA}$ , the wavelength of the H Ly  $\gamma$  line, is caused by a large spike in the  $N_2$  absorption cross section. Since absorption by  $N_2$  does not produce ionization, radiation at this wavelength produces ionization very inefficiently. The main effect, however, is that the ionization it produces is mainly at heights well above 200 km (Ohshio et al., 1966), i.e. above the height of reflection for the case considered. Other peaks and valleys in the  $N_2$  and  $O_2$  cross sections cause smaller fine structure at  $\lambda \geq 700\text{\AA}$ , which is indicated by the wiggly lines in figure 38. rate variations in the preflare electron density, solar zenith angle, or model atmosphere, the peaks and valleys in  $S(\lambda)$  caused by the absorption cross-section fine structure also vary as the  $\frac{1}{\mu}$  magnification region varies and the  $\Delta q(h)$  curve rises above or extends below the height of reflection.

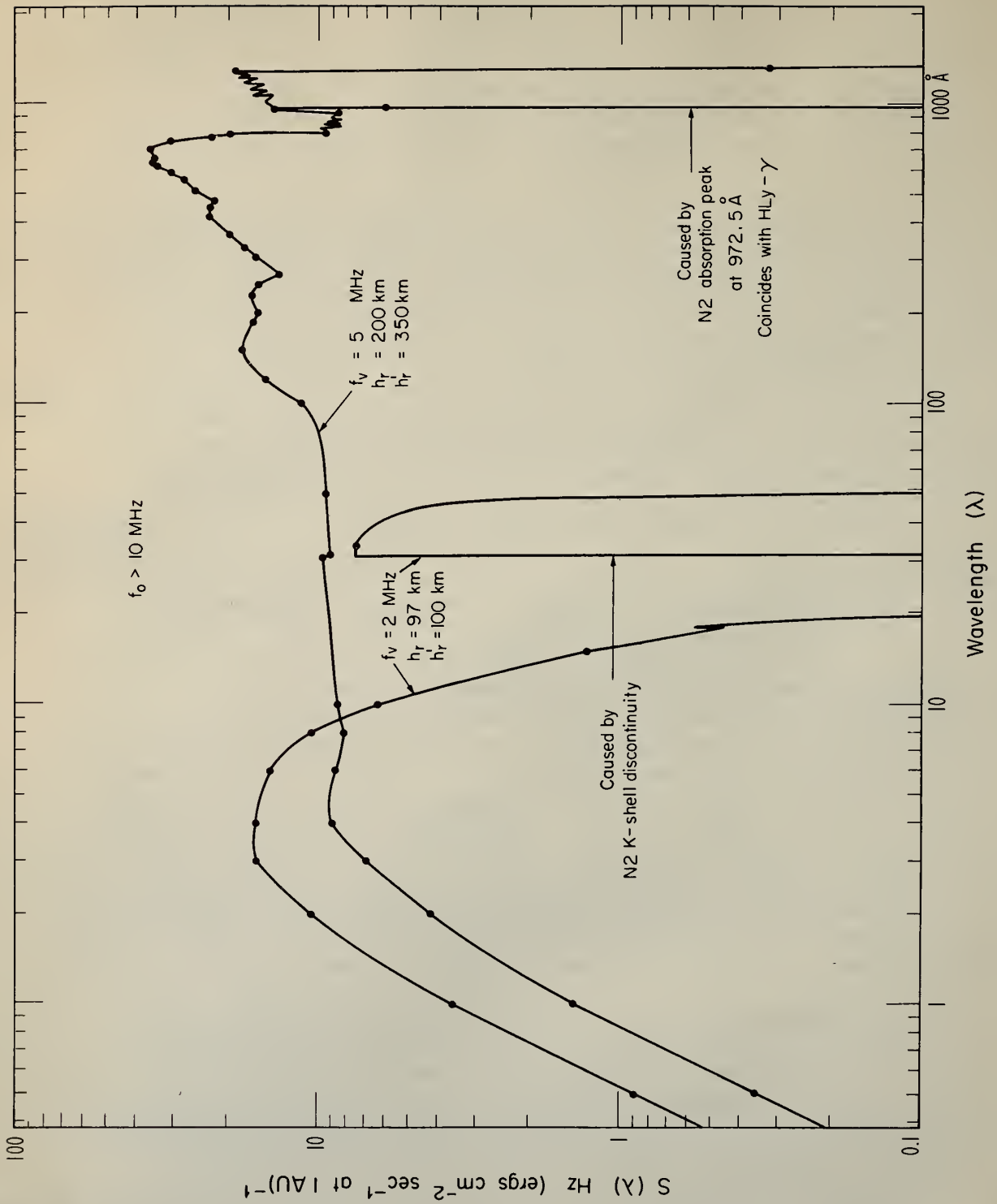


Figure 38. An example of the wavelength dependence of SFD sensitivity to ionizing radiations for  $f_0 = 2 \text{ MHz} \rightarrow f_v = 2 \text{ MHz}$ ,  $f_0 = 5 \text{ MHz} \rightarrow f_v = 5 \text{ MHz}$ .

### 3. Comments on SFD Observations

The above complications in  $S(\lambda)$  somewhat exaggerate the problems in estimating the 10-1030Å radiation flux enhancement from SFD's because the flare radiation is spread out over many wavelengths (see table 2) and complications at a few isolated wavelengths do not greatly influence SFD's. In this section, various complications in SFD observations will be discussed; but first, to put these problems in proper perspective, the usual detailed consistency in SFD data should be emphasized.

Figure 39 shows several SFD's observed one right after the other at about an hour interval. The observations at 5.1 and 5.054 MHz were at near vertical incidence but separated by nearly 1500 km. Detailed consistency in these data are evident even for the small fine structure. Similarly the oblique 10 MHz path, whose mid-point lies nearly 2,000 km east of Boulder, shows precisely the same relative shape. In general, SFD data have good consistency. See the SFD data for the March 12, 1969 event presented in section 6.

The most common complexities in SFD data, particularly for small events ( $\Delta f_{\max} < 1\text{Hz}$ ), are caused by small frequency deviations produced by acoustic-gravity waves in the ionosphere that are normally present. These cause fuzziness of the SFD data for long oblique paths and swells in the SFD data for near-vertical paths. To minimize this noise, to simplify the SFD analysis, and to minimize distortions due to flare-induced drops in the height of reflection of near vertical paths (see sec. 6), one-hop propagation paths with  $f_o \geq 10$  MHz with great-circle path lengths in the 500-1500 km range are best. Probably about 800 km is optimum, since the angle between the one-hop E-bottom and one-hop F paths and that between the one-hop F and two-hop F paths are large enough that practical HF antennas can partially suppress the unwanted two-hop F path and the bottom of the E layer path. It is also long enough that the horizontal extent of the path in the F-region is large enough compared to the local ionospheric irregularities that the swells should be smoothed out, yet short enough that the fuzziness shouldn't build up too much.

### 4. Miscellaneous Unpublished Studies of SFD's

A special study of  $\Delta f(f_v)$  was made primarily by Mr. Dennis L. Anderson of the NOAA Space Disturbances Lab. during the summer of 1968. The goals of the study were to determine the minimum number of transmissions needed for SFD observations, to search for patterns in  $\Delta f(f_v)$  that might be helpful in simplifying the analysis of SFD data and to evaluate several analysis procedures. A total of 70 SFD's from September 18, 1966 through August, 1967, each observed at Boulder on nine different transmissions (see table 3), were studied.

No simple pattern for  $\Delta f(f_v)$  was found. In general  $\Delta f_{\max}$  was small and slowly increased with  $f_v$  up to 3.3 MHz. Above  $f_v = 5$  MHz,  $\Delta f$  decreased with increasing  $f_v$ , but it wasn't always of the form  $\Delta f \propto \frac{1}{f_v}$ . The variation in  $\Delta f(f_v)$  for  $3.3 < f_v < 5$  MHz varied greatly from one event to the next. Also,  $\Delta f(f_v)$  did not closely fit the form of (4) for many events (see Agy et al., 1965, pp 22-31). This indicates that the  $\Delta q(h)$  assumptions in analysis methods 3-5 above may be inadequate, particularly for  $f_v < 5$  MHz; however, for  $f_v \approx 5$  MHz, that  $\Delta q(h)$  assumption is believed to be sufficient for 10-1030Å flux estimates accurate in absolute flux intensity to within a factor of four.

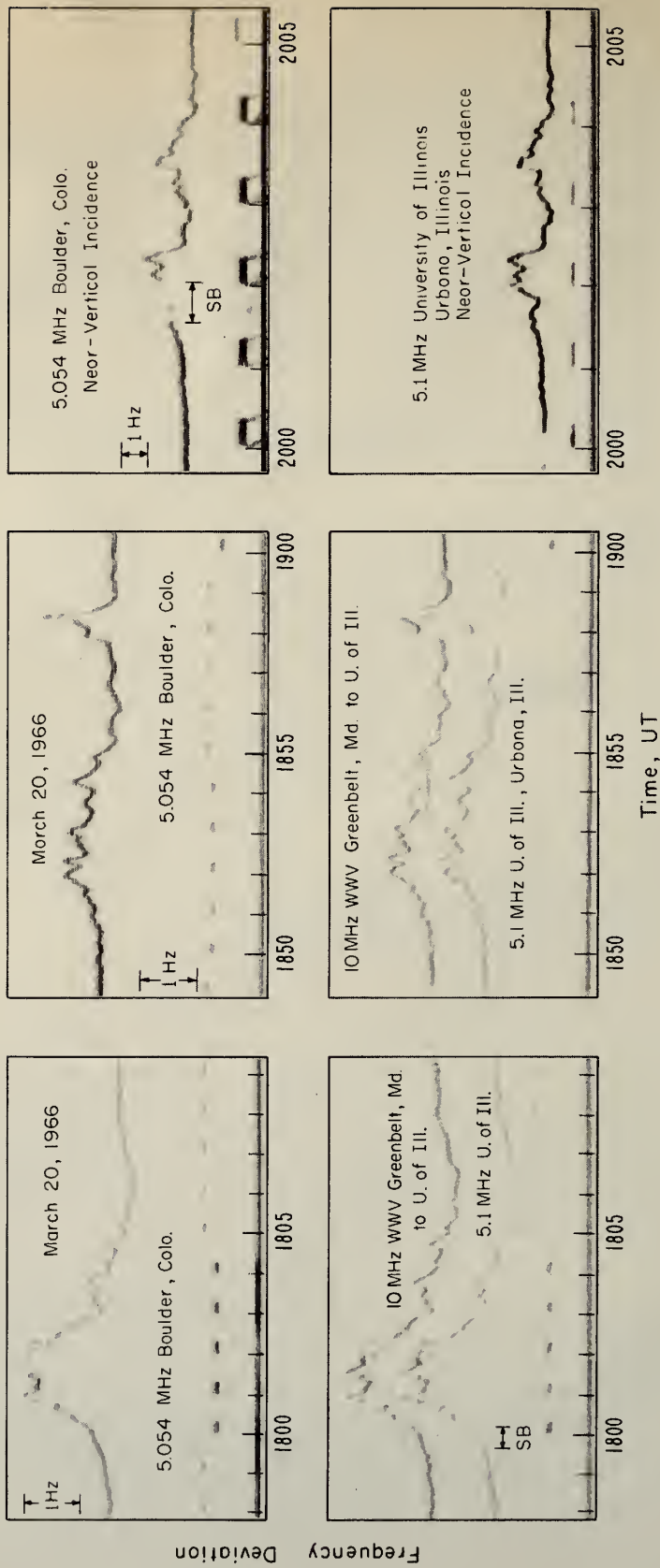


Figure 39. Examples of consistency in midlatitude SFD observations.

Additional results showed that Newbern Smith transmission-curve solutions for the propagation paths gave, for all practical purpose, as good of solutions for the ray path take-off angle, the virtual height of reflection ( $h_p$ ) and the equivalent vertical incidence frequency ( $f_v$ ) as did detailed ray-tracing calculations for about 90% of the ray-path calculations. Also, two-hop propagation that dominated the SFD observations occurred far more frequently for 8.9 MHz and 9.9 MHz WWI, Havana, Illinois, to Boulder, Colorado, than had previously been realized.

The minimum number of transmissions needed for SFD observations for accurate estimation of  $\Delta\phi(10-1030\text{\AA})$  was not determined. A minimum of three transmission frequencies spaced in frequency for the particular path length and latitude involved to provide one-hop heights of reflection near 150, 180, and 200 km at summer solstice is recommended in order to provide redundancy against equipment failure, to minimize the cut-off effects of  $E_s$ , to provide some height information, and to minimize the effects on just one path of diurnal and seasonal variations in the preflare electron density.

Another short and inconclusive study was made of the association of SFD's with short events of particle interference observed by NRL Explorer 30 soft X-ray measurements in the 0.5-3 $\text{\AA}$ , 0.5-8 $\text{\AA}$ , and 8-20 $\text{\AA}$  wavelength bands. Because the Explorer 30 satellite spun, one could easily distinguish the detector response to solar X-rays from its response to X-rays and energetic particles arriving from other directions. While scaling the X-ray flux as a function of time, it was noticed that the non-solar response due to "particle interference" often had an impulsive rise at the time of the SFD, sometimes having a time dependence more similar to the SFD than the solar soft X-rays. Out of one set of 13 SFD's and X-ray flares, two events showed no particle interference, five showed particle interference with a time dependence unrelated to that of the SFD, and six exhibited an impulsive time dependence very similar to the SFD and peaking at times in the range from the time of SFD maximum to one minute later. Certainly the number of events studied is too small to support any definite conclusions. Since small patches of particle interference frequently occur, these latter six cases could be simply the coincidental time agreement of unrelated phenomena; but since the timing agreed so closely, these phenomena might be related. For example, the ionization produced by the EUV flash at high altitudes, where the collision frequency for upward traveling electrons is small, may result in some of the freed electrons of moderate energy traveling upward along the magnetic field lines to the altitude of the satellite. Since this curious coincidence was not pertinent to the main goals of our work, we have not pursued it further.

Finally, an inconclusive study was made of the relation between large SFD's and major proton events. One main problem was the lack of a well defined list of "major" proton events. About 80% of the major proton flares that occurred during Boulder SFD observations were accompanied by SFD's, most with peak frequency deviations  $\geq 3$  Hz, i.e. large SFD's. Since some so called proton flares were not accompanied by SFD's, this study was never published. Proton flares tend to be large  $H\alpha$  flares and large  $H\alpha$  flares tend to be accompanied by large fluxes of all types of radiation, e.g., radio

bursts, hard X-rays, etc., so 80% of the flares being accompanied by SFD's was not considered to be important. However, SFD's are relatively insensitive to limb flares (sec. 5.6.5) and the events that were poorly associated with SFD's included events like the one at 1953 UT September 10, 1961, which was one of the long duration events (studied in sec. 5.6.5.b). Consequently, a more rigorous study of the relation between SFD's and proton emission should be made which considers the CMD dependence of SFD's.

# APPENDIX B

## BOULDER SFD OBSERVATIONS

DATE			UNIVERSAL TIME			TRANSMITTER	PEAK	COMMENTS
MONTH	DAY	YEAR	START	MAXIMUM	END	CALL LETTERS	FREQUENCY DEVIATION	
							Hz	
1	4	1968	1643.5	1644.0	1648.0	WMI	8.900	0.18
1	4	1968	1655.6	1657.2	1706.0	WMI	8.900	0.5
1	4	1968	1719.3	1720.3	1725.0	WMI	11.100	0.2
1	4	1968	1750.6	1752.4	1803.0	WMI	11.100	0.4
1	4	1968	2238.0	2239.8	2245.0	WMI	8.900	0.3
1	6	1968	1953.9	2001.0	2004.0	WMI	11.100	1.2
1	7	1968	2123.2	2124.1	2127.0	WMI	8.900	0.14
1	7	1968	2154.0	2154.4	2204.0	WMI	8.900	0.2
1	7	1968	2242.4	2243.2	2252.0	WMI	9.900	0.3
1	8	1968	1816.4	1816.9	1818.0	WMI	11.100	0.9
1	8	1968	1913.8	1914.2	1915.0	WMI	11.100	0.5
1	8	1968	2010.0	2011.7	2018.0	WMI	8.900	0.3
1	9	1968	1658.3	1659.8	1702.0	WMI	11.100	0.3
1	9	1968	1838.3	1839.8	1847.0	WMI	11.100	0.3
				1840.4				0.35
1	10	1968	2110.3	2111.4	2114.0	WMI	9.900	0.13
1	10	1968	2121.0	2122.7	2127.0	WMI	9.900	0.2
1	10	1968	2145.0	2147.7	2152.0	WMI	9.900	0.2
1	11	1968	1615.3	1617.3	1623.0	WMI	8.900	0.7
				1618.3				0.7
1	11	1968	1659.2	1700.2	1713.0	WMI	11.100	3.
				1703.2				0.5
1	12	1968	1712.0	1713.0	1717.0	WMI	8.900	0.16
1	12	1968	1721.0	1725.5	1731.0	WMI	8.900	0.25
1	12	1968	1808.3	1809.5	1820.0	WMI	11.100	1.2
1	13	1968	1847.0	1847.9	1857.0	WMI	11.100	0.55
1	14	1968	1839.7	1839.4	1845.0	WMI	11.100	0.2
1	14	1968	1843.0	1849.2	1855.0	WMI	11.100	0.15
1	14	1968	1918.0	1918.5	1925.0	WMI	11.100	0.17
1	14	1968	2010.0	2011.5	2030.0	WMI	11.100	1.7
1	16	1968	1540.0	1541.7	1550.0	WMI	8.900	0.18
				1542.2				0.2
1	15	1968	1855.0	1901.2	1907.0	WMI	11.100	0.25
1	18	1968	1513.0	1514.2	1528.0	WMI	8.900	0.2
1	23	1968	1538.2	1538.7	1600.0	WMI	8.900	2.3
				1543.0				0.4
1	23	1968	1730.2	1730.4	1732.5	KKE42	5.100	0.4
1	29	1968	2009.4	2009.8	2012.0	WMI	11.100	0.85
1	29	1968	2218.9	2219.3	2224.0	WMI	11.100	0.4
1	30	1968	1509.0	1511.4	1525.0	WMI	11.100	0.33
				1512.8				0.33
1	30	1968	1604.3	1604.9	1607.0	WMI	8.900	1.1
1	30	1968	1902.8	1904.2	1907.0	WMI	8.900	0.3
1	30	1968	2014.0	2016.6	2022.0	WMI	11.100	0.35
2	1	1968	1435.6	1437.1	1452.0	WMI	8.900	0.2
2	1	1968	1801.7	1802.7	1818.0	WMI	11.100	3.0
2	1	1968	1917.1	1917.9	1925.0	WMI	11.100	2.7
				1919.2				2.2
2	1	1968	2301.0	2301.3	2306.0	WMI	8.900	0.2
2	6	1968	1558.5	1559.0	1606.0	WMI	11.100	0.3
				1559.9				0.4
2	10	1968	1605.0	1615.5	1645.0	WMI	8.900	0.2
				1621.2				0.3
2	10	1968	1914.3	1915.2	1924.0	WMI	11.100	0.9
				1916.1				1.1
2	10	1968	2055.0	2055.8	2105.0	WMI	8.900	0.2
2	14	1968	1534.2	1535.2	1539.5	WMI	11.100	2.2
				1535.4				1.6
2	15	1968	1500.0	1501.2	1510.0	WMI	9.900	0.3
2	16	1968	1603.3	1604.2	1614.0	WMI	8.900	0.4
				1605.8				0.2
2	16	1968	2011.5	2013.0	2018.0	WMI	11.100	0.3
2	18	1968	1925.2	1927.1	1928.	WMI	13.000	0.7
2	25	1968	2149.5	2150.3	2153.0	WMI	11.100	0.3
2	28	1968	1936.2	1936.6	1941.0	WMI	11.100	0.3
3	2	1968	1410.0	1411.6	1419.0	WMI	11.100	0.5
3	17	1968	1758.0	1801.0	1811.0	WMI	8.900	0.2

MAIN PEAK OBSCURED  
BY THE STATION BREAK  
NO H-ALPHA FLARE REPORTD

TWO SHARP PKGS LOCATED  
ON A SLOW RISE AND FALL

A SERIES OF  
SMALL EVENTS

DATE			UNIVERSAL TIME			TRANSMITTER	PEAK	COMMENTS
MONTH	DAY	YEAR	START	MAXIMUM	END	CALL LETTERS	FREQUENCY DEVIATION	
							MHZ	
3	21	1968	1422.7	1423.8	1428.0	WWI	8.900	0.3
3	21	1968	1913.3	1914.6	1930.0	WWI	11.100	4.2
3	21	1968	2202.0	2203.7	2227.3	WWI	11.100	0.3
3	24	1968	1635.0	1643.1	1700.0	WWI	13.000	0.3
3	25	1968	1459.2	1504.7	1515.0	WWI	11.100	1.7
3	27	1968	1757.7	1800.4	1830.0	WWI	13.000	0.3
4	2	1968	1614.7	1615.1	1616.0	WWI	11.100	0.3
4	2	1968	2002.8	2003.2	2009.0	WWI	13.000	0.6
4	3	1968	2042.0	2005.3	2046.0	WWI	12.100	0.1
4	15	1968	1507.4	2043.0	1508.3	WWI	11.100	0.2
4	15	1968	1609.7	2044.1	1612.7	WWI	11.100	0.2
4	16	1968	2247.7	1507.7	2248.5	WWI	13.000	0.3
4	25	1968	1255.3	1610.4	1257.2	WWI	9.900	0.45
5	1	1968	1943.7	2247.7	1944.7	WWI	11.100	0.5
5	3	1968	1651.0	2248.5	1654.4	WWI	11.100	0.4
5	3	1968	2040.0	2251.0	2040.7	WWI	11.100	0.3
5	3	1968	2125.4	2251.0	2127.6	WWI	8.900	2.5
5	3	1968	2224.9	2226.0	2229.4	WWI	11.100	0.8
5	4	1968	1549.9	2226.0	1552.3	WWI	13.000	0.3
5	5	1968	1407.2	1552.3	1408.7	WWI	13.000	0.3
5	7	1968	2034.6	1557.1	2035.2	WWI	9.900	0.3
5	9	1968	1814.7	1557.1	1819.3	WWI	11.100	0.45
5	10	1968	1558.3	1557.1	1559.7	WWI	9.900	0.7
5	10	1968	2112.7	2113.4	2115.2	WWI	11.100	0.4
5	10	1968	2244.8	2245.6	2250.7	WWI	9.900	0.3
5	15	1968	1901.5	1902.8	1904.3	WWI	11.100	0.3
5	15	1968	2054.0	2055.3	2059.4	WWI	11.100	0.8
5	17	1968	1605.1	1606.7	1609.6	WWI	11.100	0.68
5	18	1968	1953.8	1954.4	1956.2	WWI	11.100	0.75
5	19	1968	1225.6	1228.2	1233.6	WWI	8.900	0.3
5	19	1968	1815.4	1815.8	1820.0	WWI	9.900	0.3
5	19	1968	1906.4	1907.8	1910.5	WWI	13.000	0.2
5	22	1968	1825.8	1828.2	1833.3	WWI	11.100	0.8
5	23	1968	1218.8	1219.4	1220.1	WWI	11.100	0.35
5	24	1968	1253.8	1254.4	1257.4	WWI	8.900	0.8
5	26	1968	1740.8	1741.9	1747.0	WWI	11.100	0.5
5	30	1968	1918.1	1918.8	1921.0	WWI	12.100	0.2
5	31	1968	2044.7	2045.4	2047.0	WWI	13.000	0.25
6	4	1968	2307.0	2308.8	2317.0	WWI	8.900	0.55
6	5	1968	2049.4	2051.5	2057.3	WWI	11.100	1.2
6	10	1968	2006.	2011.	2022.3	WWI	9.900	0.2
6	10	1968	2207.	2208.	2215.	WWI	11.100	0.7
6	11	1968	1644.3	1645.0	1648.3	WWI	11.100	0.3
6	11	1968	1902.7	1904.2	1909.3	WWI	11.100	0.2
6	13	1968	1625.3	1626.8	1628.6	WWI	9.900	0.25
6	13	1968	2133.1	2133.7	2138.5	WWI	9.900	0.3
6	15	1968	2154.8	2134.3	2155.2	WWI	11.100	0.4
6	15	1968	2333.7	2135.3	2334.6	WWI	11.100	0.2
6	16	1968	1945.0	2155.2	1946.4	WWI	11.100	0.25
6	18	1968	1929.3	2334.6	1930.	WWI	9.900	0.7
6	18	1968	2035.7	2157.1	2038.1	WWI	11.100	0.2
6	18	1968	2154.9	2337.2	2155.5	WWI	9.900	0.25
6	19	1968	1737.5	2337.2	1737.9	WWI	9.900	0.2
6	19	1968	2041.2	2045.8	2043.6	WWI	9.900	0.45
6	19	1968	2154.2	2157.3	2155.5	WWI	9.900	0.25
6	19	1968	2224.5	2228.4	2241.6	WWI	11.100	0.5
6	20	1968	2107.2	2109.2	2121.7	WWI	11.100	0.9
6	21	1968	1643.4	1644.8	1647.5	WWI	11.100	0.6
6	26	1968	2331.1	2332.6	2339.0	WWI	9.900	0.75
6	29	1968	2015.1	2016.7	2021.9	WWI	9.900	0.25
6	30	1968	1431.0	2019.6	1431.2	WWI	9.900	0.2
7	3	1968	2328.9	2329.6	2336.8	WWI	9.900	0.3
7	5	1968	2244.7	2245.6	2253.8	WWI	9.900	0.2
7	6	1968	1551.7	1552.3	1557.4	WWI	8.900	0.3

DATE			UNIVERSAL TIME			TRANSMITTER	PEAK	COMMENTS
MONTH	DAY	YEAR	START	MAXIMUM	END	CALL LETTERS	FREQUENCY DEVIATION	
							MHZ	
7	7	1968	1304.1	1304.9	1308.1	WWI	8.900	0.5
7	7	1968	1910.6	1912.5	1916.7	WWI	11.100	0.25
7	8	1968	1632.5	1633.8	1635.6	WWI	9.900	0.4
7	8	1968	1707.3	1710.0		WWI	11.100	19.5
7	8	1968	2104.0	2104.8	2105.8	WWI	9.900	0.4
								VERY LARGE, STRUCTURED
7	9	1968	1855.3	1812.2		WWI	9.900	1.6
7	11	1968	2232.4	2233.6	2241.7	WWI	9.900	0.4
7	13	1968	1451.2	1452.4	1501.7	WWI	11.100	0.85
7	13	1968	2131.2	2131.9	2145.6	WWI	11.100	0.2
7	15	1968	1935.9	1940.1	1944.1	WWI	9.900	0.35
								FINE STRUCTURE
7	15	1968	2022.5	2023.4	2029.9	WWI	11.100	0.2
7	16	1968	1325.6	1327.1	1327.5	WWI	8.900	1.2
7	25	1968	2004.1	2004.9	2010.6	WWI	9.900	0.3
7	30	1968	2029.1	2030.	2034.6	WWI	11.100	2.9
7	31	1968	1719.9	1722.1	1727.3	WWI	11.100	0.35
8	4	1968	1749.1	1749.5	1752.0	WWI	11.100	0.3
8	8	1968	1313.9	1316.8	1325.8	WWI	8.900	0.58
8	8	1968	1814.9	1816.4	1833.	WWI	9.900	53.
8	9	1968	1608.6	1610.6	1614.5	WWI	11.100	0.2
8	11	1968	1442.3	1443.4	1446.5	WWI	9.900	0.6
								LARGEST ONE-HOP FREQ DEV
8	12	1968	1759.1	1759.6	1801.9	WWI	9.900	0.2
8	12	1968	2045.8	2049.0	2051.1	WWI	9.900	0.6
8	13	1968	1254.1	1254.6	1255.6	WWI	8.900	0.6
8	15	1968	1717.5	1719.4	1723.1	WWI	9.900	0.2
8	20	1968	1525.1	1527.8	1531.0	WWI	11.100	0.3
8	20	1968	1645.3	1648.8	1657.8	WWI	11.100	0.75
8	20	1968	2315.3	2316.1	2317.7	WWI	8.900	0.7
8	21	1968	1533.6	1536.3	1541.4	WWI	11.100	0.4
8	21	1968	1837.7	1841.4	1846.3	WWI	11.100	2.6
8	21	1968	1933.2	1934.2	1945.9	WWI	11.100	1.6
								FINE STRUCTURE
8	23	1968	1459.1	1459.9	1504.	WWI	11.100	1.0
9	1	1968	2003.8	2006.4	2014.	WWI	13.000	0.7
9	2	1968	1531.0	1532.0	1533.	WWI	9.900	0.3
9	2	1968	1701.9	1702.4	1706.	WWI	11.100	0.4
9	3	1968	1620.4	1620.9	1630.	WWI	9.900	0.3
				1623.6				0.5
9	3	1968	1715.9	1719.8	1725.	WWI	9.900	0.3
9	4	1968	1333.8	1335.8	1343.	WWI	9.900	0.45
9	4	1968	1425.4	1429.8	1436.	WWI	11.100	0.4
				1433.4				0.4
9	4	1968	2158.0	2158.9	2200.	WWI	11.100	1.3
9	6	1968	1442.5	1444.7	1448.	WWI	11.100	0.35
9	10	1968	2012.1	2012.6	2023.	WWI	9.900	0.25
9	11	1968	2357.6	2358.1	0001.	WWI	9.900	0.4
9	17	1968	2025.8	2029.5	2035.	WWI	11.100	0.3
9	22	1968	2155.6	2157.6	2200.	WWI	9.900	0.25
9	27	1968	1555.6	1559.2	1607.	WWI	11.100	0.25
9	27	1968	2120.6	2121.2	2133.	WWI	11.100	0.35
9	28	1968	1741.9	1742.4	1744.	WWI	11.100	1.4
9	29	1968	1617.1	1618.3	1628.	WWI	11.100	2.8
				1618.8				3.0
				1619.2				3.4
				1619.8				3.1
				1620.5				1.3
				1622.8				1.4
9	30	1968	2215.1	2217.6	2223.	WWI	11.100	0.65
10	2	1968	2012.2	2012.9	2023.	WWI	11.100	1.0
				2015.2				0.5
				2017.9				0.45
10	4	1968	2124.4	2124.6	2130.	WWI	11.100	0.6
				2125.1				0.9
				2125.9				0.4
10	5	1968	1427.3	1429.4	1433.	WWI	11.100	0.4
10	5	1968	1349.4	1350.1	1353.	WWI	11.100	0.25
10	6	1968	1638.5	1639.4	1642.	WWI	11.100	0.3
				1640.0				0.35
				1640.4				0.4
10	6	1968	1722.9	1723.2	1727.	WWI	11.100	0.3
				1724.2				0.3
				1724.8				0.4

DATE			UNIVERSAL TIME			TRANSMITTER	FREQUENCY	PEAK	COMMENTS
MONTH	DAY	YEAR	START	MAXIMUM	END	CALL LETTERS	MHZ	FREQUENCY DEVIATION HZ	
10	6	1968	1734.6	1734.8 1735.3	1736.	WWI	11.100	0.8 0.7	
10	12	1968	2000.2	2004.1 2005.3	2012.	WWI	11.100	0.5 0.45	
10	16	1968	2138.2	2139.3	2142.	WWI	11.100	0.6	TIME ACCURACY ABOUT 2MIN
10	17	1968	1525.6	1527.2	1531.5	WWI	11.100	0.7	
10	17	1968	2008.8	2009.3	2012.	WWI	11.100	0.55	
10	17	1968	2127.3	2128.0 2131.2	2140.	WWI	11.100	0.25 0.5	
10	18	1968	2025.4	2026.2	2029.	WWI	11.100	0.35	
10	18	1968	2132.2	2134.1	2140.	WWI	8.900	0.35	
10	19	1968	1813.3	1814.2 1815.5	1828.	WWI	11.100	0.35 0.3	
10	19	1968	1850.4	1852.3 1854.5 1857.8	1900.	WWI	11.100	0.25 0.2 0.25	
10	20	1968	1803.4	1803.9	1809.	WWI	11.100	0.3	
10	20	1968	1927.5	1930.4	1935.	WWI	11.100	0.3	
10	20	1968	1941.2	1942.2	1947.	WWI	11.100	0.35	
10	20	1968	2058.1	2058.9	2102.	WWI	11.100	0.2	
10	20	1968	2120.0	2121.1	2125.	WWI	11.100	0.25	
10	20	1968	2127.6	2128.8 2130.3	2135.	WWI	11.100	0.5 0.6	
10	21	1968	1424.3	1426.2 1425.9 1432.1	1437.	WWI	11.100	0.6 0.35 0.35	
10	21	1968	1725.1	1729.6 1730.7 1731.9	1741.	WWI	11.100	1.4 1.2 1.4	
10	21	1968	2125.7	2126.2 2128.2 2129.7	2141.	WWI	11.100	0.65 0.55 0.35	
10	22	1968	1658.2	1658.8	1702.	WWI	11.100	1.3	
10	22	1968	1708.3	1708.9	1712.	WWI	11.100	0.45	
10	23	1968	1739.1	1743.1	1751.	WWI	11.100	0.2	LONG DURATION
10	23	1968	1935.6	1940.8	1949.	WWI	11.100	0.35	
10	23	1968	2000.3	2001.4	2007.	WWI	11.100	0.2	
10	26	1968	1645.4	1649.2	1702.	WWI	11.100	0.2	
10	26	1968	1845.3	1850.5	1857.	WWI	11.100	0.4	
10	29	1968	1847.4	1848.9 1851.9	1905.	WWI	11.100	0.8 0.4	
10	30	1968	1620.9	1623.0	1630.	WWI	11.100	0.3	LONG DURATION
11	1	1968	1241.9	1245.8	1254.	WWI	11.100	0.4	
11	1	1968	1438.4	1440.4	1451.	WWI	11.100	0.55	
11	1	1968	2002.7	2004.2 2004.5 2011.5	2030.	WWI	11.100	3.0 7.0 0.8	
11	3	1968	1614.4	1616.1	1627.	WWI	11.100	0.45	
11	3	1968	2037.2	2038.9 2039.4	2050.	WWI	11.100	0.8 0.7	
11	5	1968	1750.5	1752.0	1754.	WWI	11.100	0.2	
11	6	1968	1817.1	1818.1	1825.	WWI	11.100	0.3	
11	11	1968	1625.5	1626.2	1630.	WWI	11.100	0.75	
11	12	1968	2127.4	2128.2 2128.8	2139.	WWI	11.100	0.25 0.25	
11	17	1968	1918.8	1919.8 1921.0	1926.	WWI	11.100	0.3 0.2	
11	23	1968	1654.7	1655.2 1657.2	1704.	WWI	11.100	0.3 0.7	
11	24	1968	2036.8	2038.7	2044.	WWI	11.100	0.85	
11	27	1968	1722.1	1722.8	1724.	WWI	11.100	0.35	NO H-ALPHA FLARE REPORTO
12	4	1968	1542.6	1542.9 1544.1	1553.	WWI	8.900	0.25 0.3	
12	7	1968	1828.3	1828.7	1831.	WWI	11.100	0.25	
12	8	1968	1523.0	1523.7	1526.4	WWI	11.100	0.45	
12	8	1968	1809.2	1809.9	1812.	WWI	11.100	0.2	
12	8	1968	2157.6	2158.8 2200.0	2202.	WWI	11.100	0.2	
12	17	1968	1801.2	1803.3	1807.	WWI	11.100	0.3	NO H-ALPHA FLARE REPORTO
12	20	1968	1856.1	1857.6	1859.	WWI	11.100	0.3	

DATE			UNIVERSAL TIME			TRANSMITTER		PEAK		COMMENTS
MONTH	DAY	YEAR	START	MAXIMUM	END	CALL LETTERS	FREQUENCY MHZ	FREQUENCY	DEVIATION MHZ	
12	22	1968	2033.1	2035.3	2037.	HWI	11.100		0.25	
12	24	1968	1936.6	1938.0		HWI	11.100		0.25	
				1938.4					0.25	
12	24	1968	2224.4	2227.8	2239.	HWI	11.100		0.75	
				2228.8					0.65	
12	26	1968	2020.0	2022.4	2033.	HWI	11.100		0.25	
				2023.4					0.4	
				2026.4					0.3	
12	26	1968	2050.2	2053.1	2056.	HWI	11.100		0.3	
				2054.4					0.3	
12	27	1968	2015.2	2020.0	2023.	HWI	11.100		0.25	
12	29	1968	1920.0	1922.1	1950.	HWI	11.100		0.6	LOTS OF FINE STRUCTURE
				1923.5					0.6	
				1925.0					0.5	
				1927.8					0.5	
12	30	1968	1424.8	1425.4	1428.	HWI	11.100		0.3	
1	4	1969	2057.9	2059.8	2115.	HWI	11.100		0.3	
				2102.2					0.35	
				2104.4					0.4	
1	5	1969	1821.2	1825.5	1828.	HWI	11.100		0.35	
1	7	1969	1704.3	1705.3	1708.	HWI	11.100		0.5	
1	9	1969	1832.4	1834.2	1844.	HWI	13.000		0.3	
				1835.2					0.3	
1	9	1969	1854.1	1855.8	1858.	HWI	13.000		0.3	
1	12	1969	1912.8	1916.3	1923.	HWI	13.000		0.35	
1	14	1969	1744.3	1745.8	1747.	HWI	13.000		0.3	
1	17	1969	1704.1	1704.6	1715.	HWI	13.000		6.2	LARGE
				1704.8					5.2	
				1707.3					1.3	
1	19	1969	1818.4	1819.2	1827.	HWI	13.000		0.2	2 MAIN PLAKS
2	1	1969	2132.	2139.0	2210.	HWI	11.100		1.3	
2	7	1969	1644.6	1645.2	1647.	HWI	11.100		0.9	
2	8	1969	1750.	1751.2	1755.	HWI	11.100		1.5	
2	9	1969	1723.	1724.5	1745.	HWI	11.100		4.6	FAST SHARP RISE + PEAK
2	10	1969	1835.	1835.2	1840.	HWI	11.100		0.5	
2	13	1969	2012.7	2012.8	2016.	HWI	11.100		0.7	
2	22	1969	1921.5	1921.9	1923.	HWI	13.000		0.5	
2	23	1969	1828.	1831.8	1840.	HWI	13.000		0.4	
2	24	1969	2034.7	2035.1	2045.	HWI	13.000		0.3	
2	25	1969	1658.1	1658.5	1702.	HWI	13.000		0.3	
2	25	1969	1917.	1922.	1925.	HWI	13.000		0.2	
2	25	1969	1935.	1942.	1947.	HWI	13.000		0.2	
2	27	1969	1403.	1407.3	1425.	HWI	11.100		1.3	FINE STRUCTURE
2	28	1969	1912.	1914.2	1922.	HWI	13.000		0.3	
2	28	1969	1947.1	1947.5	1953.	HWI	13.000		0.2	
2	28	1969	2039.4	2041.2	2044.	HWI	11.000		0.2	
3	1	1969	2139.8	2140.9	2205.	HWI	13.000		1.0	FREQ DEV POSITIVE 5.5MIN
3	1	1969	2212.1	2212.8	2215.	HWI	13.000		1.0	2 SHARP PEAKS
3	1	1969	2252.7	2253.2	2255.	HWI	13.000		0.9	2 SHARP PEAKS
3	3	1969	2218.	2220.	2229.	HWI	13.000		0.2	
3	8	1969	2205.6	2207.1	2207.9	HWI	11.100		0.2	
3	9	1969	1916.	1919.6	1927.	HWI	11.100		0.6	LUMPY PEAK
3	9	1969	2234.6	2235.0	2239.	HWI	11.100		0.6	2 PEAKS
3	12	1969	1739.6	1740.3	1840.	HWI	13.000		10.5	LARGE, SEVERAL PEAKS
3	12	1969	2004.	2008.3	2025.	HWI	11.100		1.3	FINE STRUCTURE
3	12	1969	2226.6	2228.8	2239.	HWI	13.000		0.4	
3	13	1969	2040.	2041.	2054.	HWI	11.100		0.4	
3	13	1969	2113.4	2114.	2115.	HWI	11.100		0.3	
3	13	1969	2249.	2254.3	2307.	HWI	11.100		0.2	
3	15	1969	1405.	1405.6	1409.	HWI	11.100		0.3	
3	16	1969	1457.5	1458.4	1501.	HWI	11.100		0.2	
3	16	1969	2111.	2113.2	2123.	HWI	13.000		0.6	
3	16	1969	2337.1	2337.7	2346.	HWI	11.100		0.5	
3	17	1969	1919.	1919.6	1929.	HWI	13.000		0.7	
3	18	1969	1539.6	1540.1	1544.	HWI	13.000		0.15	
3	18	1969	1949.5	1950.4	1956.	HWI	13.000		0.17	
3	18	1969	2016.0	2017.0	2021.	HWI	13.000		0.3	
3	19	1969	1857.3	1900.4	1903.	HWI	13.000		0.25	
3	20	1969	1629.	1631.7	1647.	HWI	11.100		1.4	FINE STRUCTURE
3	20	1969	2145.4	2148.9	2205.	HWI	11.100		0.7	FINE STRUCTURE

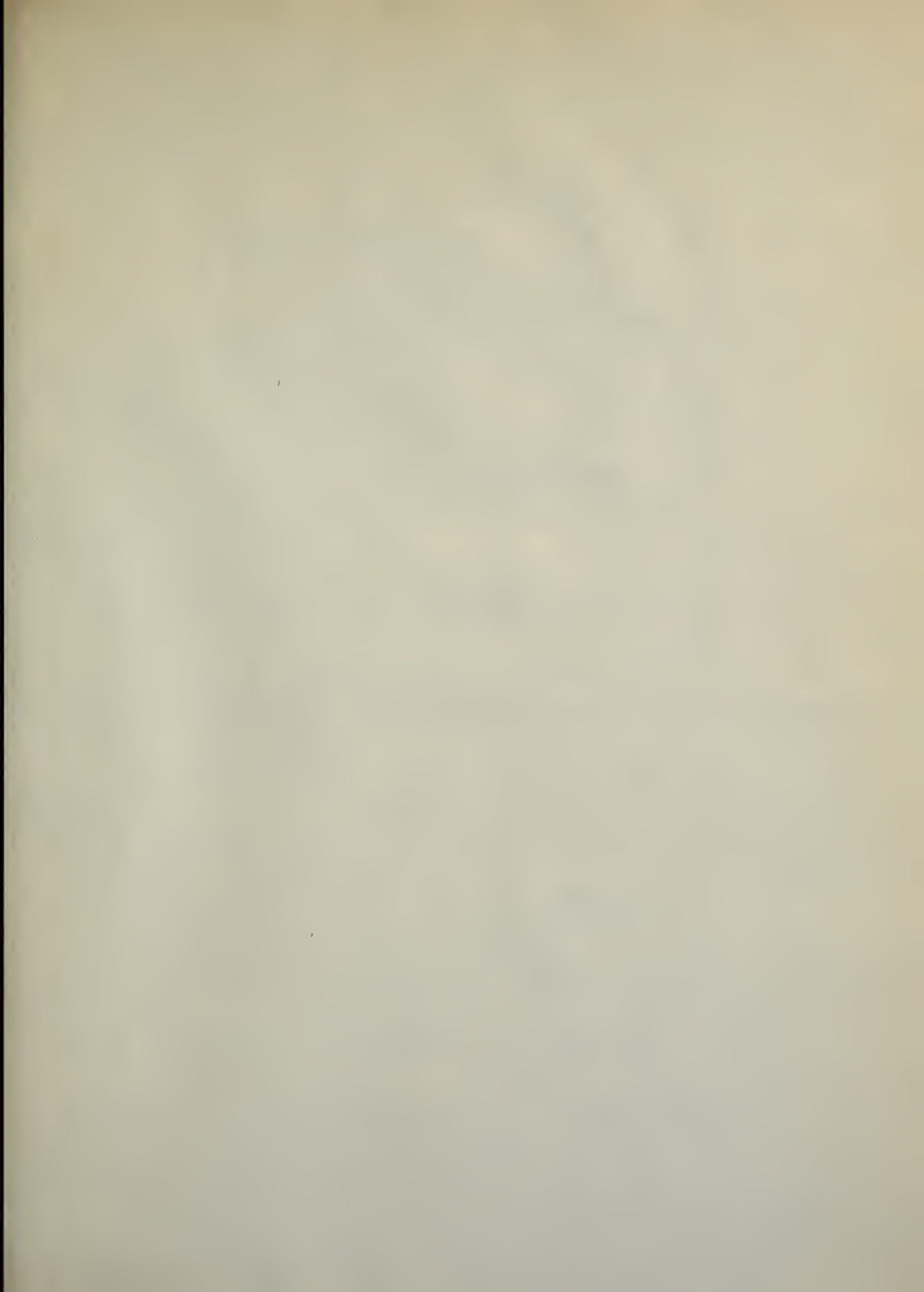
DATE			UNIVERSAL TIME			TRANSMITTER	PEAK	COMMENTS	
MONTH	DAY	YEAR	START	MAXIMUM	END	CALL LETTERS	FREQUENCY DEVIATION		
							HZ		
3	21	1969	1327.8	1332.5	1410.	WWI	11.100	0.5	
3	21	1969	1538.	1543.	1555.	WWI	13.000	0.2	
3	21	1969	1821.0	1822.4	1827.	WWI	13.000	0.2	
3	21	1969	1847.3	1848.4	1850.	WWI	13.000	0.3	
3	21	1969	1942.	1943.8	1952.	WWI	11.100	1.7	
3	23	1969	1924.1	1924.3	1926.	WWI	13.000	1.2	SINGLE SPIKE
3	25	1969	1443.	1445.	1449.	WWI	8.900	0.2	
3	25	1969	1830.7	1832.2	1841.	WWI	11.100	0.27	
3	27	1969	1323.	1326.4	1410.	WWI	8.900	0.5	FREQUENCY DEVIATION
				1328.0				0.4	GREATER THAN ZERO FOR
				1330.0				0.8	15 MINUTES
				1334.8				0.5	FINE STRUCTURE
				1339.5				0.7	
3	27	1969	1852.6	1854.4	1902.	WWI	8.900	0.2	
3	28	1969	1916.9	1918.6	1925.	WWI	13.000	0.4	
3	28	1969	2254.2	2254.7	2258.	WWI	8.900	0.6	SIMPLE SPIKE
3	29	1969	1634.1	1634.9	1637.	WWI	11.100	0.3	
3	29	1969	1920.9	1922.9	1927.	WWI	13.000	0.8	
3	29	1969	1953.8	2001.0	2004.	WWI	13.000	2.3	FINE STRUCTURE
4	2	1969	1654.2	1655.2	1657.	WWI	13.000	0.3	
4	2	1969	1728.1	1729.0	1732.	WWI	13.000	0.3	
4	2	1969	1746.0	1746.3	1748.	WWI	13.000	1.9	
4	6	1969	2308.6	2310.3	2312.	WWI	8.900	0.2	
4	14	1969	1711.	1713.3	1716.	WWI	13.000	0.6	
4	14	1969	1717.4	1719.2	1722.	WWI	13.000	0.3	
4	14	1969	1723.5	1725.0	1728.	WWI	13.000	0.2	
4	14	1969	1904.2	1905.4	1908.	WWI	13.000	0.2	
4	15	1969	1637.0	1637.7	1640.	WWI	13.000	0.5	
4	16	1969	1755.	1755.5	1800.	WWI	11.100	0.2	
4	19	1969	1840.	1841.5	1854.	WWI	13.000	0.45	
				1842.9				0.35	
4	20	1969	1734.5	1735.5	1739.	WWI	13.000	0.4	
4	20	1969	1809.	1809.	1812.	WWI	13.000	0.3	
4	20	1969	2215.2	2216.7	2219.	WWI	13.000	0.5	
4	21	1969	1557.2	1557.4	1558.3	WWI	13.000	0.3	
4	21	1969	2006.1	2008.6	2050.	WWI	13.000	12.	LARGE, FINE STRUCTURE
4	26	1969	2301.4	2303.2	2308.	WWI	13.000	2.9	
				2303.4				2.9	
				2303.8				3.0	
5	2	1969	1745.5	1749.2	1812.	WWI	13.000	2.0	LOTS OF FINE STRUCTURE
5	2	1969	2104.6	2105.2	2111.	WWI	11.100	0.75	
5	5	1969	2030.1	2031.7	2036.	WWI	11.100	0.5	
5	17	1969	1922.4	1925.1	2005.	WWI	8.900	0.6	FREQ DEV POSITIVE 12 MIN.
5	18	1969	1445.9	1447.9	1455.	WWI	11.100	0.2	
5	18	1969	1710.0	1717.7	1737.	WWI	13.000	0.9	
				1718.3				0.85	
5	18	1969	2103.7	2104.8	2120.	WWI	11.100	0.35	
5	19	1969	1432.2	1433.1	1441.	WWI	13.000	0.7	
5	20	1969	1628.0	1628.2	1634.	WWI	11.100	0.45	
				1628.8				0.4	
5	20	1969	1654.7	1656.2	1705.	WWI	11.1	1.5	
5	22	1969	1859.7	1901.1	1909.	WWI	11.1	2.5	LOTS OF FINE STRUCTURE
				1901.7				2.4	
				1902.7				1.9	
				1903.2				1.3	
5	22	1969	1931.0	1935.2	2001.	KC2X1	5.054	1.7	SMALL FINE STRUCT+SLOW RI
5	25	1969	1655.0	1656.8	1710.6	WWI	11.100	.65	LONG DURATION
5	25	1969	2238.4	2240.0	2250.	WWI	11.100	0.5	
5	28	1969	1256.8	1257.9	1302.	WWI	13.000	0.35	
5	29	1969	1422.1	1423.0	1425.0	WWI	11.100	0.6	SIMPLE SPIKE
5	29	1969	1447.	1452.4	1544.	WWI	11.100	0.8	
				1455.4				0.6	
5	29	1969	1937.2	1941.0	1955.	WWI	11.100	1.0	FAST SPIKE AT 1942.0
				1942.0				1.5	LONG DURATION
				1943.7				0.4	FINE STRUCTURE
5	30	1969	1244.6	1245.2	1311.	WWI	8.900	0.4	
6	5	1969	1450.4	1450.8	1525.	WWI	11.100	0.8	SEVERAL PEAKS ABOUT THE
				1451.2				0.8	SAME SIZE
				1455.7				0.7	
				1457.1				1.0	
				1458.0				0.9	

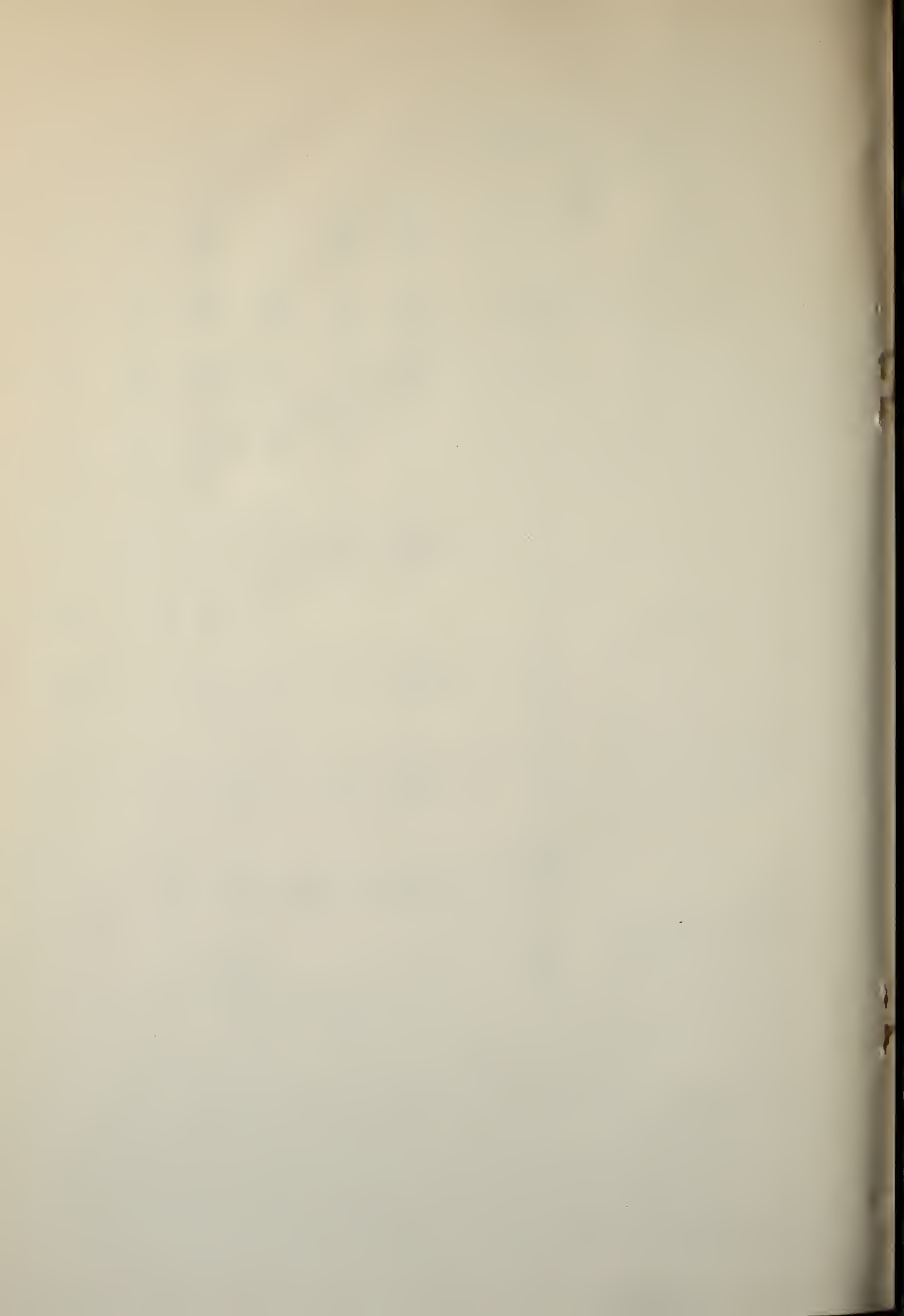
DATE			UNIVERSAL TIME			TRANSMITTER	FREQUENCY	PEAK	COMMENTS
MONTH	DAY	YEAR	START	MAXIMUM	END	CALL LETTERS	MHZ	FREQUENCY DEVIATION MHZ	
6	6	1963	0017.7	0020.3	0030.	WWI	11.100	0.35	
				0021.4				0.3	
6	6	1963	1604.1	1606.4	1640.	WWI	11.100	5.0	
				1606.9				2.0	
				1617.5				0.8	
6	6	1963	1953.3	1954.0	1955.	WWI	13.000	0.35	
6	3	1963	1511.4	1511.9	1520.	WWI	11.100	0.55	
				1512.8				0.4	
6	8	1963	1604.2	1604.4	1614.	WWI	11.100	0.5	
6	8	1963	1824.1	1824.4	1825.	WWI	13.000	1.0	MUCH FINE STRUCTURE
6	3	1963	1354.6	1357.9	1425.	WWI	11.100	0.2	
				1410.3				0.25	
				1421.2				0.3	
6	3	1963	2000.4	2007.0	2019.	WWI	11.100	0.65	
6	11	1963	1619.1	1621.0	1629.	WWI	13.000	3.2	MANY SMALL PEAKS ASSOCIATED WITH THE THREE LARGER ONES
				1621.8				2.1	
				1622.2				3.1	
6	14	1963	2102.2	2104.2	2107.	WWI	13.000	0.4	
6	16	1963	2021.3	2022.0	2024.	WWI	13.000	0.4	
6	18	1963	2339.2	2339.9	2341.	WWI	13.000	1.1	
6	19	1963	1123.3	1124.9	1130.	WWI	13.000	0.35	
6	30	1963	1708.2	1711.0	1715.	WWI	13.000	0.25	
6	30	1963	1805.4	1807.7	1811.	WWI	11.100	0.4	
7	1	1963	1624.7	1628.0	1635.	WWI	13.000	0.6	
7	1	1963	1650.0	1651.8	1659.	WWI	13.000	0.3	
7	1	1963	1712.1	1715.1	1720.	WWI	13.000	0.35	
7	3	1963	1516.4	1516.9	1543.	WWI	13.000	2.4	
7	5	1963	1229.8	1230.5	1244.	WWI	8.900	0.45	
				1231.4				0.5	
7	8	1963	2207.1	2210.9	2220.	WWI	11.100	0.25	
				2215.8				0.25	
7	14	1963	1429.8	1430.1	1432.	WWI	11.100	0.25	
				1430.9				0.3	
				1431.4				0.45	
7	15	1963	1922.3	1924.5	1927.	WWI	11.100	0.25	
7	31	1963	1549.2	1550.4	1600.	WWI	11.100	0.2	
8	1	1963	1719.8	1720.0	1721.	WWI	13.000	0.9	
8	2	1963	1911.4	1911.9	1914.	WWI	13.000	0.25	
8	5	1963	1846.8	1847.9	1852.	WWI	13.000	0.25	
8	5	1963	2016.7	2018.9	2022.	WWI	13.000	0.45	
8	10	1963	1421.7	1423.0	1428.	WWI	8.900	0.35	
8	11	1963	1215.4	1220.1	1226.	WWI	8.900	1.0	
8	12	1963	1554.8	1555.8	1601.	WWI	13.000	0.35	
8	14	1963	2004.4	2006.1	2012.	WWI	11.100	0.25	
8	21	1963	1411.6	1413.7	1431.	WWI	8.900	0.6	LONG DURATION
8	22	1963	1907.5	1908.3	1911.	WWI	13.000	0.35	
8	24	1963	1349.7	1352.2	1356.	WWI	8.900	0.45	
8	25	1963	1827.7	1829.5	1834.	WWI	11.100	0.55	
8	25	1963	1839.0	1841.1	1854.	WWI	11.100	0.8	
8	25	1963	2049.6	2050.0	2100.	WWI	13.000	0.45	
8	30	1963	1550.0	1551.0	1554.	WWI	13.000	0.25	
9	13	1963	1746.7	1749.9	1757.	WWI	11.100	0.45	
9	12	1963	2050.4	2053.3	2056.	WWI	13.000	0.35	
				2054.5				0.2	
9	15	1963	1530.5	1530.9	1533.	WWI	11.100	0.32	
9	17	1963	1800.4	1804.8	1811.	WWI	13.000	0.30	
				1810.0				0.35	
9	17	1963	1859.7	1904.4	1909.	WWI	8.900	0.25	
9	17	1963	2248.4	2251.3	2255.	WWI	11.100	0.23	
9	18	1963	2029.6	2035.5	2037.	WWI	11.100	0.25	
9	21	1963	2058.5	2101.0	2104.	WWI	13.000	0.30	
9	22	1963	1408.0	1412.0	1418.	WWI	13.000	0.45	LONG DURATION
9	27	1963	2125.4	2125.7	2128.	WWI	13.000	0.5	
10	1	1963	1950.0	1953.6	1956.	WWI	13.000	0.30	
10	3	1963	1713.8	1715.3	1721.	WWI	13.000	0.40	
10	7	1963	1722.2	1723.9	1726.	WWI	13.000	0.30	
10	3	1963	1630.2	1630.8	1633.	WWI	13.000	5.70	LARGE
10	10	1963	2224.5	2224.4	2228.	WWI	8.900	0.40	
10	13	1963	1632.5	1633.7	1641.	WWI	13.000	0.30	
				1635.3				0.30	
				1636.3				1.30	

DATE			UNIVERSAL TIME			TRANSMITTER	PEAK	COMMENTS
MONTH	DAY	YEAR	START	MAXIMUM	END	CALL LETTERS	FREQUENCY MHZ	
10	19	1963	1717.4	1720.0	1731.	HWI	13.000	0.45
10	24	1963	2111.8	2112.2	2120.	HWI	8.900	0.70
				2114.0		HWI	8.900	1.60
10	25	1963	1530.6	1535.8	1538.	HWI	13.000	0.33
10	26	1963	1631.9	1632.4	1635.	HWI	13.000	2.30
10	27	1963	1428.0	1435.8	1458.	HWI	13.000	0.42
10	28	1963	1607.1	1608.6	1610.	HWI	13.000	0.30
11	4	1963	2015.2	2025.9	2038.	HWI	13.000	0.30
11	4	1963	2125.5	2127.3	2154.	HWI	13.000	0.30
				2129.9		HWI	13.000	0.40
				2132.8		HWI	13.000	0.20
11	4	1969	1514.0	1515.0	1523.	HWI	8.900	0.30
				1516.3		HWI	8.900	0.30
				1521.9		HWI	8.900	0.15
11	5	1963	1758.6	1759.7	1805.	HWI	11.100	0.70
				1800.2		HWI	11.100	0.60
				1800.7		HWI	11.100	1.00
				1803.8		HWI	11.100	6.30
11	5	1963	1812.2	1816.9	1823.	HWI	13.000	0.25
11	18	1963	1636.2		1705.	HWI	13.000	
11	18	1963	2121.3	2122.8	2129.	HWI	13.000	3.65
				2125.0		HWI	13.000	0.50
11	20	1963	1619.6	1620.4	1625.	HWI	13.000	2.60
				1620.9		HWI	13.000	3.50
11	21	1963	2126.3	2133.8	2146.	HWI	13.000	0.70
				2131.9		HWI	13.000	1.00
11	22	1963	2123.6	2124.5	2129.	HWI	8.900	5.50
11	27	1963	1522.2	1524.2	1532.	HWI	13.000	0.50
				1525.3		HWI	13.000	0.75
12	20	1969	2012.3	2013.8	2020.	HWI	8.900	0.95
1	3	1970	1914.0	1916.3	1933.	HWI	13.000	0.75
				1923.9		HWI	13.000	0.42
1	5	1970	1803.4	1805.0	1810.	HWI	13.000	0.51
1	10	1970	2025.7	2026.7	2032.	HWI	8.900	0.43
				2028.0		HWI	8.900	0.20
				2029.6		HWI	8.900	0.15
1	11	1970	1420.5	1424.8	1430.	HWI	13.000	0.65
1	13	1970	1924.3	1925.1	1929.	HWI	11.100	0.20
				1926.5		HWI	11.100	0.25
1	23	1970	1353.3	1400.0	1409.	HWI	11.100	0.30
1	26	1970	1806.2	1808.0	1813.	HWI	13.000	0.20
1	28	1970	1916.9	1918.7	1937.	HWI	13.000	11.20
				1919.4		HWI	13.000	7.20
1	30	1970	1821.9	1823.3	1826.	HWI	13.000	0.30
1	31	1970	1647.5	1648.8	1651.	HWI	13.000	0.30
1	31	1970	1818.0	1820.2	1821.	HWI	13.000	0.25
2	11	1970	2106.8	2114.2	2145.	HWI	13.000	0.70
2	17	1970	2018.7	2019.1	2022.	HWI	13.000	0.20
2	18	1970	1923.2	1925.4	1928.	HWI	13.000	0.25
2	19	1970	1711.2	1713.4	1717.	HWI	13.000	0.30
2	23	1970	1449.5	1455.3	1500.	HWI	11.100	0.35
2	23	1970	1541.0	1544.8	1546.	HWI	11.100	0.28
2	27	1970	1906.7	1911.9	1922.	HWI	8.900	0.30
2	27	1970	2318.3	2319.8	0000.	HWI	8.900	0.30
				2321.5		HWI	8.900	0.70
				2322.4		HWI	8.900	0.80
2	28	1970	2007.8	2011.0	2030.	HWI	13.000	1.20
				2011.6		HWI	13.000	.4
3	1	1970	1530.1	1530.8	1539.	HWI	8.900	4.60
				1531.0		HWI	8.900	4.70
				1531.3		HWI	8.900	2.30
3	1	1970	2001.8	2004.3	2115.	HWI	13.000	3.40
				2005.4		HWI	13.000	5.50
3	2	1970	1713.9	1714.8	1720.	HWI	13.000	1.20
				1715.4		HWI	13.000	1.70
				1715.8		HWI	13.000	1.30
3	2	1970	1500.6	1502.5	1512.	HWI	8.900	0.55
3	2	1970	2005.3	2007.4	2012.	HWI	11.100	0.30
				2011.6		HWI	11.100	0.20
3	3	1970	2021.8	2024.3	2030.	HWI	13.000	1.10
				2026.6		HWI	13.000	0.47

DATE			UNIVERSAL TIME			TRANSMITTER	PEAK	COMMENTS
MONTH	DAY	YEAR	START	MAXIMUM	END	CALL LETTERS	FREQUENCY DEVIATION	
							MHZ	
3	4	1970	1703.1	1705.0	1713.	WHI	13.000	0.30
3	4	1970	1810.5	1813.0	1822.	WHI	13.000	0.35
3	5	1970	1613.9	1622.8	1648.	WHI	13.000	0.50
				1625.3		WHI	13.000	0.30
3	5	1970	1909.0	1909.9	1916.	WHI	13.000	0.44
				1911.2		WHI	13.000	0.30
3	7	1970	1604.2	1605.7	1613.	WHI	11.100	0.40
				1606.6		WHI	11.100	0.55
3	7	1970	2003.0	2003.8	2110.	WHI	13.000	0.40
3	9	1970	1754.7	1755.5	1758.	WHI	13.000	0.50
3	12	1970	1842.0	1842.5	1845.	WHI	13.000	0.20
3	12	1970	1858.3	1858.9	1900.	WHI	13.000	0.20
3	17	1970	1439.3	1452.1	1454.	WHI	13.000	0.25
				1453.2				0.35
3	14	1970	1758.3	1759.2	1803.	WHI	13.000	0.25
3	19	1970	1802.0	1803.1	1809.	WHI	13.000	0.20
3	19	1970	1959.1	2003.2	2006.	WHI	13.000	0.30
3	19	1970	2016.0	2016.6	2018.	WHI	13.000	0.20
3	21	1970	1615.3	1616.3	1620.	WHI	13.000	0.20
				1617.3				0.15
3	21	1970	1756.3	1753.1	1801.	WHI	13.000	0.20
3	22	1970	1607.4	1608.0	1613.	WHI	8.900	0.15
3	22	1970	1407.4	1403.0	1412.	WHI	8.900	0.20
3	22	1970	2038.8	2043.5	2054.	WHI	13.000	0.30
3	23	1970	1544.8	1547.0	1548.	WHI	13.000	1.35
3	24	1970	1625.8	1630.3	1632.	WHI	13.000	0.50
3	25	1970	1350.2	1354.2	1357.	WHI	8.900	0.25
3	25	1970	1600.1	1601.9	1605.	WHI	13.000	0.20
3	26	1970	1447.1	1453.5	1515.	WHI	13.000	0.75
3	26	1970	1726.6	1727.5	1734.	WHI	13.000	4.0
				1729.3				4.70
3	26	1970	2004.3	2007.8	2012.	WHI	13.000	3.40
3	26	1970	2332.4	2333.3	2342.	WHI	8.900	0.25
4	5	1970	1745.1	1745.8	1751.	WHI	13.000	0.80
4	6	1970	1803.0	1805.2	1806.	WHI	13.000	0.25
4	8	1970	1638.5	1643.0	1650.	WHI	13.000	0.20
4	8	1970	1948.4	1950.2	2005.	WHI	8.900	1.60
4	9	1970	1816.0	1824.1	1825.	WHI	13.000	0.30
4	11	1970	1431.1	1432.2	1434.	WHI	13.000	0.30
4	10	1970	1627.2	1631.	1637.	WHI	13.000	0.80
				1634.9				0.60
4	10	1970	1757.0	1757.2	1758.	WHI	13.000	0.90
4	10	1970	2230.4	2234.8	2242.	WHI	13.000	0.20
4	11	1970	2312.1	2314.9	2317.	WHI	13.000	0.20
4	12	1970	1703.6	1704.2	1706.	WHI	13.000	0.30
4	12	1970	1712.	1721.	1742.	WHI	13.000	0.20
4	13	1970	1548.3	1552.2	1554.	WHI	13.000	0.20
4	13	1970	2224.3	2227.4	2230.	WHI	11.100	1.10
4	13	1970	1812.0	1815.2	1848.	WHI	8.900	0.10
4	21	1970	2124.1	2127.0	2145.	WHI	13.000	0.30
4	22	1970	1715.5	1717.3	1720.	WHI	13.000	0.15
4	23	1970	1735.3	1737.0	1739.	WHI	13.000	0.20
4	25	1970	0036.4	0037.8	0054.	WHI	8.900	0.80
4	27	1970	1715.1	1719.8	1721.	WHI	13.000	0.15
4	28	1970	2211.2	2214.3	2217.	WHI	13.000	0.25
4	29	1970	2042.2	2044.8	2047.	WHI	13.000	0.25
5	2	1970	2212.0	2212.5	2214.	WHI	8.900	0.45
5	4	1970	1815.7	1816.4	1818.	WHI	13.000	0.80
5	4	1970	1829.2	1834.0	1937.	WHI	13.000	0.20
5	6	1970	0024.	0030.	0031.	WHI	11.100	0.20
5	6	1970		1230.		WHI	8.900	0.25
5	7	1970	1601.2	1603.4	1608.	WHI	13.000	0.20
5	7	1970	1609.6	1611.2	1625.	WHI	13.000	0.20
5	7	1970	2227.1	2227.9	2234.	WHI	11.100	0.45
5	7	1970	2329.6	2330.4	2331.	WHI	11.100	0.20
5	7	1970	2334.1	2334.9	2338.	WHI	11.100	0.30
5	8	1970	1716.8	1718.9	1723.	WHI	13.000	1.70
5	8	1970	1951.5	1953.4	1959.	WHI	13.000	0.35
5	8	1970	2133.2	2134.2	2135.	WHI	13.000	0.25
5	9	1970	1559.8	1600.6	1608.	WHI	13.000	4.60

DATE			UNIVERSAL TIME			TRANSMITTER		PEAK	COMMENTS
MONTH	DAY	YEAR	START	MAXIMUM	END	CALL LETTERS	FREQUENCY MHZ	FREQUENCY DEVIATION HZ	
5	9	1970	1700.5	1701.3	1705.	WWI	13.000	0.65	
5	9	1970	2005.3	2005.9	2009.	WWI	13.000	0.30	
5	10	1970	1420.5	1422.0	1426.	WWI	13.000	0.20	
5	10	1970	1849.3	1850.5	1853.	WWI	13.000	0.45	
5	12	1970	1743.2	1744.0	1745.	WWI	8.900	0.20	
5	13	1970	1652.3	1655.9	1708.	WWI	13.000	0.20	
5	15	1970	1453.2	1457.0	1500.	WWI	8.900	0.55	
5	15	1970	1911.1	1914.6	1922.	WWI	8.900	0.90	
5	15	1970	2204.6	2207.0	2219.	WWI	13.000	0.40	
5	16	1970	1445.8	1449.2	1450.	WWI	8.900	1.90	
5	16	1970	1725.2	1725.8	1728.	WWI	13.000	0.55	
5	17	1970	2126.7	2129.6	2132.	WWI	8.900	0.20	
5	18	1970	1836.9	1839.5	1852.	WWI	13.000	0.60	
5	19	1970	1937.2	1937.7	1947.	WWI	13.000	0.30	
5	20	1970	1503.8	1513.9	1516.	WWI	8.900	0.20	3 PEAKS
5	22	1970	1534.1	1535.3	1536.	WWI	13.000	0.30	
5	22	1970	1857.0	1900.0	1931.	WWI	13.000	0.35	3 PEAKS
5	26	1970	1121.8	1123.2	1140.	WWI	8.900	1.25	
5	29	1970	1740.0	1741.1	1754.	WWI	8.900	0.25	
5	29	1970	1932.3	1937.0	1940. K	C2XME	5.100	2.0	
5	29	1970	1716.9	1720.2	1731.	WWI	8.900	0.95	
5	29	1970	2230.9	2231.9	2233.	WWI	8.900	0.50	
6	3	1970	2033.6	2034.3	2042.	WWI	13.000	0.62	
6	8	1970	1715.2	1717.7	1718.	WWI	13.000	0.30	
6	10	1970	1536.8	1538.8	1540.	WWI	13.000	0.35	
6	12	1970	1533.9	1534.6	1535.	WWI	13.000	0.75	
6	12	1970	1726.8	1729.2	1738.	WWI	13.000	0.35	
6	12	1970	1938.3	1939.4	1941.	WWI	13.000	0.65	
6	13	1970	1230.2	1232.4	1240.	WWI	13.000	0.50	LONG DURATION
6	13	1970	1752.0	1754.4	1807.	WWI	13.000	0.25	
6	13	1970	1939.5	1942.1	1945.	WWI	13.000	0.50	2 PEAKS
6	13	1970	2202.3	2204.4	2217.	WWI	13.000	0.60	
6	14	1970	0015.1	0017.0	0027.	WWI	13.000	0.70	
6	14	1970	1658.1	1701.3	1714.	WWI	13.000	3.00	
				1702.2				1.60	
				1703.8				3.0	
6	14	1970	1729.1	1749.4	1749. D	WWI	13.000	1.10	
6	15	1970	1316.4	1318.7	1328.	WWI	13.000	1.60	
6	15	1970	1837.5	1839.1	1851.	WWI	13.000	1.15	
6	15	1970	1855.5	1858.0	1912.	WWI	13.000	0.40	
				1503.3				0.25	
6	16	1970	1354.0	1355.4	1357.	WWI	5.100	0.92	
6	17	1970	1858.1	1900.6	1912.	WWI	13.000	1.20	
6	18	1970	1853.4	1856.3	1858.	WWI	13.000	0.45	
6	19	1970	1549.3	1552.6	1601.	WWI	13.000	0.30	FINE STRUCTURE
				1554.8				0.40	
				1558.1				0.25	
6	19	1970	1506.5	1509.7	1514.	WWI	13.000	0.20	
6	20	1970	0005.4	0006.9	0007.	WWI	5.100	0.60	
6	25	1970	1833.8	1836.3	1839.	WWI	13.000	2.35	
6	28	1970	1958.3	2000.7	2020.	WWI	13.000	4.20	LONG DURATION
				2001.3				2.80	FINE STRUCTURE DOMINATES
				2001.9				3.30	BEGINNING
				2002.4				1.60	
				2004.9				2.00	
7	1	1970	1546.5	1548.1	1553.	WWI	13.000	0.20	







PENN STATE UNIVERSITY LIBRARIES



A000072020050